NATIONAL ADVISORY COMMITTEE FOR AERONAUTICS

TECHNICAL NOTE 3128

COMPARISON BETWEEN THEORY AND EXPERIMENT FOR INTERFERENCE PRESSURE FIELD BETWEEN WING AND BODY AT SUPERSONIC SPEEDS

By William C. Pitts, Jack N. Nielsen, and
Maurice P. Gionfriddo

Ames Aeronautical Laboratory
Moffett Field, Calif.

NACA

Washington
April 1954

1Q

NATIONAL ADVISORY COMMITTEE FOR AERONAU

TECHNICAL NOTE 3128

COMPARISON BETWEEN THEORY AND EXPERIMENT FOR INTERFERENCE PRESSURE FIELD BETWEEN WING AND BODY AT SUPERSONIC SPEEDS

By William C. Pitts, Jack N. Nielsen, and
Maurice P. Gionfriddo

SUMMARY

Pressure-distribution data were obtained for a wing-body combination at Mach numbers of 1.48 and 2.00 and at Reynolds numbers of 0.6, 1.2, and 1.5×10^6 to investigate the effects of wing-body interference. The model was a single-wedge, rectangular wing mounted on a cylindrical body with an ogival nose. The body angle of attack ranged between $+6^\circ$ and -6° and the wing-incidence angle ranged from 0° to -5.7°. The experimental pressure-distribution and span-loading results are compared with the linear, wing-body interference theory of NACA TN 2677.

For small values of angle of attack and wing-incidence angle it was found that the experimental pressure-distribution results compared well with linear theory, but for larger angles, nonlinear effects of angle caused large differences from linear theory. The nonlinear effects of angle on the wing were fairly well predicted by shock-expansion theory for the wing incidence case. In contrast with the pressure-distribution results, the lift loading was found to be very nearly linearly dependent on angle. Reynolds number and Mach number were found to have only a small effect on the difference between experiment and linear theory except near the wave traversing the body from the wing-body juncture where the effects of both of these parameters were large.

INTRODUCTION

In recent years much interest has been manifested in wing-body interference. Some of the theories that have been developed for computing the effects of wing-body interference on pressure distribution have been compared by Phinney (ref. 1) and Lawrence and Flax (ref. 2). Ferrari (ref. 3) presented an iterative method based on linear theory. Morikawa (ref. 4) obtained an approximate solution by solving a boundary-value problem, and also obtained a closed solution by approximating the three-dimensional model by a planar model. Bolton Shaw (ref. 5) obtained a solution by satisfying boundary conditions at a finite number of points rather than over a surface.

A method of solving a wide class of wing-body interference problems is presented in references 6 and 7 together with a numerical application to the special case of a flat, rectangular wing mounted at incidence on a cylindrical body at zero angle of attack. The method determines an interference potential that satisfies the boundary conditions on both the wing and the body when the body is introduced into the field of the wing alone. This interference potential is determined as the sum of a number of Fourier components. Since no assumptions are made beyond those of linear theory, the exact linear-theory solution could be obtained from this method by taking a sufficient number of terms. The numerical application shows that except near the wing leading edge, the Fourier series converges so rapidly that, generally, only four Fourier components give a close approximation to the exact linear-theory solution.

Some experimental pressure-distribution data, such as those of references 8, 9, 10, 11, and 12, are available for comparison with theory. However, a complete, systematic set of data which cover the effects of angle of attack, wing incidence, Reynolds number, and Mach number on the pressure distribution on both the wing and body of a wing-body combination is not available. It is the primary purpose of the present report to present such a set of data and to compare them with the theory of references 6 and 7 to determine the accuracy of the theory. Another purpose is to compare the calculated results of this report with those of other theories.

SYMBOLS

a	body radius, in.
A	aspect ratio of wing formed by joining exposed half-wings together
c	chord of rectangular wing, in.
$f_{2n}(x)$	velocity amplitude function of n'th Fourier component, in./sec
i_W	wing-incidence angle, radians except where otherwise designated
L	lift of combination back to wing trailing edge, lb
M	free-stream Mach number
n	number of Fourier component
p	static pressure, lb/sq in.
p_1	static pressure at any particular orifice of wing-body combination when $\alpha = i_W = 0$, lb/sq in.

P	pressure coefficient, $\frac{p - p_1}{q_o}$
P_{2n}	interference pressure coefficient due to n'th Fourier component
q	dynamic pressure, lb/sq in.
r,θ,x	cylindrical coordinates: $y = r \cos \theta$, $z = r \sin \theta$ (See fig. 1.)
R	Reynolds number based on wing-chord length
R.P.	real part
s	semispan of wing-body combination, in.
V	free-stream velocity, in./sec
$W_{2n}(x,r)$	characteristic functions
x,y,z	Cartesian coordinates: x, axial coordinate; y, lateral coordinate; z, vertical coordinate, in. (See fig. 1.)
α	body angle of attack, radians except where otherwise designated
α_W	wing angle of attack, deg
β	$\sqrt{M^2 - 1}$
ξ,η	dummy variables of integration
Φ_W	total wing-alone perturbation velocity potential
Φ_{W_R}	wing-alone perturbation velocity potential due to the exposed right half of the wing
Φ_{W_L}	wing-alone perturbation velocity potential due to the exposed left half of the wing
Φ_{W_B}	wing-alone perturbation velocity potential due to the portion of wing inside the region occupied by body

Subscripts

i	integer ranging from 1 to ∞
L	lower surface
T	wall of wind tunnel

u upper limit of integration

U upper surface

o free-stream conditions

EXPERIMENTAL CONSIDERATIONS

Apparatus and Procedure

The investigation was made in the Ames 1- by 3-foot supersonic wind tunnel. This wind tunnel was equipped with a flexible-plate nozzle that could be adjusted to give test-section Mach numbers from 1.2 to 2.2. The pressure measurements are obtained as photographic recordings of a multiple-tube manometer board using dibutyl phthalate as the fluid.

Since this investigation required a comparison of the data for several Mach numbers and Reynolds numbers at the same values of α and i_W, it was necessary to set α and i_W accurately for each measurement while under tunnel test conditions. The values of i_W were accurately set by means of angle blocks in the body. The angle of attack was set by a special image projection device. A mirror was inserted in the schlieren system so that an image of the model was cast upon a screen. With the wind off, the model was set at the desired value of α and the inclination of the model image was marked on the screen. With the tunnel in operation at the desired pressure, the angle of attack of the model was adjusted until the inclination of its image was parallel to the calibration line made on the screen with the wind off. To check this method, a horizontal and vertical wire grid was placed on the tunnel window and schlieren pictures were taken of the model while the tunnel was in operation. These pictures showed that the image projection device set α to within $\pm 0.07^\circ$ of the desired value. It was especially necessary to set α accurately for the small angles to avoid large percentage errors in the angle setting.

The model angle of attack ranged from $+6^\circ$ to -6° in 2° increments and the wing-incidence angle ranged from 0° to -5.7° in 1.9° increments. The test was performed at the two Mach numbers 1.48 and 2.00 and at the Reynolds numbers of 0.6, 1.2, and 1.5 million, based on the wing chord. The model was tested for all combinations of these values of the four parameters investigated.

Model and Support

The sting-supported model, which is diagrammed in figure 1, was a combination consisting of a cylindrical body with an ogival nose and a rectangular, wedge-shaped wing. The dimensions of the model are given in

figure 1. The wing was made 10 percent thick to minimize aeroelastic effects. It was mounted in the body by means of a set of angle blocks which enabled the flat wing surface containing the orifices to be set at 0°, -1.9°, -3.8°, and -5.7° angles of incidence with respect to the body center line. The pressure orifices were all located on the upper surface of the model. The 47 orifices were distributed along seven spanwise stations in order to give a comparison with theory for the wing and the body. The locations of the orifices are given in table I.

Reduction and Accuracy of Data

Reduction of data.- All data are reduced to the coefficient form $(p-p_1)/q_o$. Actually the quantity $(p-p_T)/q_T$ was measured and subsequent corrections were applied to change the reference static pressure to p_1 (p_1 is the static pressure at the particular orifice in question when $\alpha = i_W = 0^\circ$) and the reference dynamic pressure to q_o. Since p_1 includes the effects of nose thickness and stream angle, using p_1 as a reference pressure minimizes these effects and essentially gives only the pressures due to the angle settings of the model. The dynamic pressure was adjusted from q_T to q_o on the basis of a previous pressure survey of the tunnel. This later adjustment was negligible for $M = 1.48$ and amounted to less than a 3-percent correction for $M = 2.00$. For the purpose of comparison with theory the pressure coefficient $(p-p_1)/q_o$ is reduced to the parameters $\beta P/\alpha$ for $i_W = 0^\circ$ and $\beta P/i_W$ for $\alpha = 0^\circ$.

Accuracy of data.- There are two types of errors that enter into an experimental investigation: systematic errors and random errors. In this paper accuracy will be taken as the ability of the experiment to give the true values without nose effect or stream angle and, hence, is a measure of the systematic errors. Precision will be taken as the ability to repeat the data and, hence, is a measure of the random errors in the experiment.

Several factors contributed random errors. The major factor was the error in the angle-of-attack setting. The uncertainty in each angle setting was $\pm 0.07^\circ$, but each measurement was dependent upon two angle settings: the setting for the condition represented and the setting to determine the zero correction. This leads to a net uncertainty of 0.1° which would account for a 5-percent error for angles of $\pm 2^\circ$. Most of the remainder of the uncertainty in the data is due to the fact that the reference wall static pressure in the tunnel changed slightly from run to run while the total pressure remained constant. Although the magnitude of this pressure change was quite small, it was large enough compared to the small pressure differences for the 2° angle settings to cause as much as a 3-percent error. In addition to these factors, between 1-percent and 2-percent uncertainty was observed in reading the data from the manometer board pictures.

To determine experimentally the precision of the data, a large number of repeat measurements were taken and compared. It was found that for α or $i_W = \pm 2^\circ$, two independent determinations of $\beta P/\alpha$ or $\beta P/i_W$ differed from each other by ±7 percent on the average. For α or $i_W = \pm 4^\circ$ and α or $i_W = \pm 6^\circ$, the experimentally determined precision of $\beta P/\alpha$ and $\beta P/i_W$ is ±4 percent and ±2 percent, respectively. The precision in $\beta P/\alpha$ increases with the magnitude of the angle because a large part of the random error is due to the angle setting. The known major experimental errors are due to stream angle and body nose effects. The effect of these factors was not determined, but, as described in the reduction of data section, corrections were applied to minimize their effect, assuming the effects did not vary appreciably with angle-of-attack settings. This assumption should be good for the body-thickness effect. However, it is not necessarily a good assumption for the stream-angle effect since the stream angle varies slightly at different positions in the tunnel and the model moves approximately 6 inches in a vertical direction between $\alpha = +6^\circ$ and $\alpha = -6^\circ$. Since the stream-angle correction that was used was obtained for the $\alpha = 0^\circ$ position in the tunnel, data obtained at $\alpha = 0^\circ$ should have no appreciable error due to stream angle. For other values of α, some error due to stream angle is possible.[1]

For the purposes of this paper, the important question is, "How well does theory predict the experimental data?" Direct comparisons between linear theory and experiment will be made only for $\alpha = \pm 2^\circ$ and $i_W = -1.9^\circ$ data. In figure 2, experimental pressure distributions in the wing-body juncture obtained from two independent measurements with $i_W = -1.9^\circ$ and $\alpha = 0^\circ$ are shown together with a faired curve of their average values. The ±7-percent limit of precision about the average value is represented by the dotted lines. The figure shows that the theoretical value generally lies between these dotted lines and therefore the theory predicts the experimental values within the precision of the data in this example.

THEORETICAL CONSIDERATIONS

The theory of this report is a direct application of the general linear theory of references 6 and 7 to two special conditions of a rectangular wing and body combination. The mathematical model consists of a rectangular, flat-plate wing mounted on an infinitely long circular-cylinder body. The aspect ratio of the wing is large enough so that the Mach lines from the leading edge of the wing tips do not intersect the wing-body juncture. The two special conditions treated are the angle-of-attack case (variable angle of attack with $i_W = 0^\circ$) and the wing incidence case (variable wing-incidence angle with $\alpha = 0^\circ$). A detailed example calculation of the wing-incidence case is given in reference 7, so it will

[1]A stream-angle and pressure survey of the wind tunnel indicated that stream-angle variation caused the magnitude of the experimental values of $\beta P/\alpha$ to be 4 percent high on the average.

not be discussed in detail here. The calculations involved in the angle-of-attack case will be outlined in the following section. The differences from linear theory due to finite values of α and i_w are predicted by shock-expansion theory.

In the analysis of references 6 and 7 and in the calculations for this report the body radius is taken as unity, and M^2 is taken as 2 so that $\beta = \sqrt{M^2 - 1} = 1$. Any formula can be generalized to any body radius by dividing all length symbols by a and can be generalized to any Mach number by dividing all streamwise lengths by β, by multiplying all pressure coefficients by β, and leaving all potentials and span loadings unaltered.

Summary of Method for Angle-of-Attack Case

As in all applications of the theory of references 6 and 7, the velocity potential of the combination is considered to be the sum of the wing-alone potential and an interference potential. Since the wing-alone potential can be determined by existing methods, the essential problem is to determine the interference potential. This is done by developing a potential that cancels the flow, due to the wing alone, across the body surface as well as satisfying the two other boundary conditions, (1) that it does not distort the shape of the wing and (2) that it is zero ahead of the wing leading edge.

The first step in calculating the pressure coefficients is to determine the wing-alone potential. From this, the normal velocity, and hence the boundary condition on the body surface, is obtained. The expression for the normal velocity is expanded in a Fourier series of the form $\sum_{n=0}^{\infty} f_{2n}(x) \cos 2n\theta$ where $f_{2n}(x)$ is called the velocity amplitude function. After the velocity amplitude functions are determined, the interference pressure coefficient at any point in the flow field can be directly found in series form with the aid of the universal $W_{2n}(x,r)$ functions developed and tabulated in references 6 and 7 for $r = 1$. By adding the interference pressures to the wing-alone pressures, the pressure coefficients for the wing-body combination are obtained. The details of the calculation for the angle-of-attack case are presented in Appendixes A, B, and C. It is shown that the interference pressure coefficient for $r = a$ is

$$P_{2n} = \frac{2}{V} \cos 2n\theta \left[f_{2n}(x) - \int_0^x f_{2n}(\xi) W_{2n}(x-\xi) d\xi \right]$$

Wing-Incidence Case

The theoretical values for the wing-incidence case used in this report are taken directly from reference 7. The only exception is the pressure distribution on the $\theta = \pi/4$ meridian on the body which is not presented in reference 7. However, it was calculated in the same manner as was used for the top meridian of the body so no further discussion is necessary here.

RESULTS AND DISCUSSION

A complete set of data in the form of P for the Reynolds numbers 0.6, 1.2, and 1.5×10^6 at $M = 1.48$ and for $R = 1.5\times10^6$ at $M = 2.00$ is presented in table II. These values of P are, for the most part, averages of two readings.

General Physical Principles

Before discussing the results of the investigation in detail, it is well to give first a general physical description of the effects to be expected. Figures 3 and 4 show qualitatively the pressure distributions to be expected on a rectangular wing and body combination for the angle-of-attack case and the wing-incidence case, respectively. The chordwise variations of the coefficient, $\beta P/\alpha$ or $\beta P/i_W$, are shown for five stations by the shaded areas.[2] The variation in the pressure coefficient is somewhat exaggerated for emphasis. These figures show that Mach cones emanating from the wing-body juncture determine the points at which the various effects of wing-body interference are felt. On the cylindrical body the pressure coefficient is zero in front of the Mach helix originating at the leading edge of the wing-body juncture. However, as shown by the two stations on the body, the pressure rises abruptly behind this Mach helix, point 1, in both figures. The Mach helices from the two wing panels cross the $\theta = \pi/2$ station simultaneously so that there is only one large increase in the magnitude of the pressure coefficient. These Mach helices cross the $\theta = 3\pi/4$ station at two different points so that beyond point 1 there is a secondary increase in the pressure coefficients at point 2. These Mach helices continue to curl around the body until they strike the wing panel at points 3, where part of the pressure disturbance continues along the wing and part of it is reflected along another Mach helix on the

[2] At $y/a = 3$ in figure 3 the shape of the curve behind the Mach wave has been inferred from the wing-incidence-case calculations.

The pressure distribution shown for the $\theta = 3\pi/4$ station on the body is identical to the pressure distribution for the $\theta = \pi/4$ station due to the symmetry of the model.

body, causing a further increase in the magnitude of the pressure coefficients at points 4. Another pressure disturbance originates at the trailing edge of the wing-body juncture that causes the decrease in the magnitude of the pressure coefficients noted at points 5 of the two figures.

On the wing of the combination the pressure coefficient is the same as that for a wing alone in front of the Mach wave from the wing-body juncture, except that when the body is at an angle of attack the body upwash effectively twists the wing in a manner such that $\alpha_w = \alpha(1+a^2/y^2)$. Figure 3 shows this effect of body upwash along the leading edge of the wing where the pressure coefficient decreases as y/a increases because of the effective twist of the wing. The importance of body upwash can be seen by comparing the pressure distribution along the leading edge in figure 3 with that in figure 4. The pressure coefficient at the wing-body juncture in figure 3 is twice that in figure 4 where there is no body upwash. The pressure coefficient at any given spanwise station remains nearly constant between the wing leading edge and the Mach wave from the wing-body juncture. Behind the Mach wave, interference from the wing-body juncture causes the pressure coefficient to decrease in magnitude as shown in the two figures.

Effects of Angle of Attack

Comparisons between theory and experiment for the angle-of-attack case are made in figure 5 for data at a Reynolds number of 1.5×10^6 and Mach numbers of 1.48 and 2.00 with $i_w = 0^\circ$ and $\alpha = \pm2^\circ$ and $\pm6^\circ$.

Pressure distribution in juncture of wing-body combination.- A comparison between linear theory and experiment for the pressure distribution in the wing-body juncture is made in figures 5(a) and 5(b) for both Mach numbers. The sketches show the pertinent Mach lines and the spanwise location of the orifices.[3] The experimental data points from the wing surface on which a compression occurs (negative angle of attack) are represented by flagged symbols, and the data points from the surface on which an expansion occurs (positive angle of attack) are represented by unflagged symbols. The figures show that the theory predicts the magnitude of $\beta P/\alpha$ about 5 percent below the average of the $\alpha = \pm2^\circ$ experimental values at $M = 1.48$ and about 15 percent below experimental values at $M = 2.00$. The chordwise variation is well predicted by the theory.

Linear theory predicts that the parameter $\beta P/\alpha$ is independent of angle of attack. Actually it is not, and the nonlinear effects of angle of attack cause a spread in the data. The magnitude of the spread to be

[3]The location of these Mach lines is only qualitative because the calculations were made using shock-expansion theory, with the assumption that there was no local Mach number variation behind the leading edge of the wing. To simplify the sketches, the Mach helices on the body are represented as straight lines.

expected between $\alpha = +6^\circ$ and $\alpha = -6^\circ$ was calculated at the leading edge of the wing by shock-expansion theory. As in the calculation of first-order effects, the local angle of attack was determined using Beskin upwash theory. For $M = 1.48$ body upwash caused the shock wave to be detached from the wing in the wing-body juncture so that no calculation of the spread could be made there. For $M = 2.00$ it was found that near the wing-body juncture the predicted spread was about twice the experimental spread, whereas for y/a greater than about 1.5 the experimental spread was fairly well predicted. This difference between shock-expansion theory and the experimental data in the wing-body juncture is probably due to the combination of two things. First, near the wing-body juncture the body upwash is modified by viscous effects. Second, the theoretical spread was calculated at the leading edge of the wing and this value was assumed to apply rearward to the first orifice. This assumption is probably good beyond $y/a = 1.5$ where the chordwise changes in pressure are small back to the first orifice, but, in the juncture, the changes in the chordwise direction are large near the wing leading edge so that this assumption is probably invalid.

Another phenomenon not predicted by linear theory is shown by figure 5(a). The linear theory predicts that the Mach helix from the opposite wing panel (see sketch) should intersect the wing-body juncture at point 1, causing an increase in the magnitude of $\beta P/\alpha$. This effect is observed experimentally for negative values of α but in front of point 1 rather than exactly at point 1. The reason is that for negative values of α a compression occurs on the orificed surface reducing the local Mach number from the free-stream Mach number, thus increasing the Mach angle and causing the Mach helix to shift forward. The result is the spread of the data shown in figure 5(a) near point 1. This effect is not shown by figure 5(b) because the wing chord is effectively shorter for $M = 2.00$ so that the orifices do not extend to the Mach helix as shown by the sketch.

Figures 5(a) and 5(b) show that Mach number has no effect upon the magnitude of the higher-order spread due to angle of attack or upon the chordwise variation of $\beta P/\alpha$, but on the average the magnitude of $\beta P/\alpha$ is about 10 percent higher for $M = 2.00$ than for $M = 1.48$.

Pressure distribution on top meridian of body of wing-body combination.- A comparison between the linear theory and experiment for the pressure distribution on the top meridian of the body is made in figures 5(c) and 5(d). These figures show that theory and experiment are in good accord for $\alpha = \pm 2^\circ$, particularly at $M = 1.48$. However, nonlinear effects due to α cause a large spread between the data for $\alpha = +6^\circ$ and $\alpha = -6^\circ$. All the effects predicted to occur on the body in the section of the report "General Physical Principles" are observed experimentally, but not exactly at the points predicted because of nonlinear effects. The pressure rise predicted at point 1 of figures 5(c) and 5(d) occurs prematurely and is less abrupt than expected for all angles of attack because of the boundary layer on the body. The variation in local Mach number

causes the Mach helices to shift forward for the negative angles of attack as discussed in the section treating the wing-body juncture. The increase in the magnitude of $\beta P/\alpha$ expected at point 2, $x/\beta a = 3\pi/2$, actually occurs at about $x/\beta a = 4$ for $\alpha = -2^\circ$. The decrease in magnitude of $\beta P/\alpha$ that is expected at point 3 actually occurs at about $x/\beta a = 4.0$ for $\alpha = -6^\circ$. For the positive angles of attack the Mach helices are shifted rearward so that these effects are not observed experimentally in the range of $x/\beta a$ measured.

Figures 5(c) and 5(d) show that, in general, the $M = 1.48$ data are predicted better by the theory than are the $M = 2.00$ data. For $M = 2.00$ there is an unexpectedly large pressure coefficient in front of point 1 for negative angles of attack.[4] For $\alpha = -2^\circ$ and $M = 2.00$, $\beta P/\alpha$ dips slightly near point 1 and then rises and overshoots the $\alpha = -6^\circ$ data. This effect is due to the boundary-layer condition on the body and will be discussed in detail in the section dealing with Reynolds number effect.

Pressure distribution on $\theta = 45^\circ$ meridian of body.- A comparison between the linear theory and experiment for the pressure distribution on the $\theta = 45^\circ$ meridian of the body is made in figures 5(e) and 5(f). Essentially the same effects are shown on this meridian as on the top meridian.

Just as for the top meridian of the body the experiment is, in general, better predicted by the theory for $M = 1.48$ than for $M = 2.00$, and the same boundary-layer effects are evident near point 1 for $M = 2.00$.

Pressure distribution on wing of wing-body combination.- Experimental chordwise pressure distributions on the wing are shown in figures 5(g) to 5(n) for the four spanwise orifice stations $y/a = 1.25$, 1.92, 2.58, and 3.92. In front of the Mach cone from the wing-body juncture no interference is felt from the wing-body juncture so that the theoretical pressure distribution for a wing alone in the body upwash field is used in this region (see Appendix C). The theoretical results behind the Mach cone from the wing-body juncture (the region beyond point 2 in the figures) are not available because the $W_{2n}(x,r)$ functions for $r > a$ have not been calculated. Figures 5(g) to 5(n) show that, in general, the wing-alone theory predicts magnitudes of $\beta P/\alpha$ about 5 percent below the measurements for $\alpha = \pm 2^\circ$ for $M = 1.48$ and about 12 percent below the measurements for $M = 2.00$. The spread in the data between $\alpha = +6^\circ$ and $\alpha = -6^\circ$ is fairly well predicted by shock-expansion theory for y/a greater than about 1.5 (figs. 5(i) to 5(n)). At $y/a = 1.25$ the predicted spread is too large, just as was the case for the wing-body juncture.

Some of the interference effects discussed in the section of the report entitled "General Physical Principles" are illustrated in figures 5(g) to 5(n). The interference effect from the opposite wing panel is observed in figure 5(g) where, just in front of point 1, the same spread

[4]The possibility that this large pressure coefficient was due to body crossflow was considered by including the second-order terms in Bernoulli's equation in the calculation of the body-alone pressure coefficients, but this predicted only a small part of the observed values.

in the data occurs as in the wing-body juncture. According to linear theory the disturbance originating at the nearer wing-body juncture should be felt at point 2 of figures 5(i) to 5(m), and the magnitude of $\beta P/\alpha$ should begin to decrease from the wing-alone value there. These figures show that the magnitude of $\beta P/\alpha$ does decrease in the neighborhood of point 2. They also show that, in general, the $\alpha = +6^\circ$ and the $\alpha = -6^\circ$ data converge in the neighborhood of point 2. This convergence is due to a variation in the local Mach number with α. This is shown by the sketch in figure 5(j) where the disturbance from the wing-body juncture is first felt at point 3 for $\alpha = -6^\circ$, whereas it is first felt at point 4 for $\alpha = +6^\circ$. Since the magnitude of $\beta P/\alpha$ begins to decrease as soon as this disturbance is felt, the magnitude of $\beta P/\alpha$ begins to decrease at a smaller value of $x/\beta a$ for $\alpha = -6^\circ$ than for $\alpha = +6^\circ$, thus causing the convergence observed. The sketches in figures 5(k) and 5(m) show that the disturbance from the wing tip should also cause the $\alpha = +6^\circ$ and $\alpha = -6^\circ$ data to converge beyond point 6 in these figures. The figures show that the data not only converge but actually cross over and reverse order just beyond point 6.

The only significant effect of Mach number shown by figures 5(g) to 5(n) is the approximately 10-percent-larger values of $\beta P/\alpha$ for $M = 2.00$ than for $M = 1.48$. Nearly 40 percent of this difference may be due to differences in stream angle in the wind tunnel for the two Mach numbers.

Span loading distribution.- Span loading is defined for both the body and the wing as the integral

$$-\int_0^{c/\beta a} \left[\left(\frac{\beta P}{\alpha} \right)_L + \left(\frac{\beta P}{\alpha} \right)_U \right] d\left(\frac{x}{\beta a} \right)$$

The experimental results for the span loading distribution on the wing and body of the combination are presented in figure 6 and a comparison is made with theory on the body. As has been mentioned, the theoretical results on the wing in the interference region between the body and point 1 were not available for the α case at the time this paper was written. The theoretical pressure-distribution curves shown beyond point 1 are those of a wing alone with no body upwash present since outboard of this point its effect is small. The decrease in span loading beyond point 2 due to wing-tip interference is calculated by Busemann theory, reference 13. Figure 6 shows that theory, on the average, predicts the experimental span loading on the body within 10 percent. Of particular interest is the fact that, in general, the higher-order differences due to α that were so large for the pressure-distribution results are negligible for the span loading distribution. The only exception is on the top of the body, $y/a = 0$, at $M = 2.00$ where the effects of boundary-layer and shock-wave interaction are large. The explanation for the independence from α is

that the higher-order effects on the top surface are compensated for by higher-order effects of the same magnitude on the lower surface so that the net loading per unit angle is very nearly independent of angle of attack.

The theoretical span loading distribution shown in figure 6(b) can be applied to wings of higher aspect ratio by simply translating the tip solution shown beyond point 2 to the tip of the wing. The span loading will have the two-dimensional value of a wing alone between points 1 and 2. When the interference from the body and wing tip overlaps as in figure 6(a), the effects of these two factors must first be separated before translating the tip solution.

Effect of Wing-Incidence Angle

Comparison is made between theory and experiment for the wing-incidence case for data taken at a Reynolds number of 1.5×10^6 and Mach numbers of 1.48 and 2.00 with $\alpha = 0^\circ$ and $i_W = -1.9^\circ$ and -5.7°. It will be remembered from the section on the accuracy of data that there is no appreciable error due to stream angle for the wing-incidence case.

Pressure distribution in wing-body junctures.- The linear theory and experimental pressure distributions in the wing-body juncture are compared in figures 7(a) and 7(b). The symbols in the figures are flagged to be consistent with the use of flagged symbols for negative angle-of-attack data. The figures show that the experimental values are about 5 percent below those predicted by the theory for $i_W = -1.9^\circ$. The magnitude of the nonlinear effects due to i_W is predicted at the leading edge by shock-expansion theory. Figures 7(a) and 7(b) show that the spread predicted in this manner is in good accord with the experimental results. The premature increase in the magnitude of $\beta P/i_W$ near point 1 is due to the effect of the opposite wing panel and variation of the local Mach number as discussed in the angle-of-attack section. No significant effect of Mach number was found on the parameter $\beta P/i_W$.

Pressure distribution on top meridian of body of wing-body combination.- A comparison between the linear theory and experiment for the pressure distribution on the top meridian of the body is made in figures 7(c) and 7(d). These figures show that theory and experiment are in good accord for $i_W = -1.9^\circ$. However, nonlinear effects due to i_W cause much larger differences between theory and experiment for $i_W = -5.7^\circ$. This is consistent with the angle-of-attack case where the higher-order effect due to α was large for negative angles of attack.

All of the effects observed for the angle-of-attack case due to disturbances from the wing are also shown to occur for the wing-incidence case in figures 7(c) and 7(d). The paths of these disturbances as predicted by linear theory are shown on the sketch and the positions at which the effects are expected to occur are shown on the abscissa.

The only significant effect of Mach number apparent in figures 7(c) and 7(d) is the larger boundary-layer and shock-wave interaction for $M = 2.00$ than for $M = 1.48$ near point 1. The $M = 2.00$ experimental data for $i_W = -1.9^\circ$ dip and then overshoot at this point. This phenomenon is discussed in more detail in the section of the report on Reynolds number effect.

Pressure distribution on $\theta = 45^\circ$ meridian of body of wing-body combination.- Linear theory is compared with experimental results for the pressure distribution on the $\theta = 45^\circ$ meridian of the body of the combination in figures 7(e) and 7(f). The effects shown by the figure are consistent with those shown for the angle-of-attack case and for the wing-incidence case on the top meridian of the body. No unusual effects are observed.

Pressure distribution on wing of wing-body combination.- A comparison between linear theory and experiment for the pressure distribution along several spanwise stations is made in figures 7(g) to 7(n). The theoretical values behind the Mach wave were obtained directly from reference 7. These values were calculated by essentially the same method used in the present report, but without the aid of the $W_{2n}(x,r)$ functions. The experimental data (figs. 7(k) and 7(l)) show that, in general, $\beta P/i_W$ for the $i_W = -1.9^\circ$ data is constant and nearly equal to -2 in front of the Mach cone. Behind the Mach cone the theory generally predicts values about 5 percent above the experimental data for $i_W = -1.9^\circ$. The higher-order effects due to i_W cause larger differences between linear theory and experiment for $i_W = -5.7^\circ$. The figures show that these differences are well predicted by shock-expansion theory. The effects due to the influence of the Mach waves are the same as those discussed for the angle-of-attack case. There is no effect of Mach number evident on the wing of the wing-body combination other than that predicted by linear theory.

Span loading distribution.- A comparison between the theoretical and experimental results for span loading distribution on the wing and body of the combination is made in figure 8 for $i_W = -1.9^\circ$. The decrease in the span loading due to the wing tip was calculated by the method of Busemann (ref. 13). In part (a) of figure 8, interference from both the body and the wing tip is felt between points 1 and 2, but in part (b) no interference is felt between points 1 and 2, and the span loading is that of a two-dimensional wing alone.

Figure 8 shows that, in general, the experiment is 5 percent lower than the linear-theory prediction. Since all pressure measurements for the wing-incidence case were made for negative values of i_W, the experimental values used in this figure were obtained by doubling the values of $\beta P/i_W$ obtained for $i_W = -1.9^\circ$ rather than by considering two surfaces as for the angle-of-attack case. Since this increases the nonlinear effects of i_W rather than minimizing them, only the $i_W = -1.9^\circ$ data (for which the nonlinear effects are small) were plotted. However, the method of references 6 and 7 is applicable to the prediction of the net

span loading for larger values of i_W because the nonlinear effects on the upper and lower surfaces tend to cancel each other, as shown for the angle-of-attack case.

Effect of Reynolds Number

The primary effect of Reynolds number in this investigation was on the body. Reynolds number was found to have no significant effect on the pressure distribution on the wing of the combination for the range investigated. Figure 9 shows the boundary-layer condition, as observed in schlieren pictures, on top of the body at the point of intersection with the Mach wave from the leading edge of the wing-body juncture for $R = 0.6$ and 1.5×10^6. The transition and separation regions shown in figure 9 indicate approximately the ranges of α and i_W in which the boundary layer changes from laminar to turbulent or separated flow at the Mach wave from the wing-body juncture. In laminar and turbulent regions the flow remains laminar or turbulent across the Mach wave. Some of the Reynolds number effect shown by figure 9 may be due to changes in the turbulence level of the wind tunnel.

It is to be expected that data obtained for several angle combinations within any one of the regions shown in figure 9 would show no significant differences due to viscous effects, but that these data would differ from data in other regions. For example, for $M = 1.48$ and $R = 0.6 \times 10^6$ the data for $\alpha = -2^\circ$ with $i_W = 0^\circ$ should differ from the data for $\alpha = -6^\circ$ with $i_W = 0^\circ$ because transition occurs at the shock wave for the latter case but not for the former. That there is a difference is shown in figure 10 where the pressure distributions on top of the body for these two conditions are compared. In front of the shock wave the flow is laminar for both angles of attack so that there is no difference in the two sets of data. However, for $\alpha = -6^\circ$ transition occurs at the shock wave and the pressure rises as predicted, while for $\alpha = -2^\circ$ laminar flow persists behind the point at which the shock is expected and the pressure rise occurs much later than predicted. In fact, the pressure rise does not occur until the transition point shown in the figure is reached and then it tends to overshoot. This phenomenon of the delayed pressure rise was observed to occur whenever laminar flow persisted beyond the point at which a shock wave from the wing was predicted to exist. When the disturbance from the wing is an expansion wave, the pressure-coefficient curves rise approximately as predicted, regardless of the type of boundary layer. The conditions for which this delayed pressure rise was observed to occur are shown by the dotted areas in figure 9. Two other examples of this phenomenon may be seen near points 1 of figures 5(d) and 7(d) for $\alpha = -2^\circ$, $i_W = 0^\circ$ and $\alpha = 0^\circ$, $i_W = -2^\circ$, respectively.

In figure 11, the pressure distributions on top of the body are compared for three Reynolds numbers. It is shown that data for the two highest Reynolds numbers, R = 1.2 and 1.5×10^6, agree almost identically, while the data for the lowest Reynolds number differ considerably.

Comparison With Theory From Other Sources

The three theories for which numerical results are available are compared in figure 12. The theory due to Ferrari was obtained by cross-plotting from a figure in reference 8 so that the curve shown is only approximate. The theoretical curve due to Morikawa is obtained from tabulated results given in reference 4. The experimental data region was determined by the extreme values obtained for $\alpha = \pm 2^\circ$ for Mach numbers 1.48 and 2.00. From this figure it appears that either the theory of Morikawa or the theory of Nielsen may be used to predict the pressure distribution on the wing of a wing-body combination. Ferrari's theory predicts values that are somewhat low at the leading edge of the wing, but it appears that if numerical results were available beyond $x/\beta a = 0.7$, they would lie within the experimental range. For a more complete comparison of the theories of Ferrari and Nielsen, see references 1 and 2. Except for Nielsen's theory, no numerical results for the pressure distribution on the body were available for comparison.

CONCLUSIONS

An experimental investigation was made of the effects of angle of attack, α, wing-incidence angle, i_W, Mach number, and Reynolds number on the pressure distribution on a rectangular-wing and cylindrical-body combination. The Mach numbers were 1.48 and 2.00; the Reynolds numbers were 0.6, 1.2, and 1.5×10^6; α ranged from $+6^\circ$ to -6° in 2° increments; and i_W ranged from 0° to -5.7° in 1.9° increments. On the basis of comparisons made between the results of this investigation and the theory of NACA TN 2677, the following conclusions can be drawn:

1. The theory of NACA TN 2677, in general, predicts the pressure coefficients within ± 10 percent for values of α and i_W between $+2^\circ$ and -2°. For the wing-incidence case, $\alpha = 0^\circ$, the theory predicts magnitudes of pressure coefficient above the experimental values. For the angle-of-attack case, $i_W = 0^\circ$, the theory predicts magnitudes of pressure coefficient below the experimental values.

2. Nonlinear effects due to angle of attack and wing-incidence angle are large. On the wing the difference from linear theory due to nonlinear effects of angle can be predicted by shock-expansion theory, except near the wing-body juncture for the angle-of-attack case.

3. Span loading was shown to be predicted within ±10 percent for the wing-incidence case for all measured values of i_w on both the body and the wing. Where comparison was possible, span loading in the angle-of-attack case was also found to be predicted within ±10 percent. The predicted span loadings are high for the wing-incidence case and low for the angle-of-attack case.

4. For the angle-of-attack case, the pressure coefficients on the wing are experimentally about 5 percent higher for $M = 2.00$ than for $M = 1.48$, when reduced to a form that is theoretically independent of Mach number. Otherwise Mach number has no important effect.

5. Viscous effects are important only on the body where the shock wave from the wing causes large boundary-layer and shock-wave interactions for some angle conditions.

Ames Aeronautical Laboratory
National Advisory Committee for Aeronautics
Moffett Field, Calif., Jan. 4, 1954

APPENDIX A

DETERMINATION OF WING-ALONE POTENTIAL FOR ANGLE-OF-ATTACK CASE

The first step in determining the potential for the wing alone is to set up a mathematical model. Since the exposed wing of the combination operates in the body upwash field which effectively twists the wing, the wing-alone model[5] is considered to be twisted in the manner predicted by Beskin upwash theory for $y \geq a$

$$\alpha_W = \alpha \left(1 + \frac{a^2}{y^2} \right) = \alpha \left(1 + \frac{1}{y^2} \right) \tag{A1}$$

The concealed wing may be extended through the body region in any manner but, since equation (A1) gives $\alpha_W = 2\alpha$ at both wing-body junctures, it is taken as a flat plate at angle of attack 2α (see fig. 13).

The twisting of the wing is accomplished by superimposing a series of flat-plate wings upon a basic flat-plate wing at $\alpha_W = 2\alpha$ (see fig. 14). Each of the superimposed wings is at an incremental angle of attack and each successive wing terminates at an incremental value of y greater than the previous one. As these incremental values of α and y become infinitesimally small, the resulting potential approaches that of a wing with the twist defined by equation (A1).

For the purposes of determining the wing-alone potential, the wing is considered to be composed of the three parts shown in figure 13: the right exposed half-wing, the left exposed half-wing, and the wing section inside the body. The perturbation velocity potential is determined for each of these wing sections and the results added together to obtain the potential for the entire wing alone. Thus,

$$\varphi_W = \varphi_{W_R} + \varphi_{W_L} + \varphi_{W_B} \tag{A2}$$

Since the wing may be considered to be composed of an infinite number of flat, rectangular wings, the expression

$$\varphi(\alpha_W, y) = \frac{V\alpha_W}{\pi} \left(- x \cos^{-1} \frac{-y}{\sqrt{x^2 - z^2}} - y \cosh^{-1} \frac{x}{\sqrt{y^2+z^2}} + z \cos^{-1} \frac{-xy}{\sqrt{y^2+z^2}\sqrt{x^2-z^2}} \right) \tag{A3}$$

[5]Both a and β are taken as unity. See Theoretical Considerations section of text for method of generalization to other values of these parameters.

from reference 14 for the velocity potential of a flat, rectangular wing will be used as the basic relation for the calculations. Equation (A3) gives the velocity potential at any point (x,y,z) due to a flat, rectangular wing at angle of attack α_W, terminating at $y = 0$, and extending to ∞ along the positive y axis.

Since the twisted wing was shown to be equivalent to a basic flat-plate wing at angle of attack 2α plus an infinite number of modifying flat-plate wings, the potential of the right half-wing may be written as

$$\varphi_{W_R} = \varphi(2\alpha, y-1) + \Sigma_i \varphi(\Delta\alpha_i, y-\eta_i) \tag{A4}$$

The first term on the right in equation (A4) is the potential due to the basic exposed half-wing which terminates at the wing-body juncture, $y = 1$, and is at angle of attack 2α. The second term is the potential of the i modifying wings each at angle of attack $\Delta\alpha_i$ and terminating at $y = \eta_i$ where $1 < \eta_i \leq \infty$. Since equation (A3) is homogeneous with respect to α, equation (A4) may be written

$$\varphi_{W_R} = \varphi(2\alpha, y-1) + \Sigma_i \varphi(1, y-\eta_i)\Delta\alpha_i \tag{A5}$$

From equation (A1)

$$d\alpha_W = -\frac{2\alpha}{y^3}\, dy \tag{A6}$$

Therefore,

$$\varphi_{W_R} = \varphi(2\alpha, y-1) - 2\alpha \int_1^{\eta_u} \varphi(1, y-\eta)\, \frac{d\eta}{\eta^3} \tag{A7}$$

where the limits of integration are determined by the range of y on the wing included in the fore Mach cone originating from the point for which φ_{W_R} is being determined. From figure 15 it is apparent from the equation of the fore Mach cone emanating from the arbitrary point P_1 for $\beta = 1$ that

$$x_1^2 = z_1^2 + (\eta_u - y_1)^2$$

Therefore, the upper limit of integration is

$$\eta_u = y_1 + \sqrt{x_1^2 - z_1^2} \tag{A8}$$

The lower limit of integration is at the wing-body juncture, $y = 1$. From equations (A3), (A7), and (A8)

$$\varphi_{W_R} = \text{R.P.}\left\{\frac{2V\alpha}{\pi}\left[-x\cos^{-1}\frac{-(y-1)}{\sqrt{x^2-z^2}} - (y-1)\cosh^{-1}\frac{x}{\sqrt{(y-1)^2+z^2}} + z\cos^{-1}\frac{-x(y-1)}{\sqrt{(y-1)^2+z^2}\sqrt{x^2-z^2}}\right] - \frac{2V\alpha}{\pi}\int_1^{y+\sqrt{x^2-z^2}}\left[-x\cos^{-1}\frac{-(y-\eta)}{\sqrt{x^2-z^2}} - (y-\eta)\cosh^{-1}\frac{x}{\sqrt{(y-\eta)^2+z^2}} + z\cos^{-1}\frac{-x(y-\eta)}{\sqrt{(y-\eta)^2+z^2}\sqrt{x^2-z^2}}\right]\frac{d\eta}{\eta^3}\right\} \tag{A9}$$

Carrying out the integration and combining terms gives

$$\varphi_{W_R} = \text{R.P.}\left\{\frac{V\alpha}{\pi}\left[-x\cos^{-1}\frac{-(y-1)}{\sqrt{x^2-z^2}} + \left(\frac{y}{y^2+z^2} - y\right)\cosh^{-1}\frac{x}{\sqrt{(y-1)^2+z^2}} - \frac{xy}{(y^2+z^2)\sqrt{x^2-y^2-z^2}}\cosh^{-1}\frac{x^2-y(y-1)-z^2}{\sqrt{x^2-z^2}} + \left(z+\frac{z}{y^2+z^2}\right)\cos^{-1}\frac{-x(y-1)}{\sqrt{(y-1)^2+z^2}\sqrt{x^2-z^2}}\right]\right\} \tag{A10}$$

Equation (A10) gives the potential due to the exposed right half-wing. To this must be added the potentials due to the other two wing sections. The potential due to the section of the wing in the body region is simply the difference between the potentials of two flat wings at $\alpha_W = 2\alpha$. One of these wings terminates at the wing-body juncture at $y = -1$, figure 13, and extends (through the body) indefinitely in the positive direction. The other wing terminates at the other wing-body juncture, $y = +1$, and also extends indefinitely in the positive y direction. The difference between the potentials of these two wings is the potential of the wing section in the body

$$\varphi_{W_B} = \varphi(2\alpha, y+1) - \varphi(2\alpha, y-1) \tag{A11}$$

The expression for $\varphi(\alpha_W, y)$ is given by equation (A3). Since the model is symmetrical about the vertical $y = 0$ plane, the potential for the other half-wing is simply obtained by replacing y by $-y$ in equation (A10).

$$\varphi_{W_L} = \varphi_{W_R}(x, -y, z) \tag{A12}$$

Combining equations (A10), (A11), and (A12) gives the potential due to the entire wing alone.

$$\varphi_W = \text{R.P.}\,\frac{V\alpha}{\pi}\left[x\left(\cos^{-1}\frac{1-y}{\sqrt{x^2-z^2}} + \cos^{-1}\frac{1+y}{\sqrt{x^2-z^2}}\right)+ \right.$$

$$\left(\frac{y}{y^2+z^2} + y-2\right)\cosh^{-1}\frac{x}{\sqrt{(y-1)^2+z^2}} - \left(\frac{y}{y^2+z^2}+y+2\right)\cosh^{-1}\frac{x}{\sqrt{(y+1)^2+z^2}} +$$

$$\left(\frac{z}{y^2+z^2} - z\right)\left(\cos^{-1}\frac{-x(y-1)}{\sqrt{(y-1)^2+z^2}\sqrt{x^2-z^2}} + \cos^{-1}\frac{x(y+1)}{\sqrt{(y+1)^2+z^2}\sqrt{x^2-z^2}}\right)+$$

$$\left.\frac{xy}{(y^2+z^2)\sqrt{x^2-y^2-z^2}}\left(\cosh^{-1}\frac{x^2-y(y+1)-z^2}{\sqrt{x^2-z^2}} - \cosh^{-1}\frac{x^2-y(y-1)-z^2}{\sqrt{x^2-z^2}}\right) +2\pi(z-x)\right] \tag{A13}$$

Investigation of φ_W as given by equation (A13) reveals that there are three regions on the body in which the real part of this expression differs. A fourth region, region IV, is entirely on the wing and is, therefore, not necessary for determining the normal velocity distribution on the body. These regions are determined by three characteristic Mach cones. One of the Mach cones originates on the body axis at $x = 0$, and the other two originate at the leading edges of the two wing-body junctures (see fig. 16). The expressions for the real part of φ_W in the three regions on the body are:

Region I:

$$\varphi_W = -\frac{V\alpha}{\pi}\left[-x\left(\cos^{-1}\frac{-(y-1)}{\sqrt{x^2-z^2}} + \cos^{-1}\frac{(y+1)}{\sqrt{x^2-z^2}}\right) - \left(\frac{y}{y^2+z^2}+y-2\right)\cosh^{-1}\frac{x}{\sqrt{(y-1)^2+z^2}} +\right.$$

$$\left(\frac{y}{y^2+z^2}+y+2\right)\cosh^{-1}\frac{x}{\sqrt{(y+1)^2+z^2}} + \left(z-\frac{z}{y^2+z^2}\right)\left(\cos^{-1}\frac{-x(y-1)}{\sqrt{(y-1)^2+z^2}\sqrt{x^2-z^2}}+\right.$$

$$\left.\cos^{-1}\frac{x(y+1)}{\sqrt{(y+1)^2+z^2}\sqrt{x^2-z^2}}\right)+\frac{xy}{(y^2+z^2)\sqrt{x^2-y^2-z^2}}\left(\cosh^{-1}\frac{x^2-z^2-y(y-1)}{\sqrt{x^2-z^2}} -\right.$$

$$\left.\left.\cosh^{-1}\frac{x^2-z^2-y(y+1)}{\sqrt{x^2-z^2}}\right) -2(z-x)\pi\right] \tag{A14}$$

Region II:

$$\varphi_W = -\frac{V\alpha}{\pi}\left[-x\cos^{-1}\frac{-(y-1)}{\sqrt{x^2-z^2}} - \left(\frac{y}{y^2+z^2}+y-2\right)\cosh^{-1}\frac{x}{\sqrt{(y-1)^2+z^2}} - \left(\frac{z}{y^2+z^2}-z\right)\cos^{-1}\frac{-x(y-1)}{\sqrt{(y-1)^2+z^2}\sqrt{x^2-z^2}} + \frac{xy}{(y^2+z^2)\sqrt{x^2-y^2-z^2}}\cosh^{-1}\frac{x^2-z^2-y(y-1)}{\sqrt{x^2-z^2}} - 2(z-x)\pi\right] \tag{A15}$$

Region III:

$$\varphi_W = -\frac{V\alpha}{\pi}\left[-x\cos^{-1}\frac{-(y-1)}{\sqrt{x^2-z^2}} - \left(\frac{y}{y^2+z^2}+y-2\right)\cosh^{-1}\frac{x}{\sqrt{(y-1)^2+z^2}} - \left(\frac{z}{y^2+z^2}-z\right)\cos^{-1}\frac{-x(y-1)}{\sqrt{(y-1)^2+z^2}\sqrt{x^2-z^2}} + \frac{xy}{(y^2+z^2)\sqrt{y^2+z^2-x^2}}\cos^{-1}\frac{x^2-z^2-y(y-1)}{\sqrt{x^2-z^2}} - 2(z-x)\pi\right] \tag{A16}$$

APPENDIX B

DETERMINATION OF VELOCITY AMPLITUDE FUNCTIONS

The method of references 6 and 7 requires a Fourier series expansion of the expression for the normal velocity on the body surface. The coefficients, $f_{2n}(x)$, of the cosine terms in this series are called the velocity amplitude functions. The interference pressure coefficients are found directly from these functions, as will be shown in Appendix C.

The velocity normal to the body surface due to the wing alone is easily found from the wing-alone velocity potential by differentiation. The amplitudes of the Fourier series expansion of the normal velocity expression are obtained by the usual equation,

$$f_0(x) = \frac{2}{\pi}\int_0^{\sin^{-1}x}\left(\frac{\partial\varphi_W}{\partial r}\right)d\theta$$

$$f_{2n}(x) = \frac{4}{\pi}\int_0^{\sin^{-1}x}\left(\frac{\partial\varphi_W}{\partial r}\right)\cos(2n\theta)d\theta$$

The $f_{2n}(x)$ functions were obtained in closed form for the wing-incidence case, but the angle-of-attack case required the evaluation of untabulated elliptic integrals so that numerical methods had to be used to obtain $f_{2n}(x)$. The resulting $f_{2n}(x)$ functions are shown in figure 17. This figure shows that the curves of $\frac{f_{2n}(x)}{V\alpha}$ against x oscillate n times between $x = 0$ and $x = 1$ but for $x > 1$, $\frac{f_{2n}(x)}{V\alpha}$ ceases to oscillate and is nearly constant.

APPENDIX C

PRESSURE COEFFICIENTS OF THE WING-BODY COMBINATION FOR THE ANGLE-OF-ATTACK CASE

Determination of Interference Pressure Coefficients

The interference pressure coefficients are obtained directly from the velocity amplitude functions, $f_{2n}(x)$, using the universal functions $W_{2n}(x,r)$, developed in references 6 and 7. In references 6 and 7 it is shown that the interference pressure coefficients for $r = 1$ for each of the $f_{2n}(x)$ functions are

$$P_{2n} = \frac{2}{V}\cos 2n\theta\left[f_{2n}(x) - \int_0^x f_{2n}(\xi)W_{2n}(x-\xi,1)d\xi \right] \qquad (C1)$$

The integration operation requires graphical or numerical methods. The total interference pressure coefficient is the sum of the n components, P_{2n}. To get the exact linear-theory solution it would be necessary to compute an infinite number of terms, but in most cases using only four terms gives a close approximation to linear theory, as shown in reference 7 and verified by figures 18, 19, and 20. A relation similar to that of equation (C1) gives values of P_{2n} for r different from 1.

Pressure Distribution in Juncture of Wing-Body Combination

The pressure distribution of the combination is obtained by adding the interference pressure coefficients to the pressure coefficients of the wing along. The results, using four and six P_{2n} components, are shown in figure 18. This figure shows that four components give a close approximation to the linear-theory value for $x/\beta a > 1$. At $x/\beta a = 0$, the wing leading edge, linear theory using Beskin upwash gives exactly $\beta P/\alpha = -4.0$. For the region $x/\beta a < 1$ the higher harmonics have their greatest importance and many components would be necessary to get good accuracy. However, satisfactory accuracy can be obtained by fairing a curve through this region since both end points are known.

One point of interest in figure 18 is the increase in the magnitude of $\beta P/\alpha$ near point 1. This is due to the influence of the opposite half-wing reaching the wing-body juncture at this point as shown in the sketch.

Pressure Distribution on the Body of the Wing-Body Combination

The pressure distribution on the body is also obtained by adding the interference pressure coefficients to the pressure coefficients due

to the wing alone. The interference pressure distribution for any value of θ differs from that in the wing-body juncture, $\theta = 0$, only by the $\cos 2n\theta$ factor in equation (C1). For example, in the juncture, $\cos 2n\theta$ is always +1, on top of the body, $\theta = \pi/2$, $\cos 2n\theta$ alternates between +1 and -1 as n increases, and on the $\theta = \pi/4$ meridian $\cos 2n\theta$ has values of 0, +1, and -1 so that when n is odd, $P_{2n} = 0$. The pressure distributions on the top meridian of the body and on the $\theta = 45^\circ$ meridian of the body are shown in figures 19 and 20, respectively.

Several interesting effects are exhibited by figures 19 and 20. The step in the wing-alone pressure at $x/\beta a = 1$ in figure 19 is effectively canceled by the interference pressure from $x/\beta a = 1$ to $x/\beta a = \pi/2$ and for $x/\beta a > \pi/2$ the pressure increases rapidly. The effect of the interference pressure in canceling the effect of the wing alone on the top of the body from $x/\beta a = 1$ to $x/\beta a = \pi/2$ is to be expected since the wing of the combination can have no effect on the body in front of the Mach helix (point 1 of sketch) originating at the leading edge of the wing-body juncture. If an infinite number of components had been computed, the combination pressure coefficients would be identically zero from $x/\beta a = 0$ to $x/\beta a = \pi/2$. The same effects are exhibited by figure 20 except that the wing-alone step occurs at $x/\beta a = \sqrt{2}/2$ and the Mach helix intersects the meridian at $x/\beta a = \pi/4$, point 1. The Mach helix from the opposite wing panel intersects the meridian at point 2 causing an additional pressure rise. Since the region in which $\beta P/\alpha = 0$ is known and since the exact linear theory is well approximated by four components for large values of $x/\beta a$, theoretical curves of good accuracy can be faired from figures 19 and 20. The area under the high peaks in the curves near $x/\beta a = \pi/4$ would become infinitesimal if an infinite number of interference pressure components were taken.

Pressure Distributions for the Wing of Wing-Body Combinations

In region IV of figure 16, the calculation of pressure coefficients is just a wing-alone problem. The pressure coefficients in this region can therefore be obtained directly from the wing-alone potential as given by equation (A10). The result is

$$P = -2\alpha \left[1 + \frac{y}{(y^2 - x^2)^{3/2}} \right] \qquad (C2)$$

In the region behind the Mach cone the pressure coefficients can be obtained directly from the $W_{2n}(x,r)$ functions, as was done on the body.

The span loading distribution is determined by graphical integration of faired pressure-distribution curves of figures 18, 19, and 20. The pressure results of these figures are for $c/\beta a \leq 4$ and for $\beta A \geq 2$. Span loadings for any combination of $c/\beta a$ and βA in these ranges can be obtained from these pressure distributions. The theoretical and experimental span loading distributions on the body were evaluated back to the wing trailing edge.

For purposes of specifying the span loading, the following equation is used:

$$\left.\begin{aligned}\frac{L}{q_o a \alpha} &= \int_{-s}^{s}\left\{-\int_{o}^{c/\beta a}\left[\left(\frac{\beta P}{\alpha}\right)_L + \left(\frac{\beta P}{\alpha}\right)_U\right] d\left(\frac{x}{\beta a}\right)\right\} dy \\ &= \int_{-s}^{s}\left\{-\frac{1}{a}\int_{o}^{c}\left[\left(\frac{P}{\alpha}\right)_L + \left(\frac{P}{\alpha}\right)_U\right] dx\right\} dy\end{aligned}\right\} \qquad (C3)$$

The span loading is the quantity inside the bracket.

REFERENCES

1. Phinney, R. E.: Wing-Body Interference. Progress Rep. No. 4, University of Michigan, Eng. Res. Inst., 1952.

2. Lawrence, H. R., and Flax, A. H.: Wing-Body Interference at Subsonic and Supersonic Speeds. Survey and New Developments. Paper presented at the Annual Summer Meeting of the I.A.S., Los Angeles, July 15-17, 1953.

3. Ferrari, Carlo: Interference Between Wing and Body at Supersonic Speeds - Theory and Numerical Application. Jour. Aero. Sci., vol. 15, no. 6, June 1948, pp. 317-336.

4. Morikawa, George K.: The Wing-Body Problem for Linearized Supersonic Flow. Calif. Inst. of Tech. Doctoral Thesis, 1949. GALCIT, Jet Propulsion Lab. PR4-116.

5. Bolton Shaw, B. W.: Wing-Body Interference at Supersonic Speeds - Rectangular Wing at Incidence on a Body at Zero Incidence. English Electric Co. Rep. LA.t. 039.

6. Nielsen, Jack N.: Supersonic Wing-Body Interference. Calif. Inst. of Tech. Doctoral Thesis, 1951.

7. Nielsen, Jack N., and Pitts, William C.: Wing-Body Interference at Supersonic Speeds With an Application to Combinations With Rectangular Wings. NACA TN 2677, 1952.

8. Cramer, R. H.: Interference Between Wing and Body at Supersonic Speeds. Part V - Phase I Wind-Tunnel Tests Correlated With Linear Theory. Cornell Aero. Lab. Rep. No. CAL/CM-597, Dec. 1950.

9. Berler, Irving, and Nichols, Sidney: Interference Between Wing and Body at Supersonic Speeds. Part VI, Data Report. Pressure Distribution Tests of Wing-Body Interference Models at Mach Number of 2.0. Phase II, Tests of June 1949. Cornell Aero. Lab. Rep. No. CAL/CF-1569, May 1951.

10. Berler, Irving, and Nichols, Sidney: Interference Between Wing and Body at Supersonic Speeds. Part VII, Data Report. Pressure Distribution Tests of Wing-Body Interference Models at Mach Number of 2.0. Phase III, Tests of August 1949. Cornell Aero. Lab. Rep. No. CAL/CF-1570, June 1951.

11. Nichols, Sidney: Interference Between Wing and Body at Supersonic Speeds. Part VIII, Data Report. Pressure Distribution Tests of Wing-Body Interference Models at Mach Number of 2.0. Phase IV, Test of March 1950. Cornell Aero. Lab. Rep. No. CAL/CF-1571, July 1951.

12. Dye, Fulton E., Jr.: Interference Between Wing and Body at Supersonic Speeds. Part IX, Data Report. Pressure Distribution Tests of Wing-Body Interference Models at Mach Number of 2.0. Phase V, Test of August 1951. Cornell Aero. Lab. Rep. No. CAL/CF-1684, Dec. 1951.

13. Busemann, Adolf: Infinitesimal Conical Supersonic Flow. NACA TM 1100, 1947.

14. Nielsen, Jack N., and Matteson, Frederick H.: Calculative Method for Estimating the Interference Pressure Field at Zero Lift on a Symmetrical Swept-Back Wing Mounted on a Circular Cylindrical Body. NACA RM A9E19, 1949.

TABLE I.- ORIFICE LOCATIONS ON WING AND BODY OF WING-BODY COMBINATION

[Dimensions in inches measured from wing leading edge]

y/a = 1.020 (a)	y/a = 1.253	y/a = 1.916	y/a = 2.583	y/a = 3.916	$\theta = 90^\circ$	$\theta = 45^\circ$
0.400	0.400	- - -	0.400	- - -	-0.281	0.468
.775	.775	0.775	.775	- - -	.219	.968
1.150	1.150	1.150	1.150	1.150	.719	1.468
1.525	1.525	1.525	1.525	1.525	1.219	1.968
1.900	1.900	1.900	1.900	1.900	1.719	2.468
2.275	2.275	2.275	2.275	2.275	2.219	2.968
2.650	2.650	2.650	2.650	2.650	2.719	
					3.219	
					3.719	

[a] a = 0.75 inches

TABLE II.- PRESSURE COEFFICIENTS $\left(\frac{p-p_1}{q_0}\right)$

(a) M = 1.48, R = 1.5×10⁶

Station	$\frac{i_w}{x/c}$	α = -6°				α = -4°				α = -2°				α = 0°			α = 2°				α = 4°				α = 6°			
		-5.7°	-3.8°	-1.9°	0°	-5.7°	-3.8°	-1.9°	0°	-5.7°	-3.8°	-1.9°	0°	-5.7°	-3.8°	-1.9°	-5.7°	-3.8°	-1.9°	0°	-5.7°	-3.8°	-1.9°	0°	-5.7°	-3.8°	-1.9°	0°
y/s = 0.170	0.133	0.629	0.529	0.421	0.334	0.448	0.354	0.273	0.200	0.300	0.223	0.152	0.095	0.180	0.114	0.054	0.073	0.007	-0.046	-0.092	-0.046	-0.094	-0.139	-0.189	-0.143	-0.183	-0.229	-0.268
	.258	.480	.409	.329	.268	.361	.297	.229	.168	.256	.199	.132	.082	.156	.106	.051	.068	.019	-.032	-.075	-.019	-.064	-.109	-.153	-.098	-.134	-.181	-.221
	.383	.405	.354	.280	.232	.323	.253	.197	.149	.224	.169	.112	.072	.135	.088	.042	.058	.014	-.028	-.065	-.009	-.050	-.091	-.126	-.073	-.109	-.151	-.186
	.508	.406	.330	.266	.205	.307	.238	.187	.133	.211	.157	.112	.066	.129	.089	.046	.061	.020	-.017	-.058	.003	-.033	-.067	-.107	-.049	-.083	-.117	-.155
	.633	.442	.344	.270	.194	.322	.247	.176	.126	.223	.156	.104	.061	.133	.084	.042	.063	.022	-.016	-.055	.008	-.025	-.061	-.098	-.038	-.071	-.102	-.141
	.759	.432	.375	.296	.221	.351	.279	.201	.124	.262	.176	.109	.060	.155	.091	.043	.077	.030	-.013	-.052	.014	-.021	-.058	-.090	-.036	-.069	-.098	-.135
	.884	.409	.360	.297	.246	.345	.281	.232	.154	.266	.209	.125	.066	.188	.110	.046	.102	.034	-.010	-.051	.027	-.021	-.059	-.090	-.037	-.074	-.103	-.136
y/s = 0.208	.133	.579	.478	.390	.316	.434	.340	.261	.197	.307	.225	.146	.089	.177	.110	.054	.070	.007	-.043	-.092	-.047	-.094	-.147	-.196	-.145	-.193	-.238	-.272
	.258	.486	.412	.332	.266	.374	.298	.229	.174	.272	.202	.147	.095	.162	.102	.050	.072	.016	-.030	-.074	-.015	-.062	-.106	-.152	-.095	-.139	-.199	-.225
	.383	.419	.378	.293	.235	.343	.267	.205	.154	.249	.185	.128	.080	.150	.094	.043	.078	.021	-.021	-.065	-.002	-.046	-.081	-.118	-.069	-.099	-.147	-.185
	.508	.401	.334	.275	.207	.311	.247	.186	.136	.222	.166	.112	.071	.133	.083	.043	.064	.019	-.020	-.059	.005	-.034	-.072	-.111	-.050	-.084	-.127	-.165
	.633	.442	.351	.278	.209	.324	.258	.186	.134	.232	.161	.104	.069	.134	.086	.041	.068	.024	-.015	-.053	.015	-.025	-.062	-.098	-.036	-.072	-.109	-.149
	.759	.431	.371	.301	.232	.354	.288	.213	.138	.266	.187	.106	.066	.160	.094	.042	.081	.028	-.013	-.051	.018	-.023	-.059	-.095	-.033	-.070	-.102	-.137
	.884	.404	.355	.296	.250	.339	.280	.231	.166	.261	.206	.136	.071	.190	.119	.047	.102	.034	-.014	-.053	.024	-.023	-.062	-.100	-.036	-.075	-.105	-.139
y/s = 0.319	.258	.503	.432	.355	.282	.400	.319	.250	.180	.297	.224	.152	.092	.197	.127	.063	.089	.020	-.038	-.091	-.012	-.066	-.112	-.160	-.092	-.136	-.186	-.227
	.383	.437	.384	.315	.244	.364	.284	.220	.156	.262	.195	.133	.079	.172	.111	.056	.088	.025	-.038	-.081	-.002	-.058	-.109	-.162	-.088	-.138	-.192	-.234
	.508	.392	.345	.302	.224	.331	.274	.207	.144	.251	.180	.122	.071	.159	.102	.051	.085	.028	-.021	-.068	.012	-.039	-.086	-.134	-.060	-.107	-.157	-.202
	.633	.414	.314	.275	.223	.301	.257	.210	.140	.241	.179	.120	.066	.160	.099	.052	.087	.033	-.010	-.059	.032	-.034	-.070	-.113	-.039	-.085	-.133	-.179
	.759	.412	.328	.247	.204	.306	.255	.194	.143	.224	.176	.123	.066	.159	.105	.051	.088	.041	-.007	-.056	.034	-.014	-.059	-.101	-.025	-.068	-.101	-.138
	.884	.380	.323	.254	.189	.305	.231	.176	.123	.216	.159	.113	.066	.142	.096	.055	.089	.043	-.007	-.056	.031	-.016	-.059	-.095	-.036	-.058	-.092	-.140
y/s = 0.431	.133	.639	.539	.411	.285	.500	.365	.253	.167	.337	.236	.148	.078	.216	.135	.065	.116	.040	-.018	-.076	.020	-.039	-.094	-.142	-.062	-.114	-.161	-.208
	.258	.537	.476	.382	.297	.451	.354	.270	.181	.335	.246	.153	.083	.217	.135	.064	.109	.037	-.021	-.076	.014	-.043	-.097	-.144	-.069	-.118	-.161	-.209
	.383	.456	.413	.358	.266	.395	.328	.245	.170	.304	.224	.150	.085	.201	.129	.062	.099	.032	-.026	-.079	.010	-.047	-.099	-.147	-.073	-.122	-.167	-.213
	.508	.400	.364	.323	.265	.338	.308	.245	.165	.289	.221	.144	.082	.198	.123	.061	.106	.034	-.027	-.065	.010	-.051	-.102	-.150	-.071	-.120	-.170	-.211
	.633	.366	.311	.269	.229	.294	.260	.221	.162	.244	.204	.144	.080	.182	.124	.062	.114	.043	-.015	-.069	.030	-.031	-.085	-.135	-.048	-.102	-.154	-.206
	.759	.366	.266	.216	.177	.247	.206	.171	.134	.190	.157	.117	.071	.136	.099	.058	.090	.040	-.012	-.063	.029	-.026	-.080	-.128	-.046	-.101	-.154	-.202
	.884	.354	.290	.194	.146	.254	.181	.140	.101	.166	.126	.091	.056	.109	.075	.043	.068	.030	-.010	-.059	.026	-.013	-.064	-.133	-.015	-.063	-.127	-.177
y/s = 0.652	.383	.451	.406	.357	.280	.396	.339	.258	.188	.320	.239	.160	.088	.227	.150	.068	.137	.055	-.013	-.072	.046	-.021	-.083	-.144	-.055	-.093	-.143	-.195
	.508	.358	.313	.274	.227	.306	.263	.211	.148	.249	.195	.128	.072	.178	.117	.057	.105	.045	-.014	-.071	.028	-.028	-.084	-.140	-.047	-.096	-.148	-.197
	.633	.305	.263	.224	.185	.254	.212	.171	.124	.204	.157	.108	.064	.145	.096	.045	.079	.028	-.017	-.059	.012	-.032	-.076	-.120	-.048	-.087	-.135	-.184
	.759	.285	.226	.189	.154	.217	.178	.142	.105	.170	.129	.088	.052	.118	.078	.037	.062	.019	-.020	-.054	.003	-.033	-.069	-.104	-.049	-.082	-.118	-.149
	.884	.310	.206	.164	.133	.195	.155	.122	.091	.147	.111	.076	.047	.100	.066	.031	.053	.015	-.020	-.052	-.001	-.033	-.066	-.080	-.048	-.079	-.094	-.099
θ = 90°	-.094	.011	.012	.011	.012	.002	.001	.002	.001	.002	.001	.002	.003	-.002	0	0	-.003	-.002	-.002	0	.001	.002	.003	.003	.006	.008	.009	.008
	.073	.012	.002	.001	.002	.001	-.002	-.001	-.006	.002	.001	.002	.003	-.003	-.001	0	-.004	-.002	-.002	-.001	.001	.007	.003	.003	.012	.013	.013	.013
	.240	.088	.058	.035	.005	.043	.030	.015	.003	.020	.009	.005	.005	.010	.002	.001	.004	.002	-.001	-.001	.004	.003	.003	.003	.010	.009	.011	.026
	.410	.460	.345	.068	.031	.318	.139	.076	.033	.198	.115	.054	.021	.109	.056	.020	.041	.007	-.013	-.028	-.005	-.023	-.032	-.034	-.036	-.046	-.045	-.046
	.573	.469	.405	.314	.255	.384	.284	.210	.144	.250	.174	.110	.062	.150	.091	.040	.074	.021	-.020	-.050	.006	-.035	-.068	-.086	-.074	-.087	-.111	-.126
	.740	.445	.393	.334	.236	.381	.308	.211	.157	.278	.186	.119	.070	.168	.102	.048	.087	.030	-.017	-.058	.017	-.031	-.074	-.107	-.049	-.091	-.131	-.162
	.906	.411	.368	.324	.259	.356	.308	.232	.147	.288	.212	.152	.089	.197	.110	.049	.103	.036	-.015	-.059	.026	-.026	-.072	-.111	-.041	-.086	-.130	-.169
	1.073	.346	.323	.293	.265	.306	.278	.242	.178	.248	.214	.148	.070	.189	.134	.054	.124	.045	-.013	-.059	.037	-.021	-.070	-.114	-.035	-.081	-.125	-.168
	1.240	.179	.201	.214	.218	.157	.173	.176	.172	.198	.134	.129	.099	.091	.094	.069	.060	.045	-.011	-.064	.018	-.026	-.075	-.116	-.050	-.091	-.124	-.168
θ = 45°	.156	.296	.136	.025	.010	.096	.028	.045	.010	.066	.044	.025	.009	.062	.032	.012	.018	-.001	-.011	-.014	-.013	-.019	-.017	-.014	-.032	-.041	-.045	-.026
	.323	.307	.301	.250	.207	.277	.289	.167	.131	.192	.141	.086	.042	.106	.071	.033	.045	.009	-.023	-.050	-.008	-.043	-.073	-.098	-.064	-.095	-.122	-.145
	.489	.456	.334	.238	.192	.312	.224	.163	.128	.213	.150	.102	.069	.118	.076	.037	.057	.018	-.017	-.054	.006	-.033	-.069	-.092	-.047	-.083	-.112	-.145
	.696	.458	.385	.311	.209	.365	.289	.186	.124	.258	.170	.110	.067	.142	.087	.041	.071	.024	-.017	-.053	.011	-.028	-.063	-.097	-.045	-.080	-.112	-.149
	.823	.422	.374	.315	.260	.356	.298	.228	.151	.273	.208	.117	.070	.178	.100	.046	.085	.029	-.015	-.056	.016	-.028	-.067	-.104	-.046	-.083	-.118	-.156
	.990	.369	.361	.298	.248	.317	.278	.227	.185	.255	.209	.148	.074	.189	.133	.058	.119	.038	-.015	-.056	.027	-.025	-.069	-.111	-.046	-.087	-.121	-.160

TABLE II.- PRESSURE COEFFICIENTS $\left(\frac{p-p_1}{q_0}\right)$ - Continued

(b) M = 1.48, R = 1.2×10^6

Station	$\frac{l_y}{c}$ / x/c	α = -6°				α = -4°				α = -2°				α = 0°			α = 2°				α = 4°				α = 6°			
		-5.7°	-3.8°	-1.9°	0°	-5.7°	-3.8°	-1.9°	0°	-5.7°	-3.8°	-1.9°	0°	-5.7°	-3.8°	-1.9°	-5.7°	-3.8°	-1.9°	0°	-5.7°	-3.8°	-1.9°	0°	-5.7°	-3.8°	-1.9°	0°
y/s = 0.170	0.133	0.682	0.510	0.411	0.335	0.453	0.358	0.274	0.209	0.297	0.222	0.151	0.096	0.180	0.113	0.051	0.070	0.001	-0.046	-0.093	-0.048	-0.093	-0.136	-0.178	-0.151	-0.186	-0.231	-0.270
	.258	.475	.404	.322	.262	.363	.295	.230	.174	.255	.199	.132	.081	.157	.105	.048	.075	.017	-.034	-.078	-.023	-.064	-.109	-.150	-.098	-.138	-.182	-.224
	.383	.405	.356	.277	.230	.328	.255	.198	.156	.222	.170	.114	.074	.134	.087	.041	.064	.015	-.029	-.068	-.018	-.055	-.095	-.137	-.071	-.111	-.153	-.184
	.508	.415	.333	.272	.205	.317	.244	.188	.140	.214	.161	.114	.067	.128	.084	.045	.063	.019	-.017	-.059	.003	-.037	-.070	-.114	-.048	-.088	-.130	-.156
	.633	.446	.351	.281	.203	.335	.259	.182	.134	.231	.161	.109	.064	.131	.083	.040	.066	.023	-.013	-.053	.011	-.024	-.058	-.097	-.033	-.065	-.101	-.137
	.759	.434	.375	.299	.236	.352	.282	.209	.137	.263	.184	.110	.063	.160	.092	.042	.080	.031	-.010	-.050	.019	-.019	-.054	-.093	-.029	-.064	-.095	-.128
	.884	.409	.360	.299	.248	.344	.282	.232	.174	.263	.209	.136	.070	.191	.118	.043	.109	.088	-.008	-.049	.030	-.016	-.055	-.092	-.031	-.071	-.101	-.130
y/s = 0.208	.133	.580	.478	.389	.317	.442	.344	.270	.206	.303	.223	.149	.089	.181	.112	.053	.061	.002	-.047	-.100	-.049	-.098	-.146	-.195	-.155	-.191	-.240	-.280
	.258	.485	.409	.329	.264	.377	.296	.230	.176	.267	.202	.138	.083	.165	.106	.049	.072	.017	-.033	-.080	-.021	-.067	-.111	-.159	-.103	-.143	-.195	-.239
	.383	.424	.373	.298	.232	.350	.266	.206	.155	.244	.182	.129	.077	.148	.098	.045	.077	.022	-.024	-.067	-.005	-.050	-.088	-.128	-.070	-.107	-.148	-.190
	.508	.409	.344	.287	.217	.326	.253	.195	.146	.226	.169	.118	.070	.134	.088	.043	.071	.023	-.014	-.057	.006	-.034	-.074	-.116	-.044	-.083	-.126	-.164
	.633	.441	.350	.287	.222	.309	.263	.195	.143	.231	.166	.111	.068	.134	.084	.040	.070	.023	-.012	-.053	.014	-.025	-.062	-.101	-.032	-.072	-.110	-.147
	.759	.432	.372	.300	.240	.352	.287	.215	.151	.262	.192	.114	.067	.162	.095	.041	.082	.027	-.012	-.051	.021	-.021	-.057	-.094	-.028	-.067	-.101	-.134
	.884	.405	.355	.295	.248	.340	.278	.227	.174	.261	.208	.143	.076	.191	.119	.050	.108	.037	-.011	-.052	.030	-.020	-.057	-.095	-.029	-.071	-.104	-.135
y/s = 0.319	.258	.501	.430	.349	.280	.408	.319	.246	.186	.295	.224	.153	.093	.198	.127	.061	.084	.018	-.039	-.094	-.018	-.069	-.118	-.169	-.099	-.142	-.190	-.235
	.383	.437	.386	.313	.242	.378	.287	.222	.163	.263	.196	.134	.080	.173	.112	.053	.088	.023	-.029	-.083	-.008	-.058	-.111	-.163	-.090	-.143	-.191	-.235
	.508	.396	.349	.303	.229	.337	.262	.209	.151	.255	.184	.123	.073	.160	.103	.049	.090	.029	-.020	-.068	.011	-.040	-.088	-.136	-.056	-.107	-.157	-.203
	.633	.419	.319	.278	.230	.311	.264	.215	.152	.243	.188	.123	.069	.164	.101	.048	.094	.035	-.012	-.058	.024	-.024	-.068	-.116	-.032	-.085	-.134	-.187
	.759	.411	.369	.254	.207	.318	.244	.198	.153	.224	.179	.131	.072	.157	.106	.051	.101	.042	-.006	-.053	.038	-.012	-.056	-.105	-.021	-.073	-.109	-.133
	.884	.378	.319	.255	.186	.303	.230	.172	.130	.213	.154	.111	.068	.140	.094	.051	.087	.039	-.005	-.054	.034	-.013	-.056	-.105	-.018	-.047	-.094	-.124
y/s = 0.491	.133	.632	.535	.407	.284	.500	.364	.251	.178	.330	.232	.146	.080	.216	.135	.062	.112	.039	-.020	-.078	.018	-.042	-.096	-.148	-.069	-.119	-.164	-.210
	.258	.538	.473	.379	.297	.456	.354	.266	.180	.333	.247	.154	.084	.217	.135	.062	.111	.036	-.023	-.079	.014	-.044	-.096	-.147	-.070	-.117	-.164	-.209
	.383	.457	.410	.360	.270	.402	.333	.244	.178	.308	.226	.150	.089	.202	.129	.060	.101	.032	-.026	-.080	.011	-.046	-.096	-.146	-.073	-.120	-.166	-.213
	.508	.401	.361	.323	.271	.353	.309	.250	.179	.290	.226	.147	.086	.203	.126	.059	.109	.035	-.025	-.084	.012	-.050	-.104	-.154	-.070	-.122	-.170	-.214
	.633	.365	.304	.267	.227	.295	.256	.216	.170	.238	.198	.143	.084	.178	.124	.060	.115	.045	-.014	-.070	.031	-.031	-.085	-.135	-.044	-.100	-.152	-.204
	.759	.364	.264	.216	.176	.255	.204	.167	.132	.186	.152	.112	.071	.132	.094	.048	.088	.039	-.013	-.064	.027	-.026	-.081	-.138	-.041	-.100	-.154	-.199
	.884	.355	.279	.199	.151	.261	.184	.141	.109	.166	.125	.090	.056	.109	.073	.037	.068	.030	-.009	-.055	.024	-.019	-.070	-.127	-.017	-.074	-.133	-.177
y/s = 0.652	.383	.440	.396	.348	.276	.388	.331	.251	.184	.314	.237	.157	.088	.221	.147	.069	.137	.055	-.011	-.074	.046	-.022	-.080	-.136	-.031	-.091	-.146	-.190
	.508	.356	.313	.270	.225	.304	.259	.206	.154	.245	.194	.128	.071	.176	.115	.054	.103	.042	-.012	-.074	.023	-.031	-.083	-.134	-.043	-.096	-.148	-.192
	.633	.307	.264	.223	.185	.254	.211	.169	.130	.199	.155	.107	.065	.141	.095	.044	.079	.025	-.017	-.069	.011	-.036	-.076	-.118	-.048	-.089	-.132	-.176
	.759	.254	.230	.190	.157	.221	.180	.143	.112	.169	.130	.088	.054	.119	.078	.037	.061	.017	-.017	-.058	.004	-.034	-.066	-.101	-.046	-.080	-.118	-.162
	.884	.313	.211	.167	.136	.202	.158	.124	.096	.148	.112	.082	.047	.100	.067	.032	.053	.013	-.019	-.050	-.001	-.033	-.065	-.093	-.045	-.072	-.101	-.094
θ = 90°	-.094	.018	.013	.013	.014	.003	.005	.002	.007	.003	.002	.002	.001	0	.003	.001	-.002	-.004	0	-.002	.001	.003	.003	.004	.018	.012	.011	.014
	.073	.035	.010	.004	.004	.025	.010	.002	.001	.007	.006	.003	.002	-.002	0	0	-.003	-.003	0.000	0	.002	.004	.005	.006	.016	.016	.014	.019
	.240	.002	.069	.057	.029	.098	.047	.044	.027	.029	.021	.016	.009	.011	.005	.001	.005	.002	.002	.001	.006	.005	.005	.005	.018	.014	.016	.031
	.410	.449	.320	.083	.079	.315	.148	.057	.041	.198	.103	.046	.024	.112	.058	.020	.042	.007	-.011	-.020	-.003	-.020	-.029	-.031	-.031	-.042	-.042	-.036
	.573	.469	.403	.309	.249	.376	.278	.212	.111	.252	.179	.111	.054	.151	.093	.039	.078	.020	-.019	-.051	.005	-.036	-.068	-.091	-.056	-.088	-.114	-.128
	.740	.445	.396	.338	.240	.378	.311	.217	.166	.282	.190	.124	.074	.169	.102	.045	.090	.029	-.018	-.059	.017	-.033	-.075	-.112	-.048	-.092	-.134	-.164
	.906	.411	.368	.326	.273	.357	.309	.247	.157	.289	.221	.124	.071	.204	.113	.048	.109	.036	-.014	-.059	.026	-.026	-.073	-.115	-.038	-.085	-.131	-.169
	1.073	.340	.322	.292	.266	.307	.273	.245	.202	.249	.220	.162	.074	.195	.145	.059	.139	.053	-.010	-.058	.049	-.017	-.067	-.113	-.024	-.079	-.124	-.164
	1.240	.174	.196	.207	.206	.199	.169	.176	.173	.122	.133	.134	.111	.088	.093	.072	.064	.070	.001	-.062	.024	-.017	-.069	-.119	-.031	-.081	-.127	-.162
θ = 45°	.156	.268	.089	.037	.027	.066	.035	.031	.030	.040	.025	.008	.016	.056	.024	.011	.009	-.001	-.007	-.010	-.014	-.006	-.022	-.023	-.030	-.033	-.037	-.019
	.323	.357	.306	.246	.199	.260	.221	.159	.073	.206	.161	.099	.021	.111	.074	.034	.052	.009	-.023	-.052	-.011	-.043	-.070	-.096	-.062	-.098	-.124	-.145
	.489	.432	.334	.244	.192	.348	.232	.178	.141	.216	.163	.116	.082	.118	.077	.035	.059	.018	-.016	-.057	.005	-.030	-.070	-.096	-.046	-.086	-.113	-.146
	.656	.454	.384	.315	.209	.371	.296	.191	.136	.264	.177	.119	.073	.145	.090	.041	.074	.029	-.014	-.052	.012	-.027	-.062	-.097	-.041	-.077	-.111	-.143
	.823	.421	.374	.317	.265	.354	.299	.243	.168	.277	.211	.122	.072	.183	.100	.044	.090	.029	-.015	-.056	.017	-.027	-.066	-.106	-.041	-.081	-.118	-.153
	.990	.368	.340	.299	.251	.315	.279	.231	.195	.255	.211	.169	.081	.191	.143	.058	.133	.046	-.011	-.057	.035	-.020	-.069	-.108	-.037	-.080	-.120	-.156

TABLE II.- PRESSURE COEFFICIENTS $\left(\frac{p-p_1}{q_0}\right)$ - Continued

(c) M = 1.48, R = 0.6×10^6

Station	i_w / x/a	α = -6°				α = -4°				α = -2°				α = 0°			α = 2°				α = 4°				α = 6°			
		-5.7°	-3.8°	-1.9°	0°	-5.7°	-3.8°	-1.9°	0°	-5.7°	-3.8°	-1.9°	0°	-5.7°	-3.8°	-1.9°	-5.7°	-3.8°	-1.9°	0°	-5.7°	-3.8°	-1.9°	0°	-5.7°	-3.8°	-1.9°	0°
y/s = 0.170	0.133	0.662	0.525	0.421	0.338	0.470	0.379	0.288	0.218	0.320	0.252	0.187	0.100	0.202	0.121	0.054	0.087	0.002	-0.049	-0.093	-0.046	-0.089	-0.127	-0.171	-0.118	-0.160	-0.203	-0.248
	.258	.508	.408	.324	.258	.378	.300	.232	.173	.263	.211	.143	.086	.162	.111	.047	.073	.015	-.035	-.076	-.019	-.063	-.097	-.141	-.092	-.123	-.151	-.202
	.383	.466	.374	.294	.224	.344	.263	.200	.148	.228	.177	.118	.072	.133	.091	.046	.065	.023	-.019	-.060	.007	-.035	-.074	-.114	-.047	-.088	-.140	-.191
	.508	.450	.374	.308	.222	.348	.277	.198	.144	.233	.171	.114	.070	.133	.091	.046	.065	.029	-.015	-.056	.015	-.024	-.067	-.105	-.025	-.062	-.103	-.126
	.633	.444	.374	.312	.243	.348	.291	.211	.146	.250	.182	.111	.063	.141	.092	.044	.070	.038	-.011	-.057	.030	-.016	-.058	-.096	-.011	-.046	-.083	-.095
	.759	.436	.370	.307	.251	.342	.287	.238	.172	.251	.202	.124	.065	.165	.102	.047	.086	.038	-.011	-.057	.030	-.016	-.058	-.096	-.011	-.046	-.083	-.095
	.884	.388	.333	.278	.227	.309	.259	.206	.162	.232	.186	.132	.074	.161	.105	.052	.093	.046	-.011	-.063	.041	-.015	-.064	-.106	-.006	-.053	-.093	-.076
y/s = 0.208	.133	.606	.494	.398	.316	.446	.356	.276	.210	.306	.235	.159	.094	.177	.109	.052	.068	.004	-.047	-.098	-.037	-.094	-.141	-.193	-.139	-.182	-.228	-.271
	.258	.519	.428	.338	.269	.396	.311	.241	.183	.273	.215	.149	.088	.168	.107	.049	.070	.013	-.034	-.080	-.016	-.063	-.108	-.158	-.088	-.133	-.184	-.231
	.383	.478	.395	.314	.243	.367	.286	.215	.162	.247	.191	.132	.096	.154	.101	.047	.072	.021	-.024	-.068	-.008	-.048	-.086	-.125	-.065	-.098	-.183	-.187
	.508	.451	.378	.316	.237	.355	.287	.208	.150	.247	.178	.121	.071	.142	.095	.047	.073	.027	-.021	-.058	.006	-.038	-.074	-.116	-.049	-.092	-.163	-.150
	.633	.439	.371	.312	.249	.346	.289	.217	.149	.253	.185	.118	.067	.149	.095	.046	.077	.031	-.015	-.059	.016	-.028	-.068	-.107	-.026	-.069	-.125	-.130
	.759	.421	.363	.299	.245	.337	.279	.220	.160	.250	.192	.123	.070	.162	.102	.049	.090	.039	-.012	-.057	.033	-.017	-.060	-.101	-.001	-.043	-.111	-.089
	.884	.387	.332	.274	.223	.312	.251	.200	.153	.232	.177	.118	.062	.159	.098	.052	.091	.042	-.013	-.061	.044	-.009	-.061	-.106	-.012	-.045	-.116	-.058
y/s = 0.319	.258	.526	.452	.360	.282	.427	.334	.255	.191	.303	.233	.157	.094	.198	.125	.060	.093	.025	-.035	-.090	-.006	-.060	-.118	-.165	-.085	-.130	-.183	-.234
	.383	.481	.407	.346	.258	.390	.321	.234	.170	.288	.214	.144	.085	.180	.115	.053	.093	.028	-.028	-.080	.005	-.050	-.101	-.154	-.073	-.121	-.164	-.202
	.508	.449	.371	.323	.260	.353	.307	.238	.167	.276	.213	.137	.079	.178	.113	.052	.095	.034	-.019	-.067	.022	-.031	-.080	-.129	-.040	-.087	-.138	-.185
	.633	.420	.344	.289	.240	.327	.270	.224	.168	.238	.202	.136	.076	.171	.116	.054	.100	.041	-.013	-.061	.084	-.020	-.069	-.117	-.020	-.069	-.131	-.178
	.759	.395	.321	.259	.204	.298	.241	.188	.148	.206	.165	.119	.070	.141	.103	.052	.089	.042	-.012	-.059	.033	-.016	-.068	-.115	-.013	-.068	-.136	-.135
	.884	.372	.307	.245	.188	.283	.223	.167	.124	.193	.143	.097	.059	.119	.082	.043	.073	.037	-.011	-.057	.032	-.011	-.063	-.111	-.006	-.059	-.098	-.071
y/s = 0.431	.133	.641	.551	.417	.297	.516	.384	.261	.176	.344	.245	.153	.084	.211	.134	.062	.111	.040	-.022	-.079	.023	-.038	-.091	-.147	-.051	-.107	-.152	-.199
	.258	.542	.484	.404	.300	.464	.371	.274	.197	.343	.255	.166	.093	.217	.138	.063	.118	.040	-.023	-.078	.020	-.040	-.090	-.140	-.053	-.108	-.149	-.194
	.383	.479	.420	.375	.308	.408	.359	.273	.192	.333	.250	.158	.090	.215	.132	.061	.112	.039	-.084	-.078	.020	-.041	-.091	-.143	-.052	-.108	-.153	-.197
	.508	.430	.361	.319	.272	.348	.310	.259	.195	.287	.240	.165	.093	.212	.140	.064	.123	.046	-.023	-.083	.029	-.040	-.100	-.154	-.048	-.104	-.160	-.198
	.633	.380	.304	.256	.213	.283	.243	.202	.159	.218	.186	.135	.083	.163	.116	.056	.101	.042	-.018	-.072	.031	-.030	-.085	-.139	-.035	-.090	-.151	-.190
	.759	.369	.286	.225	.178	.264	.206	.163	.127	.177	.147	.104	.064	.127	.092	.046	.078	.036	-.014	-.068	.027	-.022	-.078	-.135	-.022	-.078	-.136	-.165
	.884	.368	.287	.221	.165	.260	.199	.145	.110	.168	.128	.087	.053	.109	.076	.039	.067	.038	-.010	-.050	.027	-.014	-.057	-.108	-.011	-.054	-.111	-.134
y/s = 0.692	.383	.422	.370	.323	.257	.358	.311	.236	.163	.289	.219	.148	.073	.196	.131	.061	.134	.050	-.012	-.069	.085	-.025	-.082	-.136	-.031	-.089	-.110	-.189
	.508	.372	.316	.272	.224	.303	.260	.209	.155	.239	.194	.128	.069	.173	.114	.057	.099	.039	-.013	-.064	.028	-.029	-.080	-.128	-.034	-.084	-.102	-.157
	.633	.343	.272	.226	.186	.257	.217	.173	.131	.199	.160	.109	.063	.140	.097	.046	.082	.029	-.016	-.056	.023	-.026	-.067	-.104	-.030	-.069	-.125	-.137
	.759	.334	.246	.197	.160	.229	.186	.144	.110	.169	.135	.098	.052	.117	.079	.038	.065	.022	-.016	-.048	.016	-.023	-.056	-.088	-.026	-.058	-.116	-.126
	.884	.319	.241	.181	.141	.221	.167	.126	.098	.151	.119	.082	.046	.102	.069	.033	.059	.021	-.016	-.045	.013	-.023	-.056	-.086	-.024	-.055	-.103	-.095
θ = 90°	-.094	.079	.018	.013	.012	.031	.011	.006	.006	.019	.011	.005	.001	.013	.005	.001	.009	-.003	-.003	-.004	-.002	-.002	-.001	0	.012	.010	.018	.020
	.073	.089	.061	.061	.018	.067	.066	.036	.009	.053	.050	.021	.007	.033	.025	.009	.018	.003	-.004	-.004	0	-.002	.002	-.001	.015	.018	.016	.024
	.240	.275	.110	.087	.076	.102	.074	.067	.035	.058	.056	.048	.026	.031	.032	.022	.017	.007	-.005	-.007	.003	-.003	-.006	-.006	.012	.013	.009	.019
	.410	.389	.308	.182	.086	.291	.172	.074	.066	.144	.062	.049	.038	.038	.027	.022	.013	.018	-.011	-.083	.004	-.014	-.023	-.027	-.012	-.021	-.024	-.022
	.573	.439	.383	.297	.207	.365	.273	.186	.062	.245	.165	.049	.042	.137	.030	.020	.024	.017	-.015	-.041	.014	-.024	-.054	-.078	-.030	-.064	-.090	-.090
	.740	.439	.397	.338	.269	.386	.326	.237	.167	.317	.215	.133	.033	.197	.115	.013	.101	.021	-.016	-.054	.034	-.022	-.066	-.104	-.018	-.068	-.111	-.123
	.906	.428	.364	.320	.277	.359	.312	.257	.181	.302	.248	.154	.099	.238	.145	.030	.152	.033	-.013	-.067	.049	-.015	-.073	-.119	-.001	-.061	-.115	-.145
	1.073	.348	.303	.268	.239	.295	.262	.224	.196	.246	.219	.173	.118	.204	.165	.101	.161	.094	-.008	-.062	.067	-.004	-.060	-.114	.041	-.041	-.094	-.101
	1.240	.172	.178	.189	.178	.156	.154	.154	.145	.109	.126	.118	.111	.087	.096	.099	.063	.060	-.005	-.044	.053	.010	-.044	-.088	.024	0	-.071	-.102
θ = 45°	.156	.133	.078	.063	.057	.056	.055	.050	.046	.041	.045	.038	.024	.026	.026	.018	.013	.001	-.014	-.021	-.019	-.033	-.040	-.045	-.065	-.071	-.075	-.066
	.323	.423	.267	.177	.079	.270	.195	.078	.049	.199	.088	.050	.033	.090	.033	.024	.011	.010	-.022	-.048	-.015	-.048	-.075	-.102	-.076	-.102	-.139	-.156
	.489	.471	.408	.300	.215	.376	.271	.196	.158	.286	.172	.119	.064	.128	.091	.084	.063	.018	-.018	-.054	-.004	-.040	-.068	-.099	-.020	-.050	-.083	-.109
	.656	.451	.402	.338	.248	.369	.315	.211	.138	.278	.181	.106	.066	.147	.084	.042	.069	.024	-.017	-.053	.015	-.023	-.059	-.094	-.011	-.053	-.098	-.103
	.823	.411	.374	.324	.273	.346	.299	.250	.184	.273	.227	.141	.062	.204	.117	.041	.107	.033	-.014	-.058	.042	-.012	-.060	-.102	-.002	-.052	-.099	-.112
	.990	.344	.312	.274	.236	.286	.256	.212	.169	.230	.192	.141	.092	.174	.132	.074	.122	.067	-.009	-.054	.048	.005	-.064	-.114	.018	-.043	-.104	-.100

NACA

TABLE II.- PRESSURE COEFFICIENTS $\left(\frac{p-p_1}{q_o}\right)$ - Concluded

(d) M = 2.00, R = 1.5×10^6

Station	$\frac{z_w}{c}$ / $\frac{x}{c}$	α = -6°				α = -4°				α = -2°				α = 0°			α = 2°				α = 4°				α = 6°			
		-5.7°	-3.8°	-1.9°	0°	-5.7°	-3.8°	-1.9°	0°	-5.7°	-3.8°	-1.9°	0°	-5.7°	-3.8°	-1.9°	-5.7°	-3.8°	-1.9°	0°	-5.7°	-3.8°	-1.9°	0°	-5.7°	-3.8°	-1.9°	0°
y/s = 0.170	0.133	0.390	0.337	- - -	0.231	0.288	0.247	0.196	0.149	0.211	0.164	0.116	0.077	0.113	0.072	0.035	0.024	-0.010	-0.040	-0.072	-0.050	-0.080	-0.107	-0.131	-0.183	-0.148	-0.168	-0.187
	.258	.354	.311	- - -	.214	.268	.230	.183	.138	.198	.150	.106	.070	.106	.069	.033	.030	.002	-.029	-.061	-.033	-.059	-.087	-.112	-.099	-.124	-.141	-.165
	.383	.306	.265	- - -	.191	.231	.197	.157	.129	.161	.129	.089	.057	.097	.053	.030	.022	-.002	-.032	-.058	-.034	-.057	-.080	-.105	-.093	-.116	-.134	-.155
	.508	.287	.249	- - -	.174	.218	.184	.150	.113	.152	.124	.089	.056	.087	.061	.028	.034	.010	-.017	-.048	-.013	-.037	-.062	-.087	-.093	-.108	-.107	-.133
	.633	.262	.229	- - -	.159	.198	.168	.136	.103	.136	.111	.080	.051	.081	.057	.026	.035	.011	-.016	-.045	-.010	-.031	-.056	-.080	-.051	-.072	-.092	-.119
	.759	.243	.214	- - -	.150	.184	.157	.128	.098	.128	.103	.074	.045	.077	.053	.024	.035	.013	-.013	-.040	-.005	-.025	-.049	-.074	-.041	-.061	-.081	-.106
	.884	.230	.201	- - -	.142	.170	.144	.118	.089	.120	.095	.069	.041	.075	.051	.026	.037	.014	-.010	-.035	-.002	-.022	-.045	-.068	-.035	-.055	-.074	-.099
y/s = 0.206	.133	.398	.337	- - -	.236	.317	.252	.206	.161	.212	.164	.118	.076	.113	.072	.034	.027	-.007	-.041	-.074	-.047	-.076	-.106	-.132	-.120	-.143	-.161	-.186
	.258	.347	.294	- - -	.204	.276	.225	.181	.140	.191	.148	.105	.069	.106	.067	.031	.027	-.003	-.035	-.065	-.038	-.068	-.097	-.122	-.108	-.134	-.151	-.177
	.383	.316	.270	- - -	.187	.250	.207	.166	.128	.175	.136	.097	.063	.098	.063	.029	.028	.002	-.030	-.059	-.029	-.056	-.085	-.110	-.092	-.117	-.137	-.162
	.508	.293	.251	- - -	.177	.226	.189	.152	.119	.161	.128	.091	.059	.091	.061	.028	.030	.005	-.024	-.051	-.021	-.046	-.074	-.097	-.078	-.103	-.123	-.147
	.633	.275	.236	- - -	.169	.211	.178	.144	.111	.150	.119	.086	.055	.084	.056	.027	.032	.008	-.019	-.047	-.014	-.037	-.064	-.087	-.060	-.083	-.104	-.129
	.759	.261	.229	- - -	.161	.200	.170	.137	.106	.141	.113	.081	.054	.082	.056	.026	.035	.013	-.015	-.043	-.007	-.030	-.056	-.079	-.047	-.069	-.090	-.115
	.884	.249	.220	- - -	.155	.188	.161	.130	.100	.132	.105	.075	.048	.079	.054	.026	.030	.015	-.012	-.038	-.004	-.025	-.050	-.073	-.039	-.060	-.080	-.106
y/s = 0.319	.258	.388	.324	- - -	.208	.305	.242	.195	.135	.209	.158	.107	.063	.126	.081	.038	.049	.013	-.025	-.062	-.013	-.047	-.080	-.111	-.072	-.101	-.125	-.154
	.383	.349	.296	- - -	.201	.275	.227	.180	.135	.197	.150	.103	.063	.121	.078	.037	.047	.013	-.025	-.061	-.016	-.049	-.082	-.112	-.078	-.108	-.131	-.158
	.508	.320	.273	- - -	.187	.250	.200	.165	.124	.185	.141	.099	.060	.113	.073	.034	.050	.015	-.022	-.058	-.013	-.046	-.079	-.107	-.080	-.108	-.131	-.158
	.633	.299	.256	- - -	.175	.232	.193	.152	.113	.172	.132	.091	.057	.108	.070	.034	.050	.017	-.017	-.053	-.007	-.040	-.072	-.101	-.072	-.102	-.124	-.154
	.759	.279	.239	- - -	.161	.216	.179	.141	.104	.160	.124	.085	.051	.102	.067	.032	.050	.018	-.014	-.050	-.004	-.036	-.063	-.099	-.065	-.096	-.120	-.150
	.884	.262	.224	- - -	.151	.211	.166	.130	.096	.150	.115	.079	.046	.098	.065	.031	.050	.019	-.012	-.047	0	-.028	-.058	-.086	-.043	-.076	-.100	-.132
y/s = 0.431	.133	.363	.294	- - -	.185	.274	.215	.162	.116	.193	.145	.097	.059	.124	.079	.037	.060	.023	-.014	-.050	.012	-.024	-.058	-.089	-.038	-.070	-.097	-.122
	.258	.365	.295	- - -	.188	.276	.216	.163	.115	.196	.146	.096	.053	.125	.081	.039	.060	.023	-.015	-.051	.009	-.027	-.061	-.092	-.041	-.074	-.100	-.130
	.383	.375	.303	- - -	.187	.283	.220	.165	.118	.198	.147	.097	.055	.125	.079	.037	.059	.022	-.017	-.053	.004	-.032	-.066	-.097	-.049	-.081	-.106	-.140
	.508	.357	.299	- - -	.198	.280	.224	.171	.123	.202	.151	.101	.057	.126	.081	.039	.059	.023	-.016	-.054	0	-.036	-.070	-.101	-.055	-.086	-.112	-.141
	.633	.331	.281	- - -	.184	.262	.213	.165	.120	.193	.146	.099	.057	.123	.080	.038	.057	.021	-.017	-.055	-.005	-.040	-.075	-.105	-.062	-.093	-.117	-.147
	.759	.314	.266	- - -	.176	.246	.201	.157	.115	.183	.139	.095	.056	.119	.077	.037	.056	.020	-.018	-.055	-.006	-.040	-.075	-.105	-.066	-.097	-.121	-.150
	.884	.297	.253	- - -	.166	.232	.190	.148	.108	.163	.132	.090	.053	.114	.074	.035	.057	.021	-.016	-.053	-.003	-.038	-.073	-.101	-.067	-.098	-.122	-.152
y/s = 0.692	.383	.347	.280	- - -	.170	.270	.211	.159	.112	.195	.144	.095	.052	.123	.080	.036	.063	.026	-.013	-.048	.014	-.023	-.060	-.090	-.033	-.067	-.096	-.126
	.508	.356	.286	- - -	.173	.270	.209	.156	.110	.191	.140	.092	.051	.122	.078	.036	.061	.025	-.013	-.047	.011	-.024	-.060	-.090	-.033	-.065	-.094	-.125
	.633	.359	.293	- - -	.182	.274	.215	.162	.115	.193	.142	.093	.052	.122	.078	.035	.060	.023	-.015	-.048	.008	-.027	-.061	-.090	-.035	-.067	-.094	-.123
	.759	.345	.285	- - -	.183	.263	.209	.160	.116	.186	.138	.092	.052	.118	.076	.035	.058	.022	-.016	-.049	.005	-.029	-.063	-.090	-.037	-.068	-.094	-.121
	.884	.317	.268	- - -	.177	.248	.198	.152	.112	.174	.130	.088	.050	.110	.070	.033	.053	.020	-.015	-.047	.003	-.029	-.061	-.087	-.038	-.067	-.092	-.120
θ = 90°	-.094	.040	.039	- - -	.040	.022	.020	.019	.020	.008	.007	.007	.008	-.001	-.001	-.001	-.002	-.001	-.001	-.004	.008	.007	.008	.001	-.002	-.002	-.001	-.004
	.073	.038	.033	- - -	.033	.022	.018	.018	.020	.008	.007	.007	.008	0	-.001	0	.006	.004	-.001	0	.013	.013	.013	0	.006	.006	.007	-.004
	.240	.027	.026	- - -	.027	.016	.014	.014	.016	.029	.019	.004	.002	.009	.007	.003	.010	.008	0	-.001	.011	.010	.011	.001	.005	.006	.006	-.004
	.410	.031	.042	- - -	.028	.027	.031	.014	.011	.032	.028	.020	.007	.016	.013	.007	.010	.009	-.001	-.002	.008	.007	.007	0	.003	.003	.001	-.005
	.573	.195	.073	- - -	.039	.134	.046	.039	.023	.031	.025	.021	.015	.021	.008	.004	.022	.012	0	-.001	-.001	-.007	-.013	-.015	-.024	-.027	-.029	-.033
	.740	.298	.195	- - -	.066	.198	.126	.046	.054	.118	.068	.011	.011	.061	.015	-.002	.039	.013	-.003	-.015	-.006	-.024	-.039	-.046	-.041	-.054	-.061	-.068
	.906	.272	.239	- - -	.154	.213	.160	.145	.090	.155	.115	.080	.022	.103	.070	.024	.048	.020	-.006	-.027	-.003	-.029	-.050	-.066	-.044	-.065	-.079	-.092
	1.073	.272	.242	- - -	.159	.212	.180	.199	.100	.166	.120	.084	.059	.108	.073	.041	.048	.020	-.013	-.039	-.003	-.033	-.060	-.080	-.045	-.071	-.090	-.109
	1.240	.254	.233	- - -	.147	.193	.170	.130	.090	.158	.117	.077	.046	.102	.067	.032	.040	.015	-.018	-.048	-.010	-.036	-.065	-.088	-.046	-.073	-.096	-.120
θ = 45°	.156	.004	.021	- - -	.003	.003	.026	.012	.004	.027	.022	.016	.009	.011	.009	.006	-.002	0	-.002	-.003	-.005	-.005	-.006	-.006	-.023	-.022	-.022	-.024
	.323	.108	.121	- - -	.032	.140	.062	.030	.031	.030	.022	.019	.016	.016	.009	.006	.015	.001	-.011	-.018	-.020	-.031	-.039	-.043	-.060	-.068	-.069	-.074
	.489	.146	.175	- - -	.137	.140	.138	.116	.090	.125	.100	.042	.019	.077	.044	.007	.024	.004	-.016	-.034	-.016	-.034	-.043	-.068	-.057	-.075	-.087	-.103
	.656	.217	.185	- - -	.143	.165	.142	.122	.093	.130	.106	.081	.054	.074	.053	.028	.029	.009	-.013	-.034	-.012	-.032	-.051	-.070	-.052	-.069	-.085	-.105
	.823	.257	.194	- - -	.138	.179	.141	.116	.089	.120	.077	.072	.048	.069	.048	.028	.033	.013	-.009	-.032	-.006	-.028	-.047	-.070	-.044	-.065	-.083	-.109
	.990	.263	.200	- - -	.131	.194	.141	.111	.088	.117	.090	.063	.043	.071	.046	.024	.035	.014	-.010	-.034	-.007	-.028	-.058	-.073	-.043	-.065	-.085	-.110

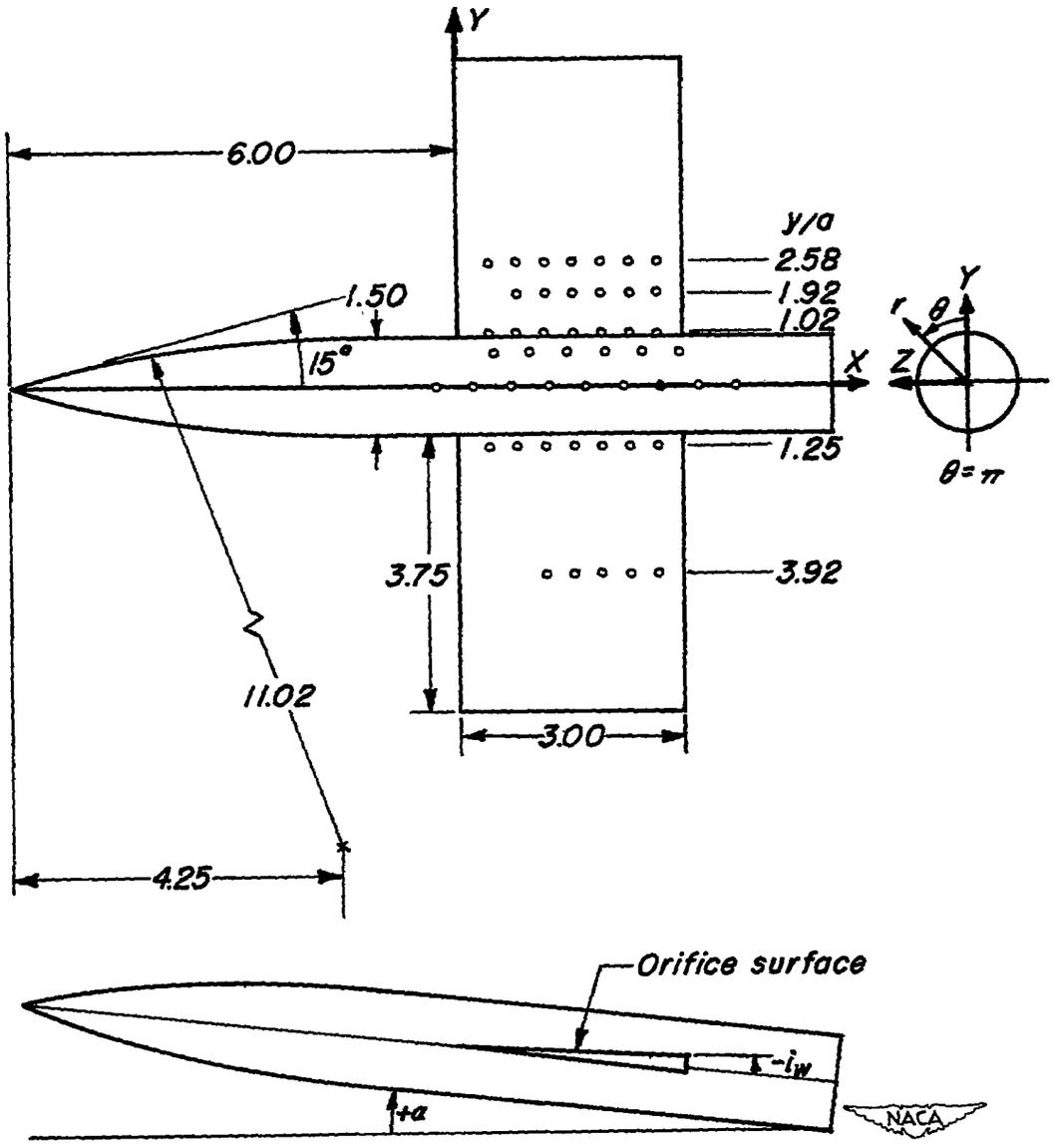

Figure 1.- Pressure-distribution model (all dimensions in inches).

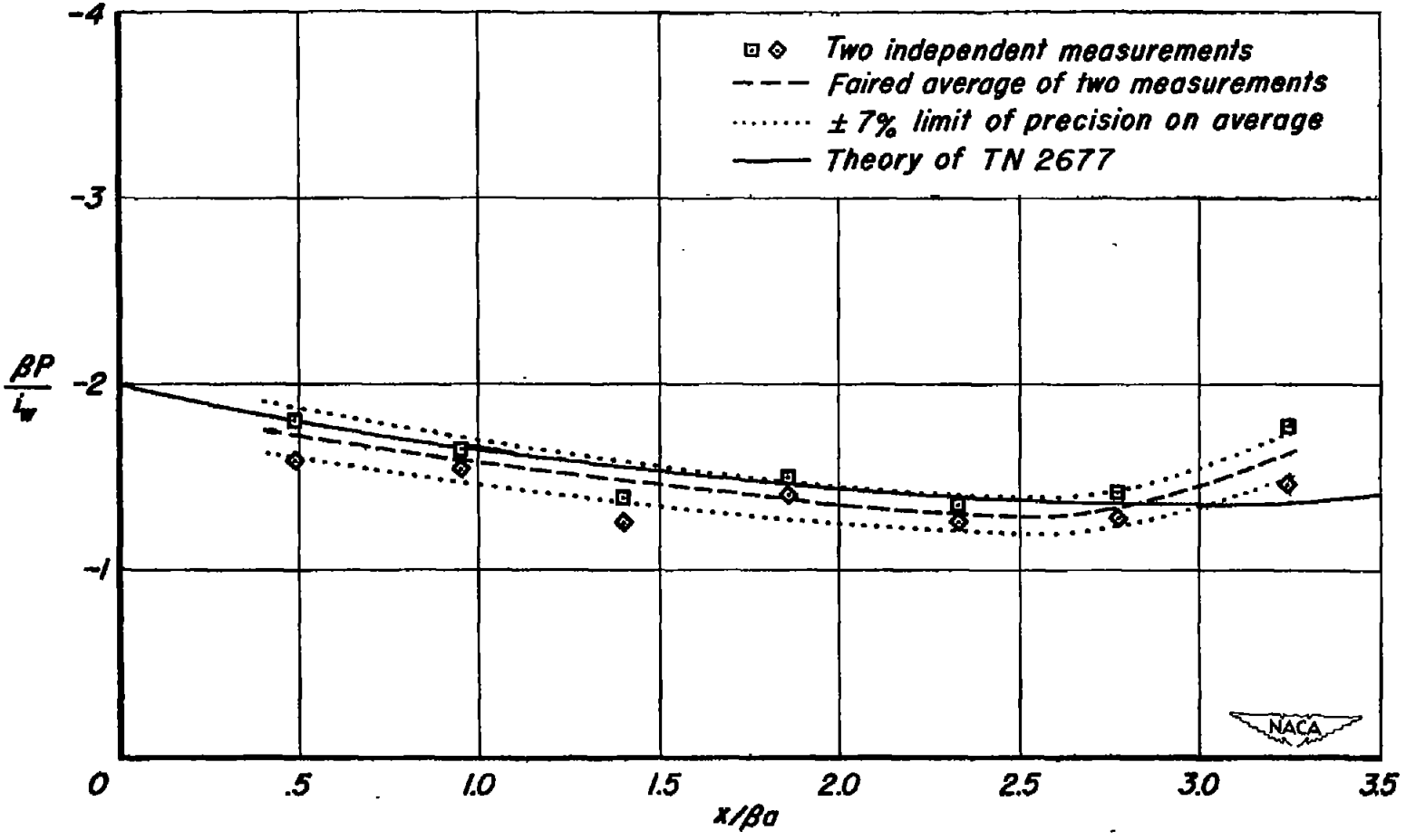

Figure 2.- Comparison between two independent readings of pressure distribution in wing-body juncture for $\alpha = 0^{\circ}$, $i_W = -1.9^{\circ}$, $M = 1.48$, and $R = 1.5 \times 10^6$.

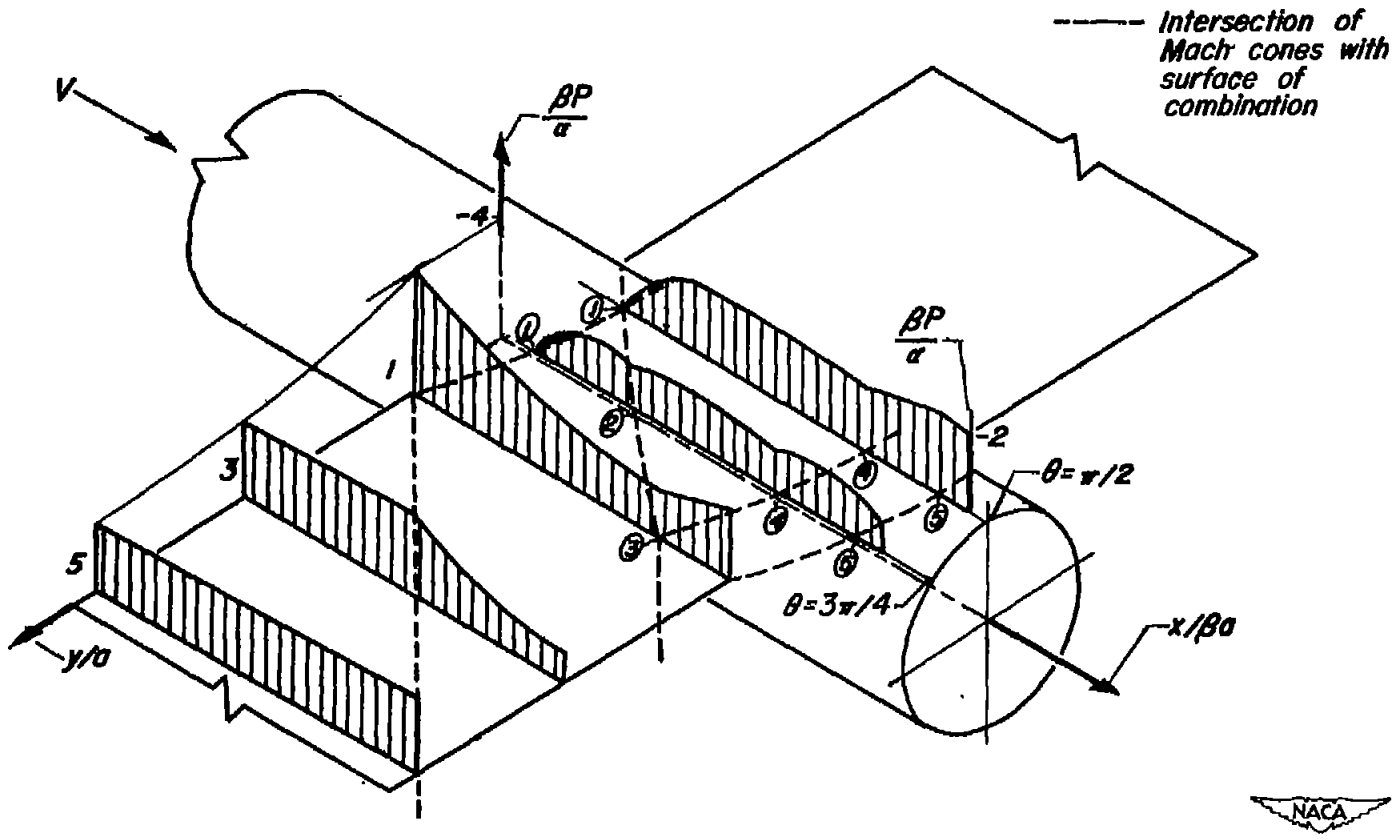

Figure 3.- Isometric drawing of pressure distribution acting on combination of body and rectangular wing for angle-of-attack case.

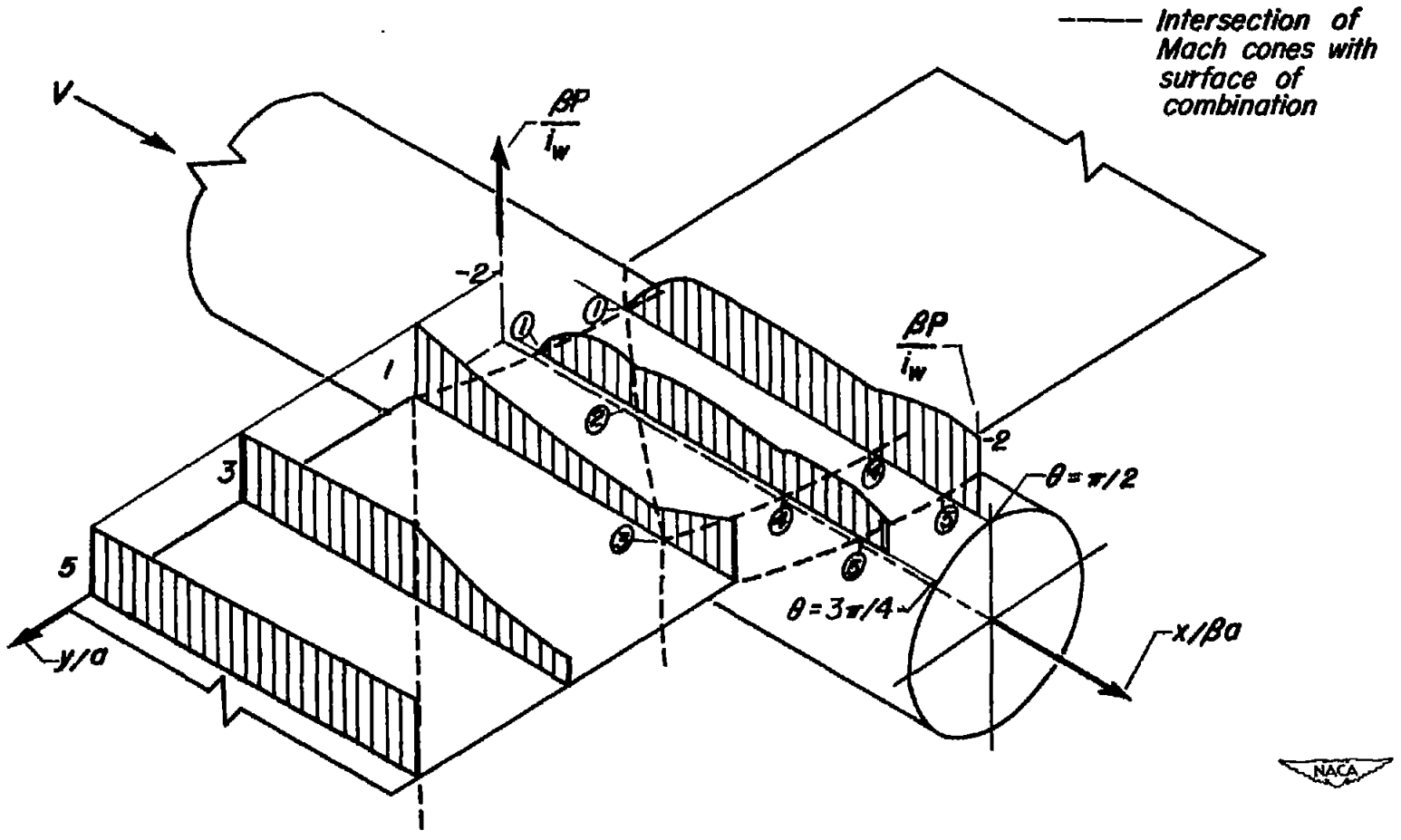

Figure 4.- Isometric drawing of pressure distribution acting on combination of body and rectangular wing for wing-incidence case.

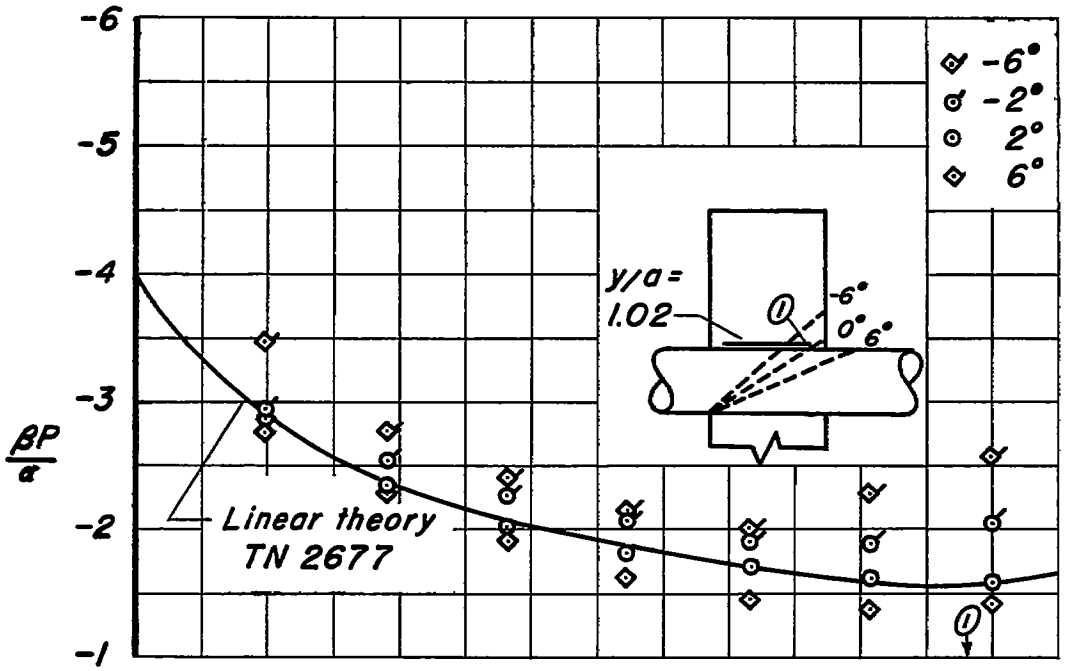

(a) M = 1.48, y/a = 1.02

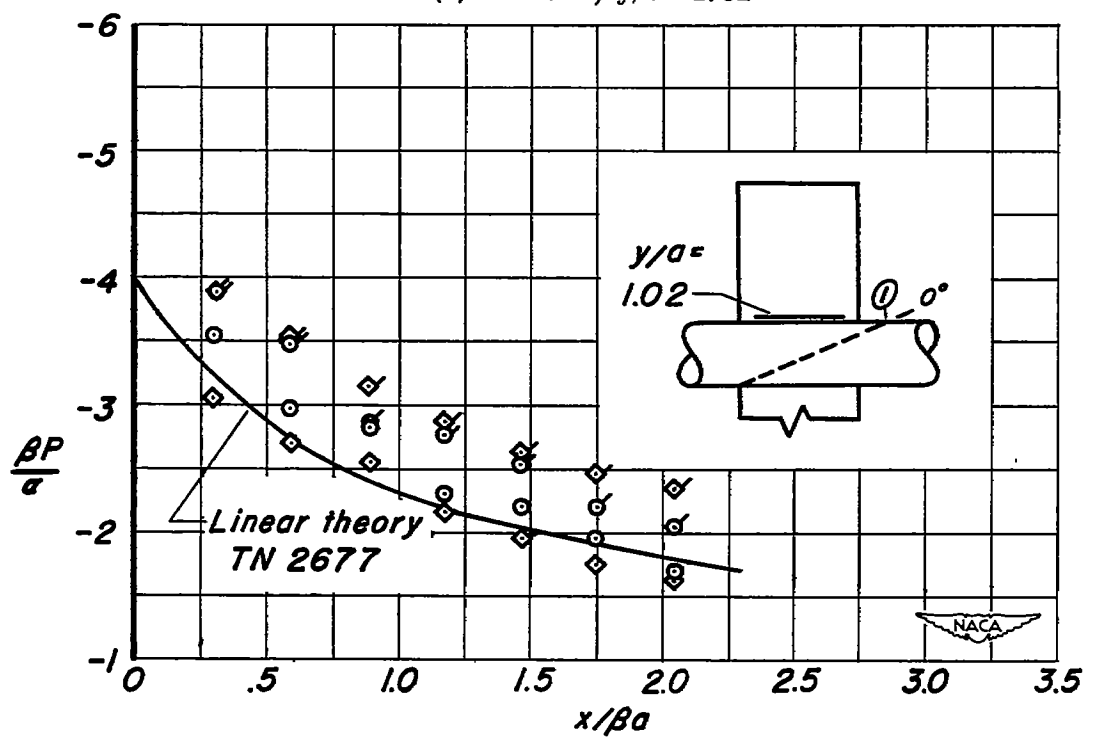

(b) M = 2.00, y/a = 1.02

Figure 5.- Pressure distribution due to α with $i_W = 0^\circ$ and $R = 1.5 \times 10^6$.

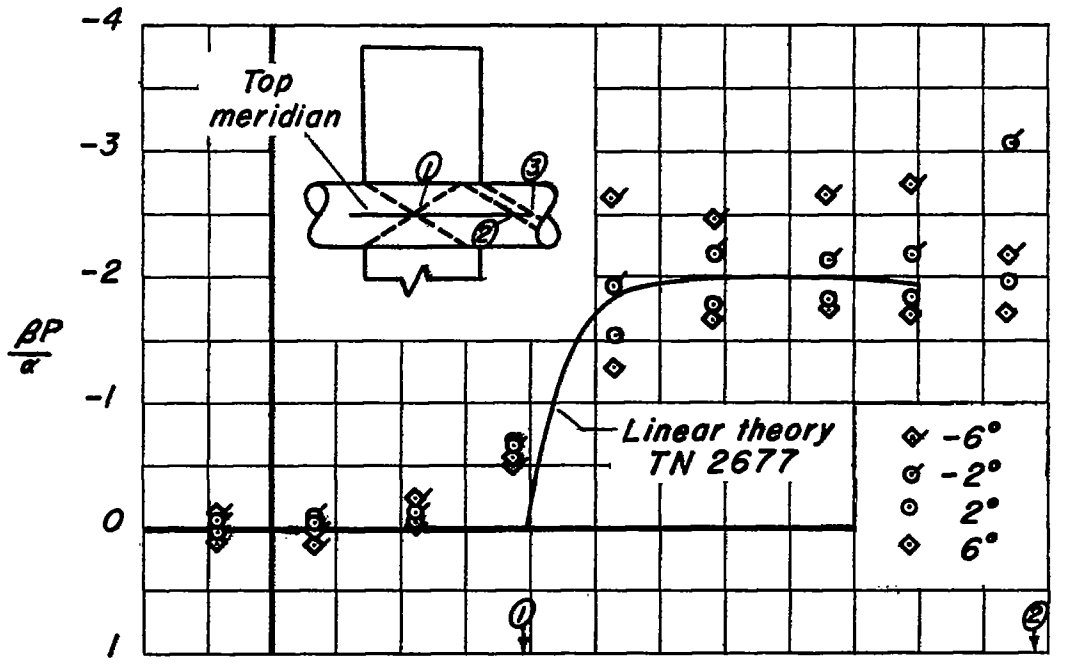

(c) M = 1.48, top meridian

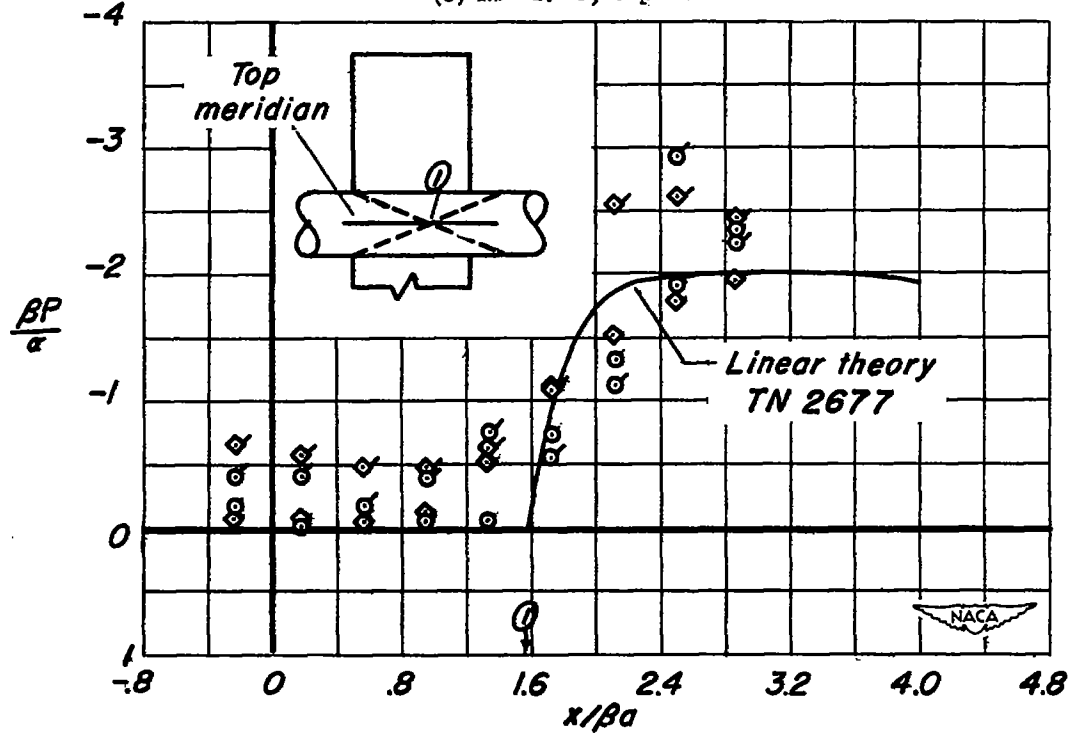

(d) M = 2.00, top meridian

Figure 5.- Continued.

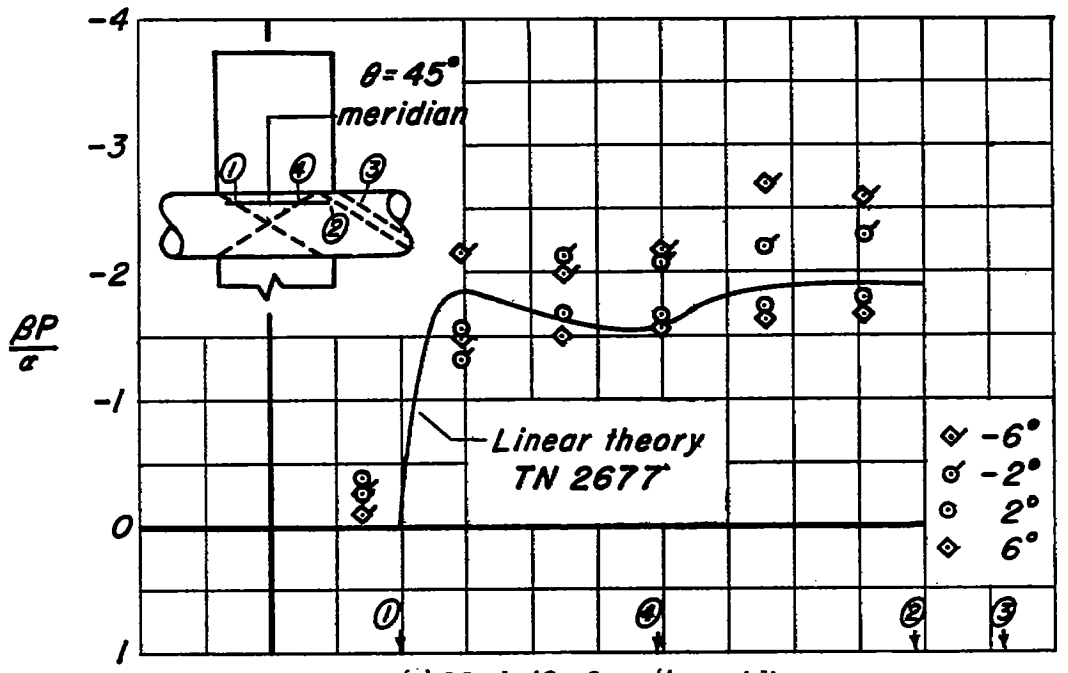

(e) M = 1.48, $\theta = \pi/4$ meridian

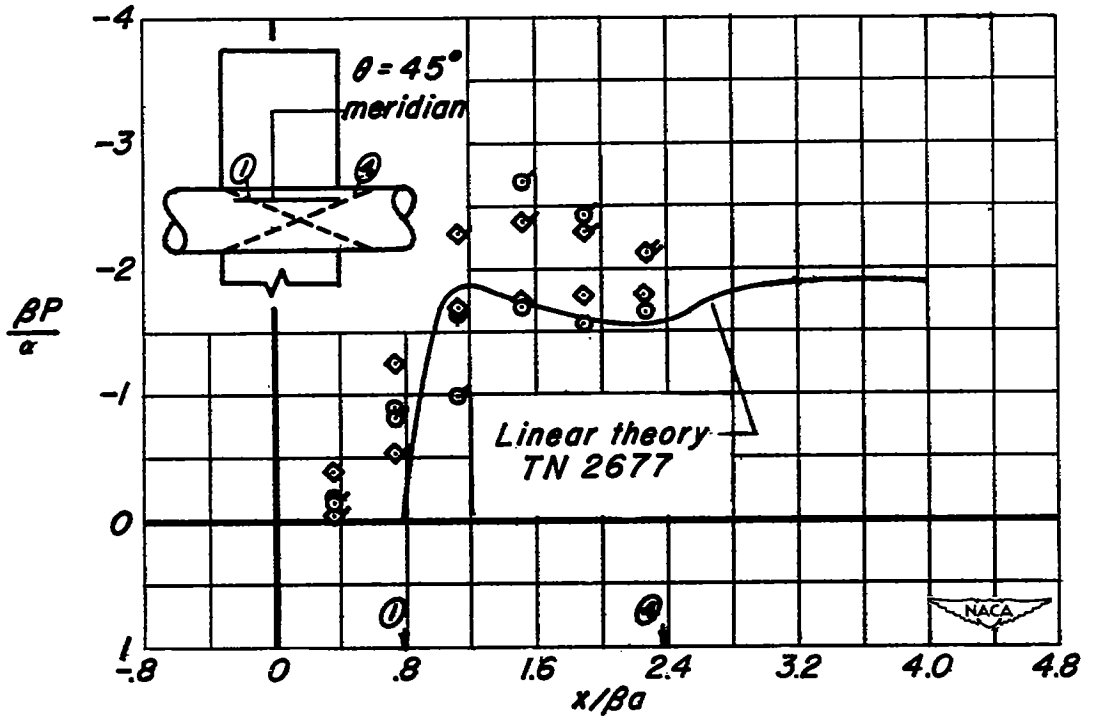

(f) M = 2.00, $\theta = \pi/4$ meridian

Figure 5.- Continued.

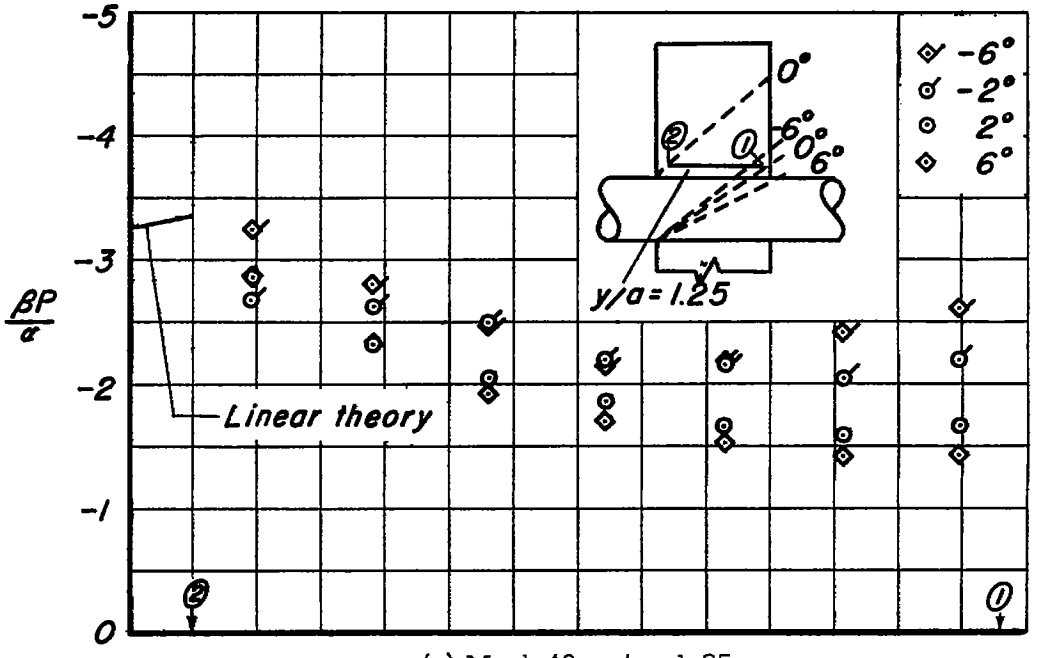

(g) M = 1.48, y/a = 1.25

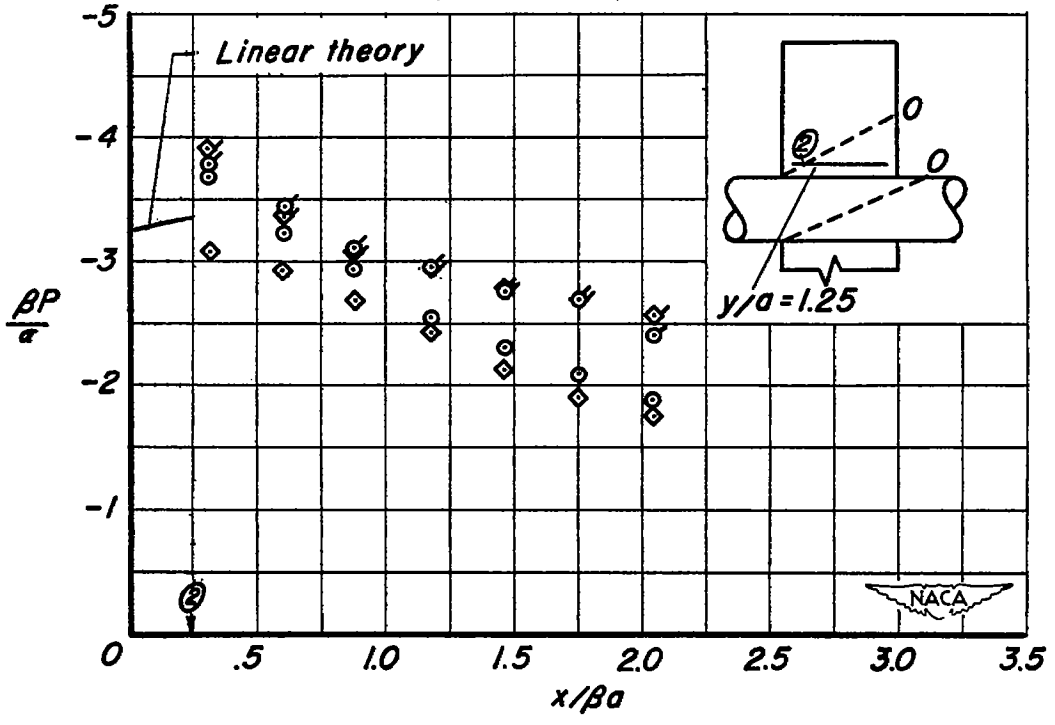

(h) M = 2.00, y/a = 1.25

Figure 5.- Continued.

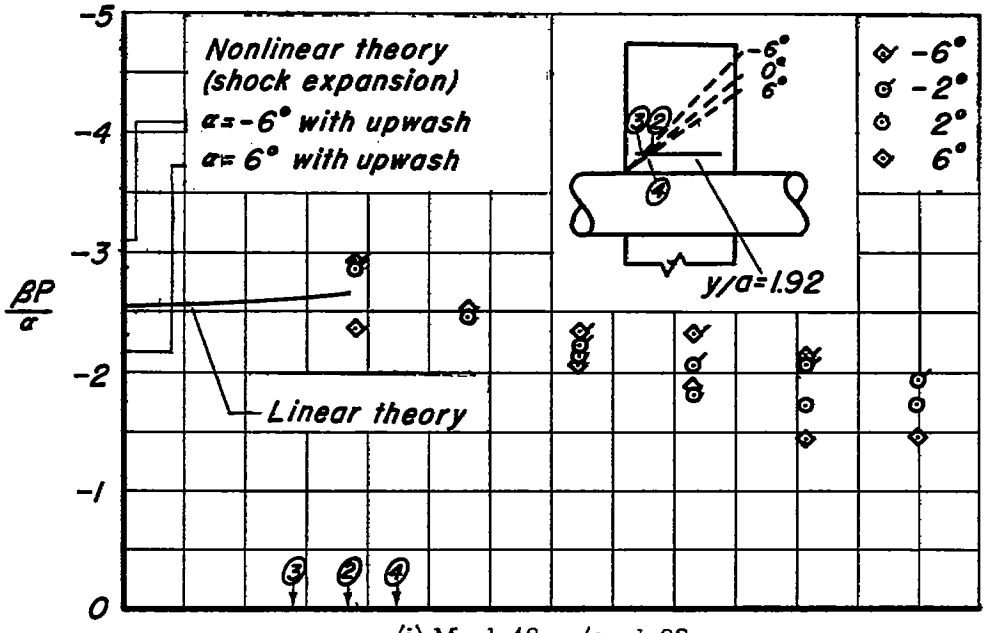

(i) M = 1.48, y/a = 1.92

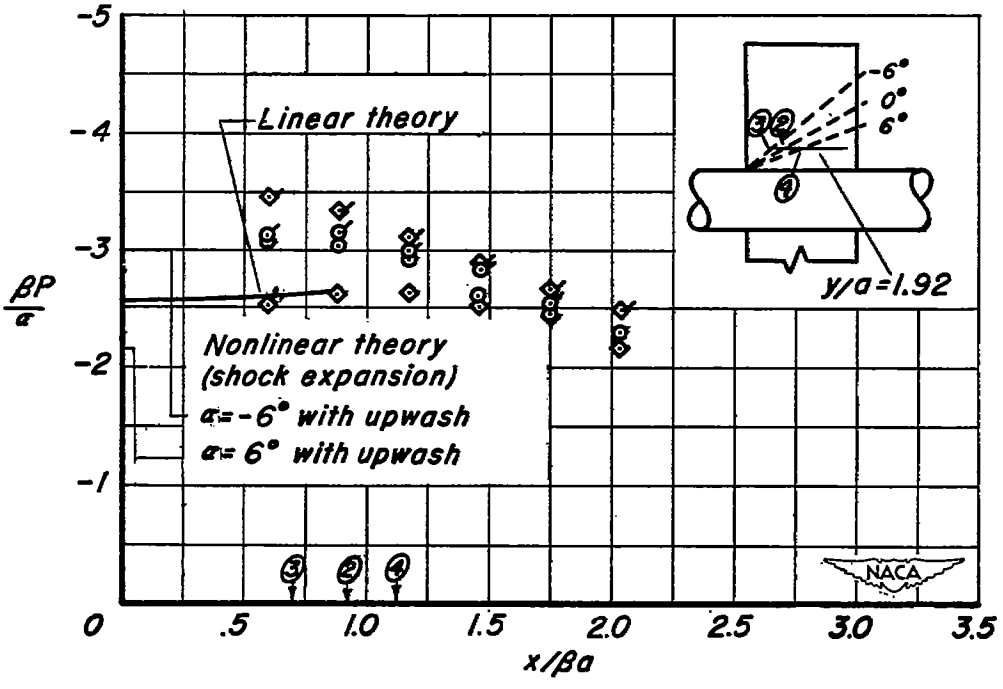

(j) M = 2.00, y/a = 1.92

Figure 5.- Continued.

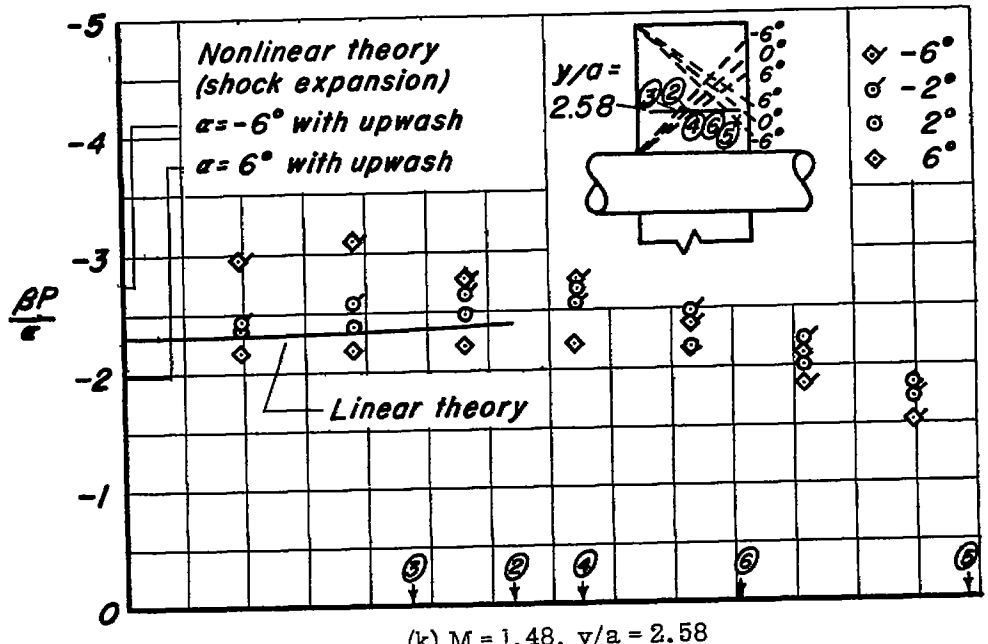

(k) M = 1.48, y/a = 2.58

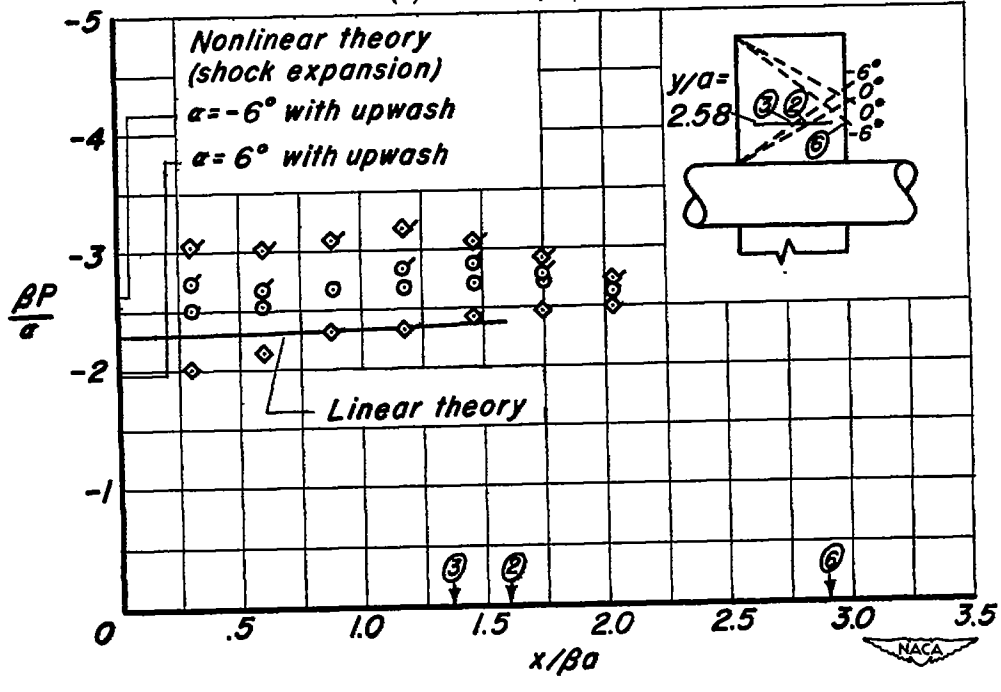

(l) M = 2.00, y/a = 2.58

Figure 5.- Continued.

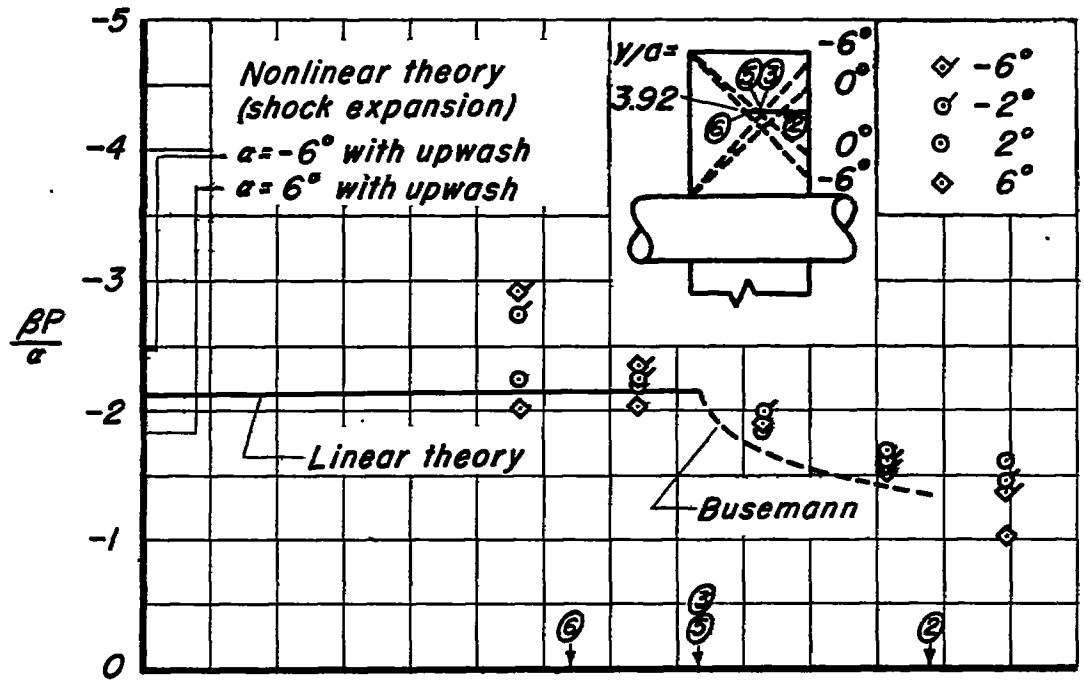

(m) M = 1.48, y/a = 3.92

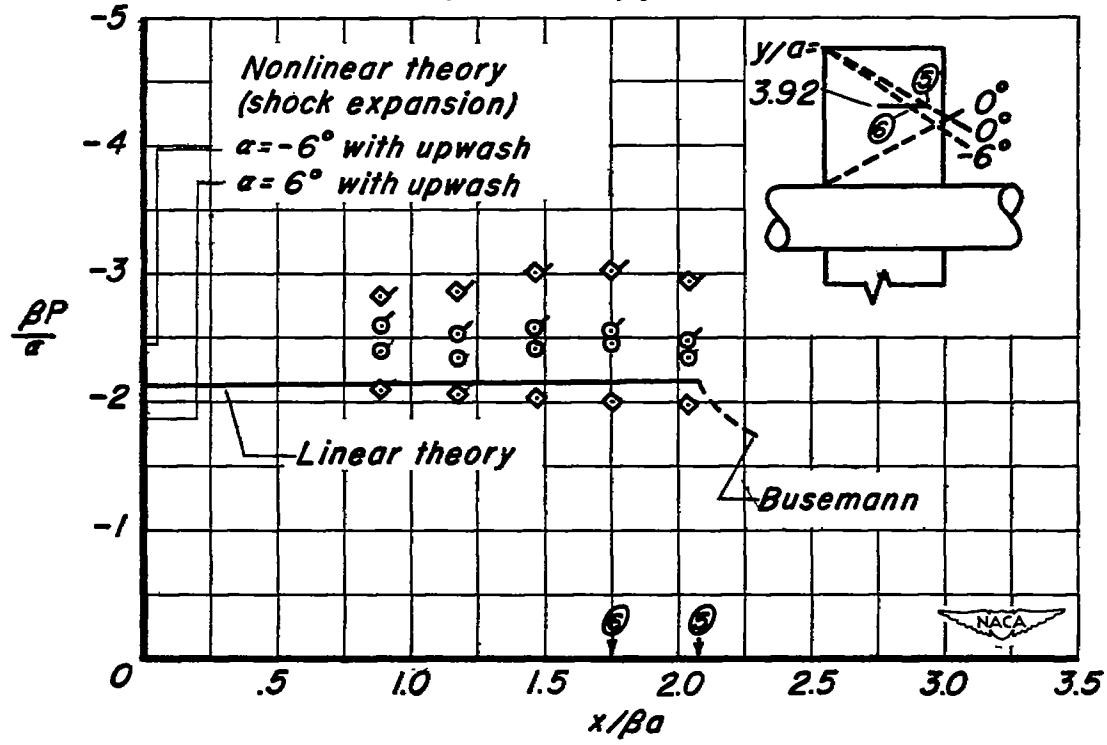

(n) M = 2.00, y/a = 3.92

Figure 5.- Concluded.

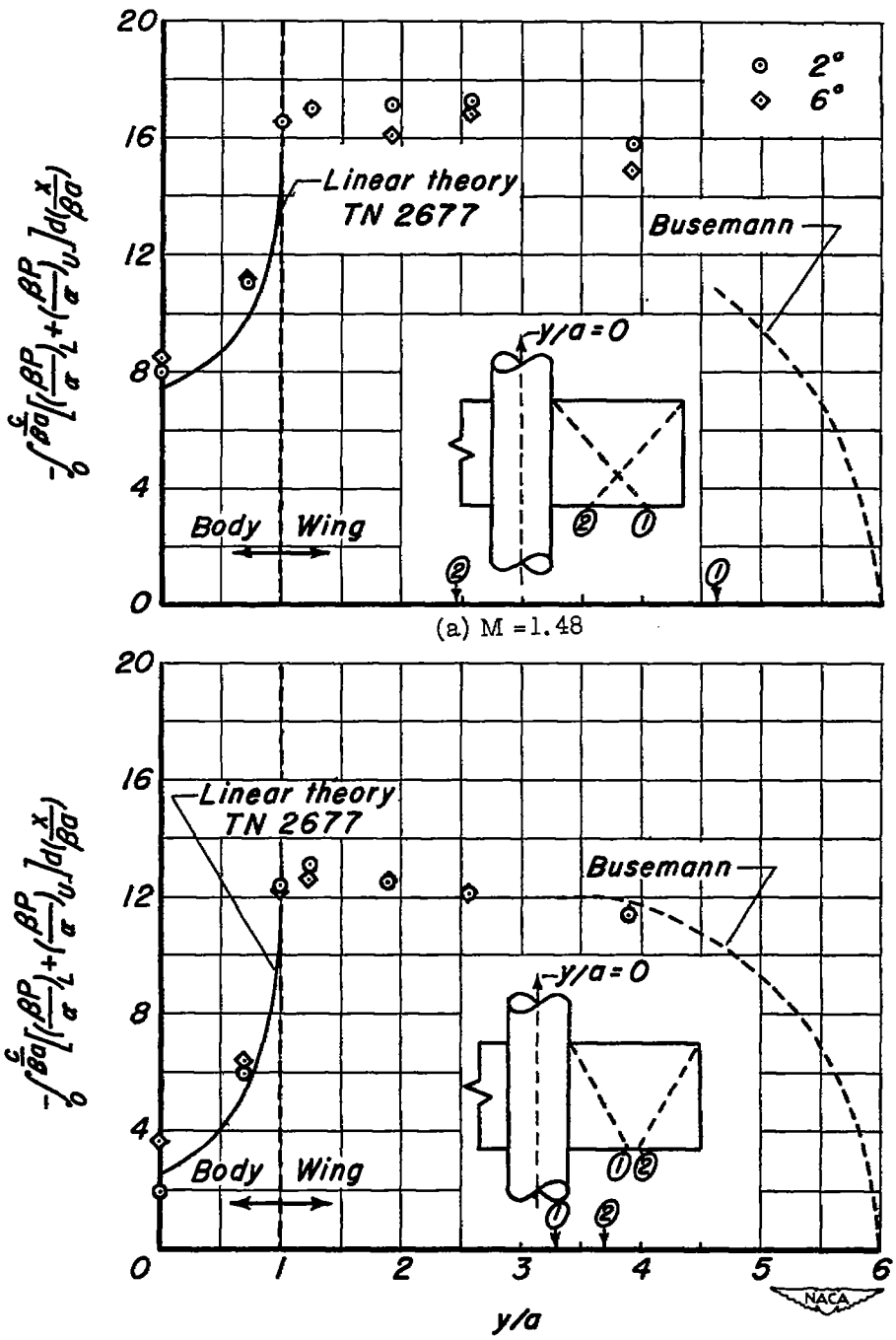

(a) M = 1.48

(b) M = 2.00

Figure 6.- Span load distribution due to α on rectangular wing-body combination with $i_W = 0^\circ$ and $R = 1.5 \times 10^6$.

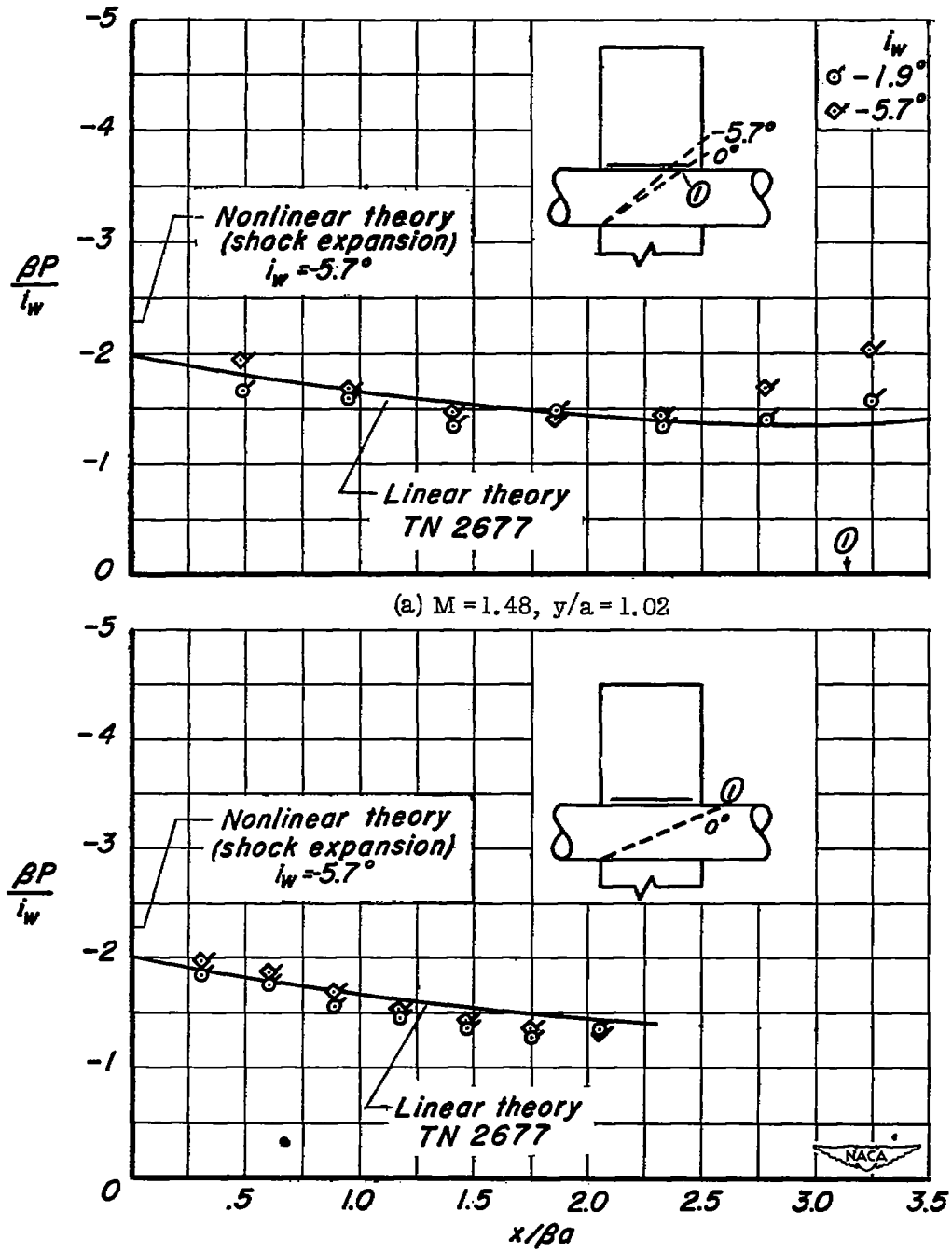

(a) M = 1.48, y/a = 1.02

(b) M = 2.00, y/a = 1.02

Figure 7.- Pressure distribution due to i_W with $\alpha = 0^\circ$ and $R = 1.5 \times 10^6$.

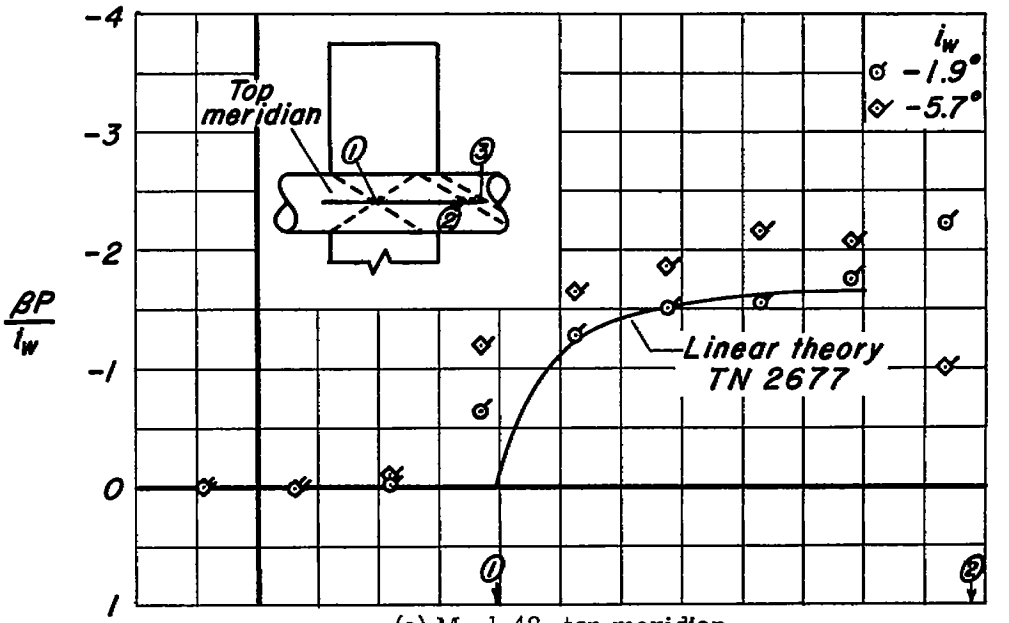

(c) M = 1.48, top meridian

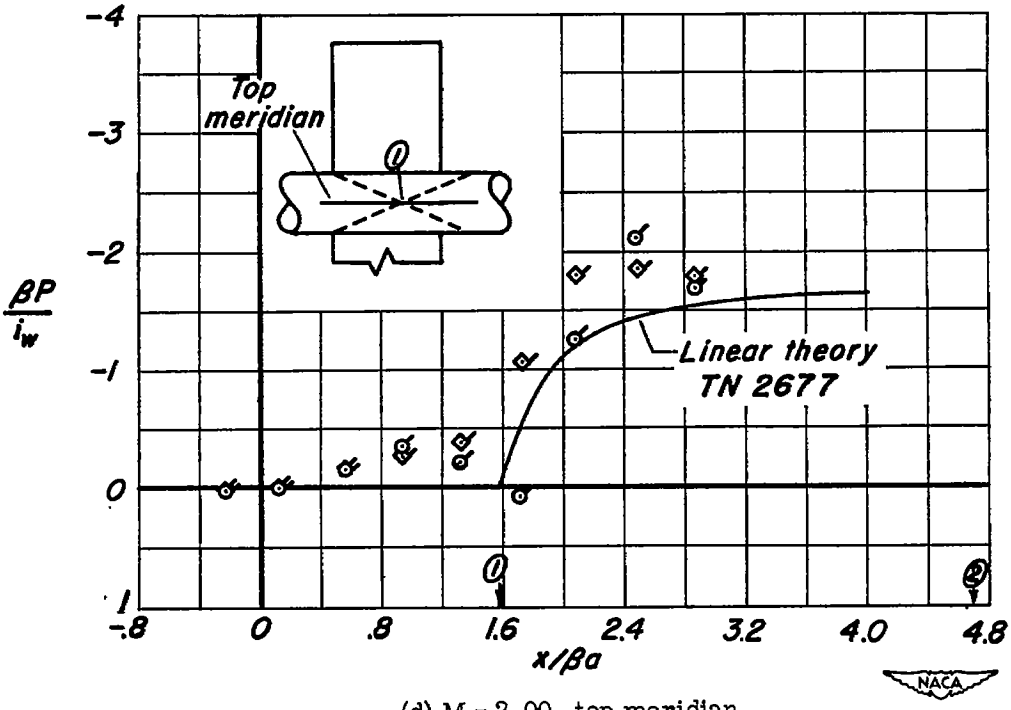

(d) M = 2.00, top meridian

Figure 7.- Continued.

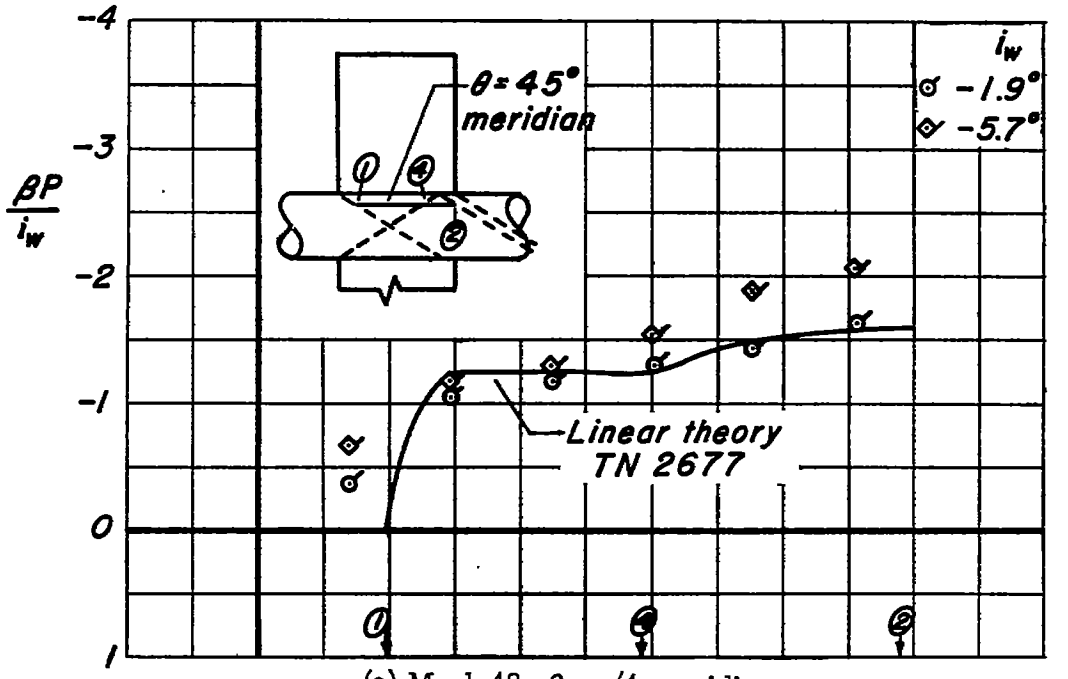

(e) M = 1.48, $\theta = \pi/4$ meridian

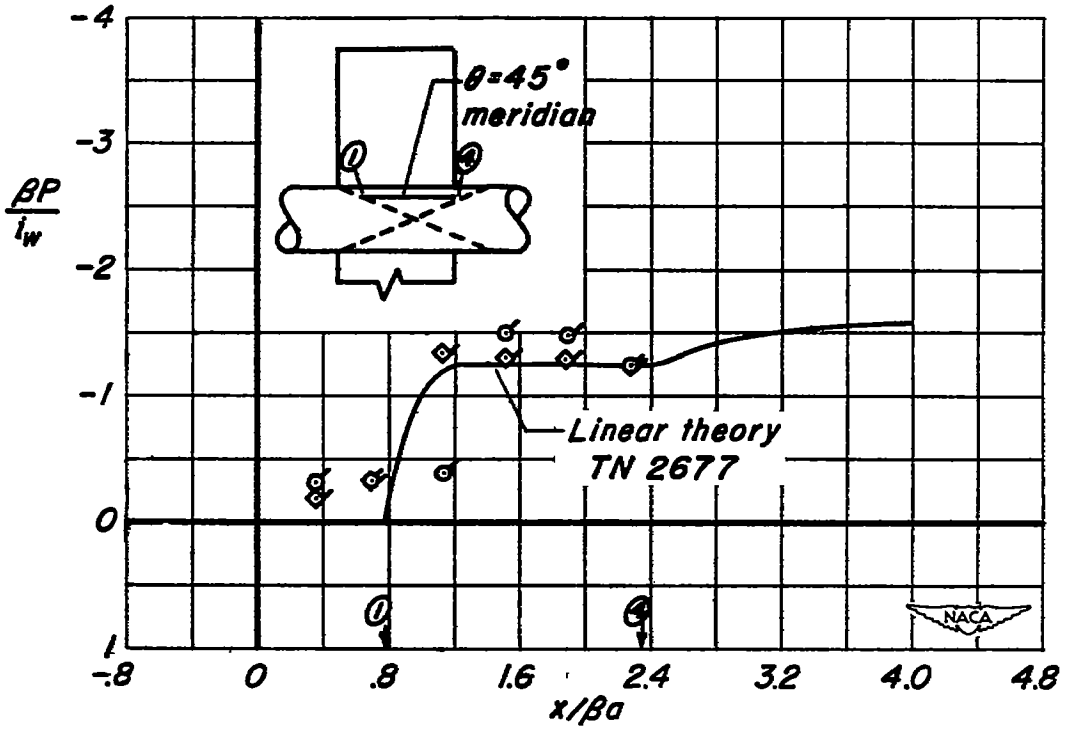

(f) M = 2.00, $\theta = \pi/4$ meridian

Figure 7.- Continued.

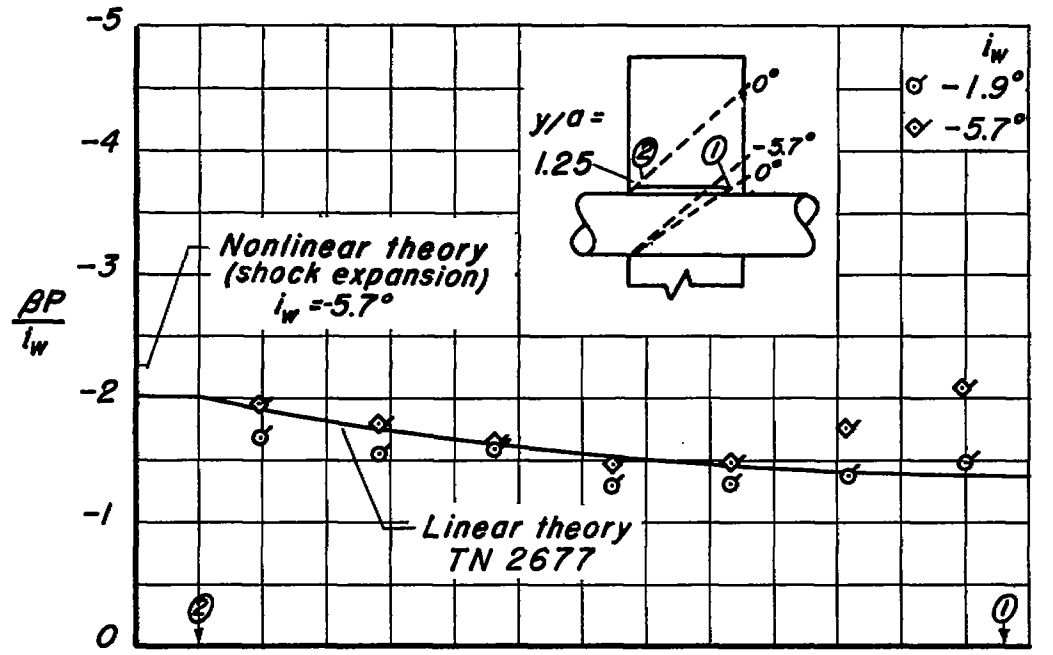

(g) M = 1.48, y/a = 1.25

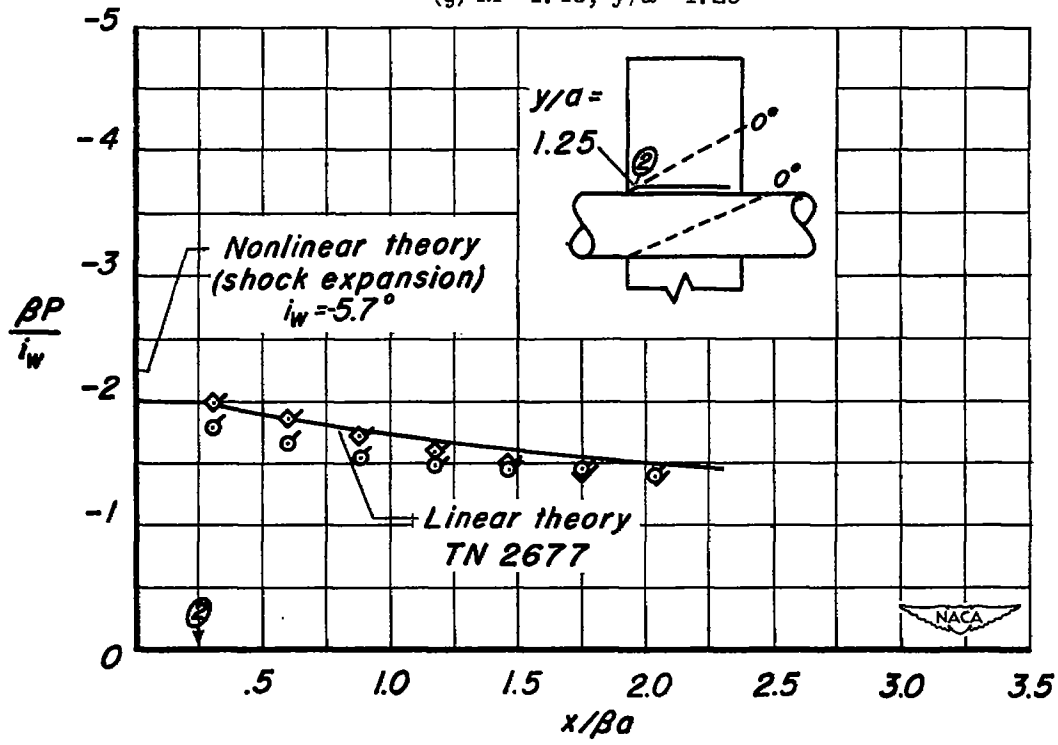

(h) M = 2.00, y/a = 1.25

Figure 7.- Continued.

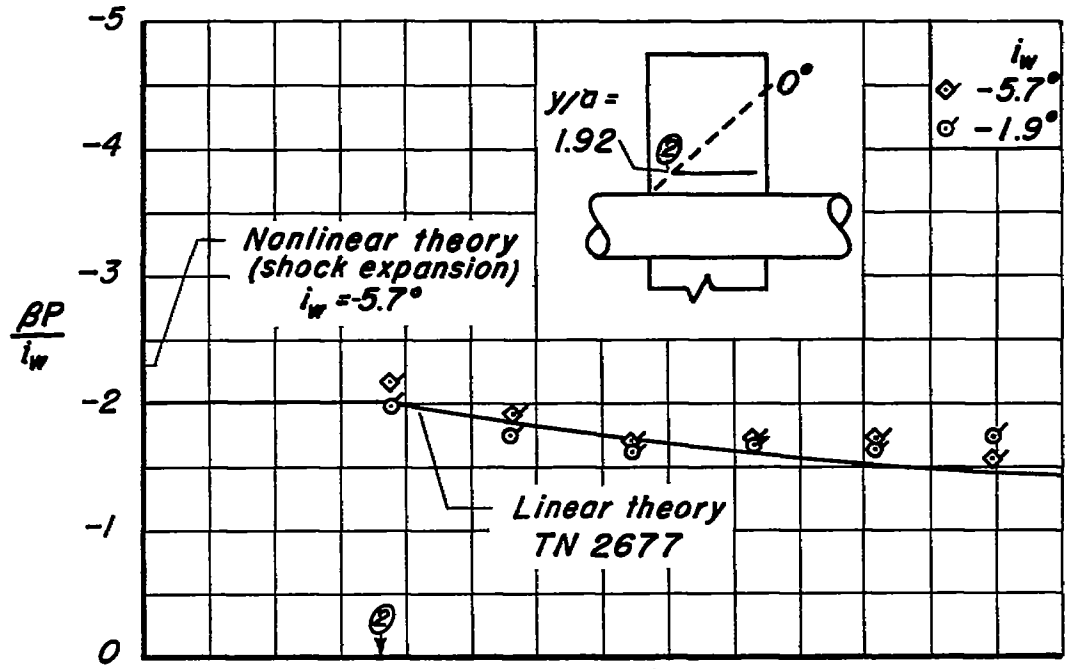

(i) M = 1.48, y/a = 1.92

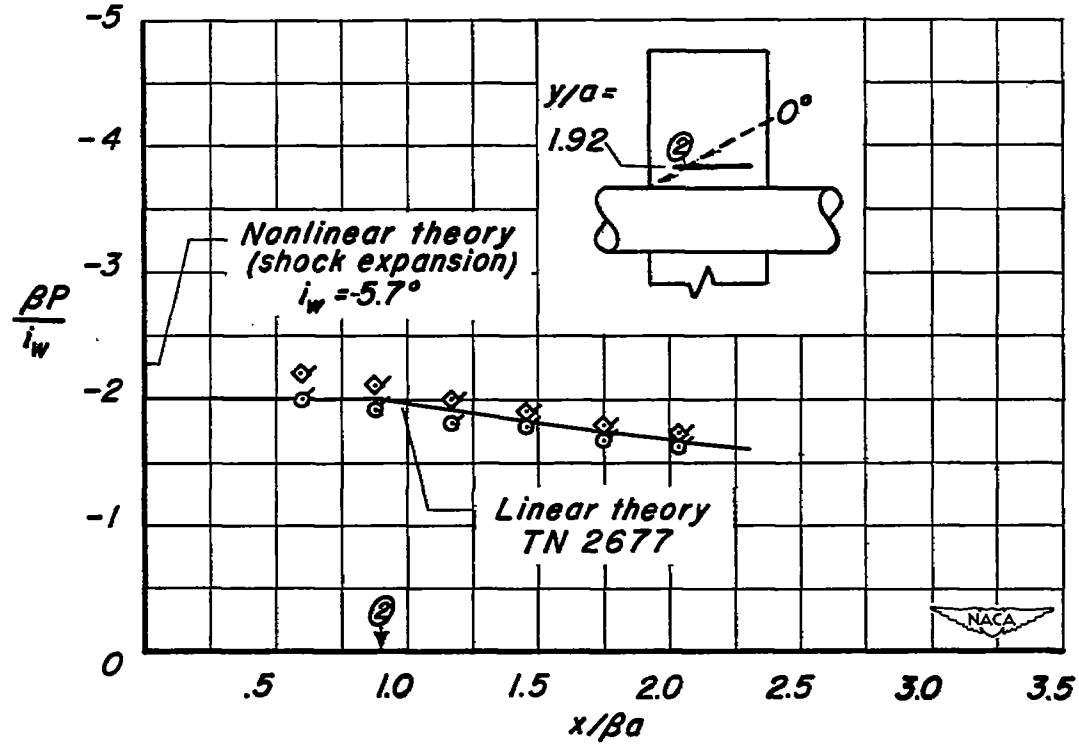

(j) M = 2.00, y/a = 1.92

Figure 7.- Continued.

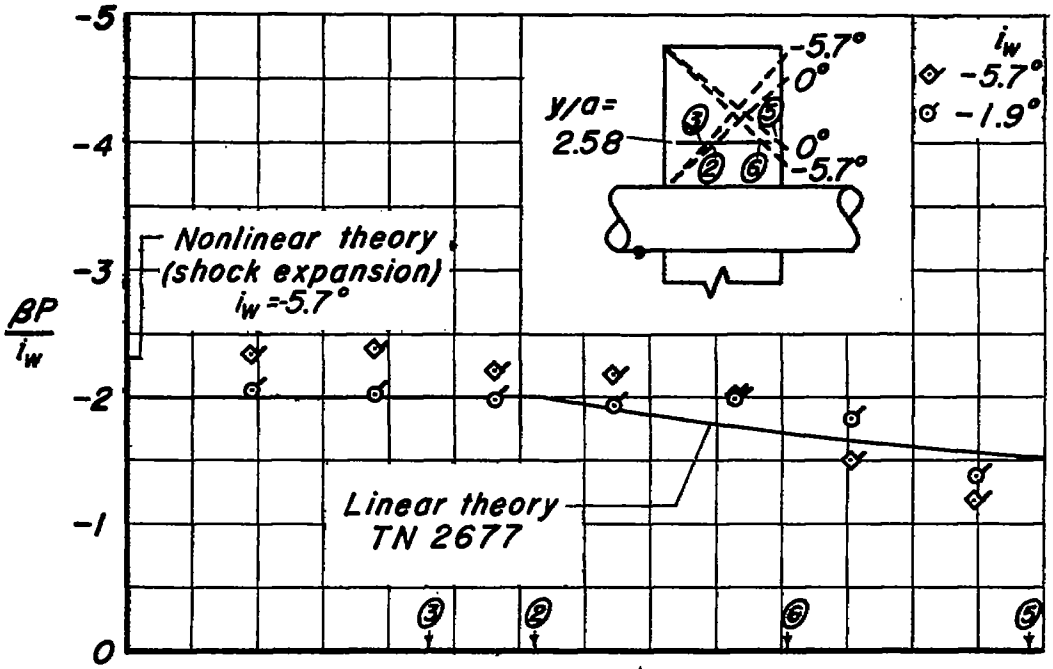

(k) M = 1.48, y/a = 2.58

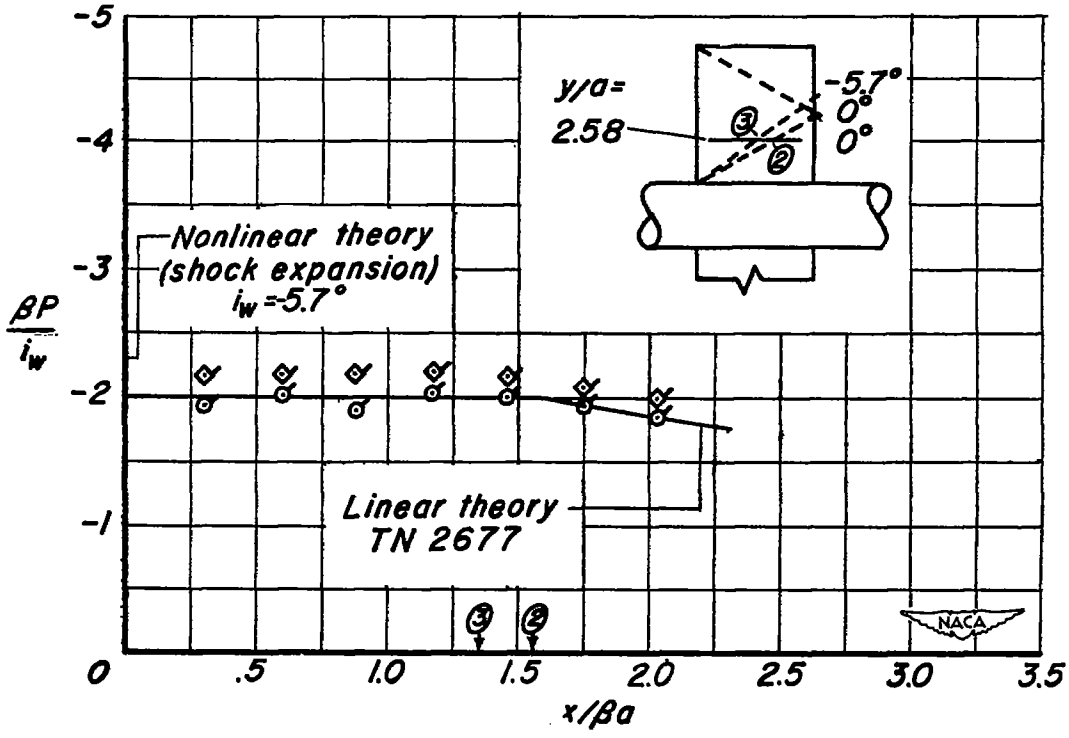

(l) M = 2.00, y/a = 2.58

Figure 7.- Continued.

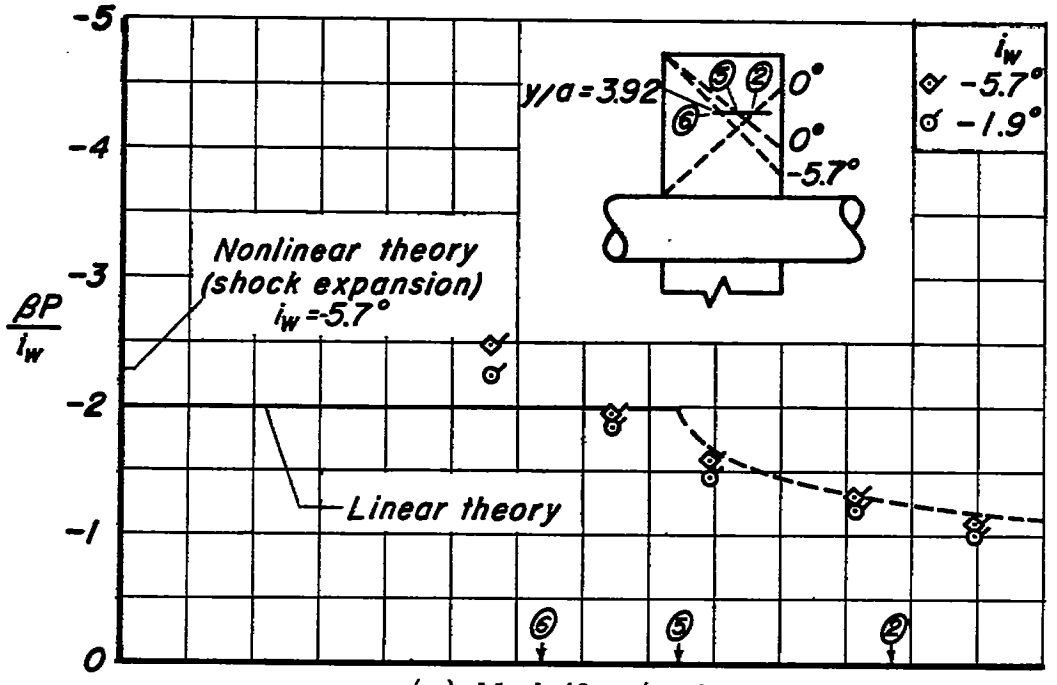

(m) M = 1.48, y/a = 3.92

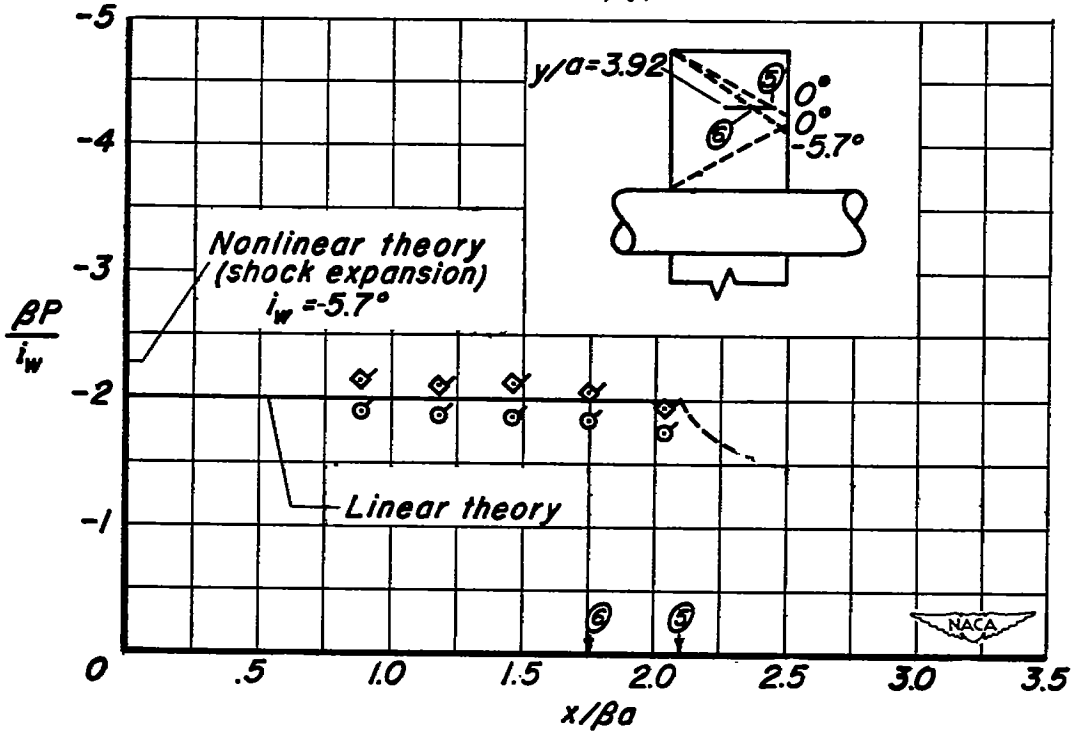

(n) M = 2.00, y/a = 3.92

Figure 7.- Concluded.

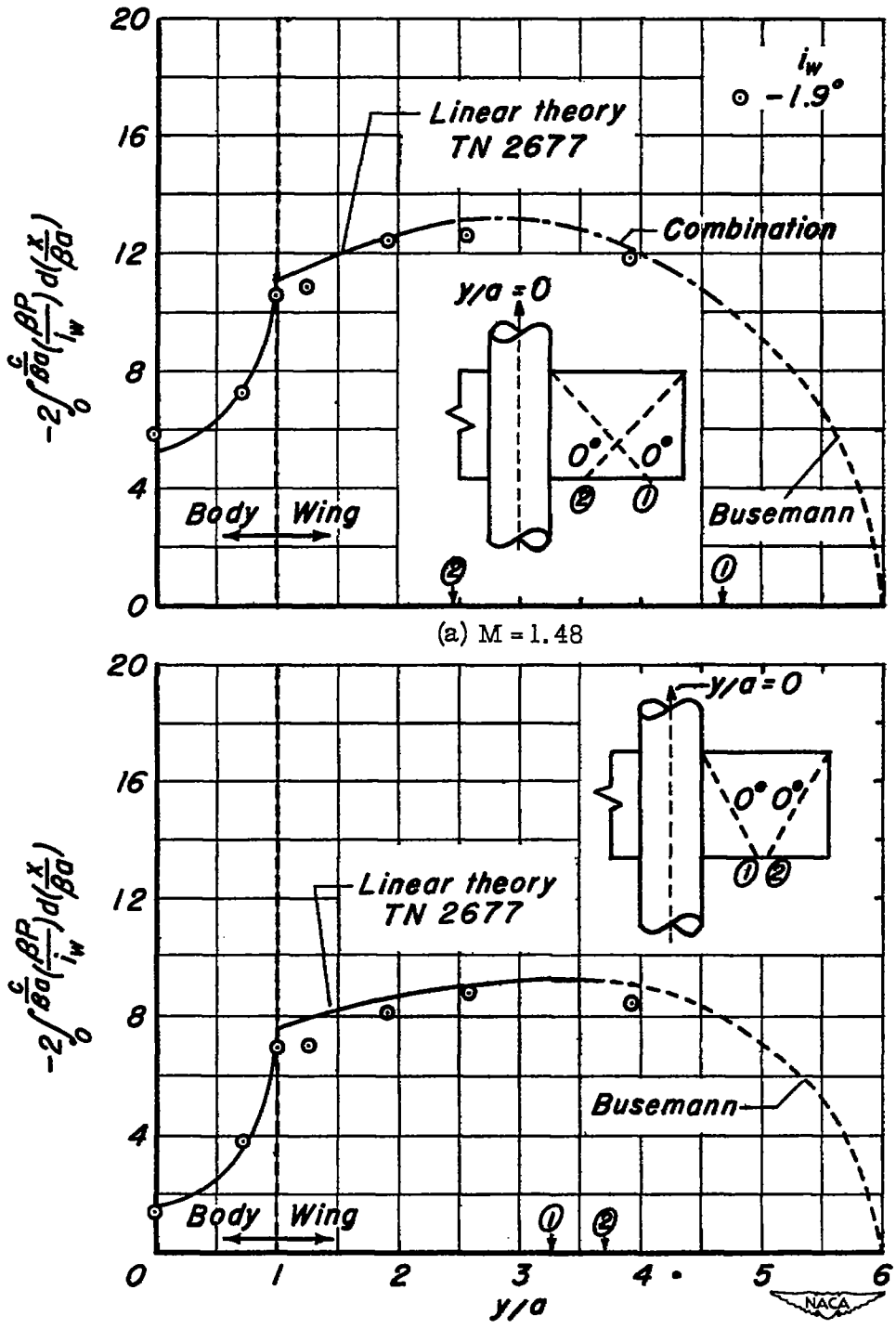

(a) M = 1.48

(b) M = 2.00

Figure 8.- Span load distribution due to i_w on rectangular wing-body combination with $\alpha = 0^\circ$ and $R = 1.5 \times 10^6$.

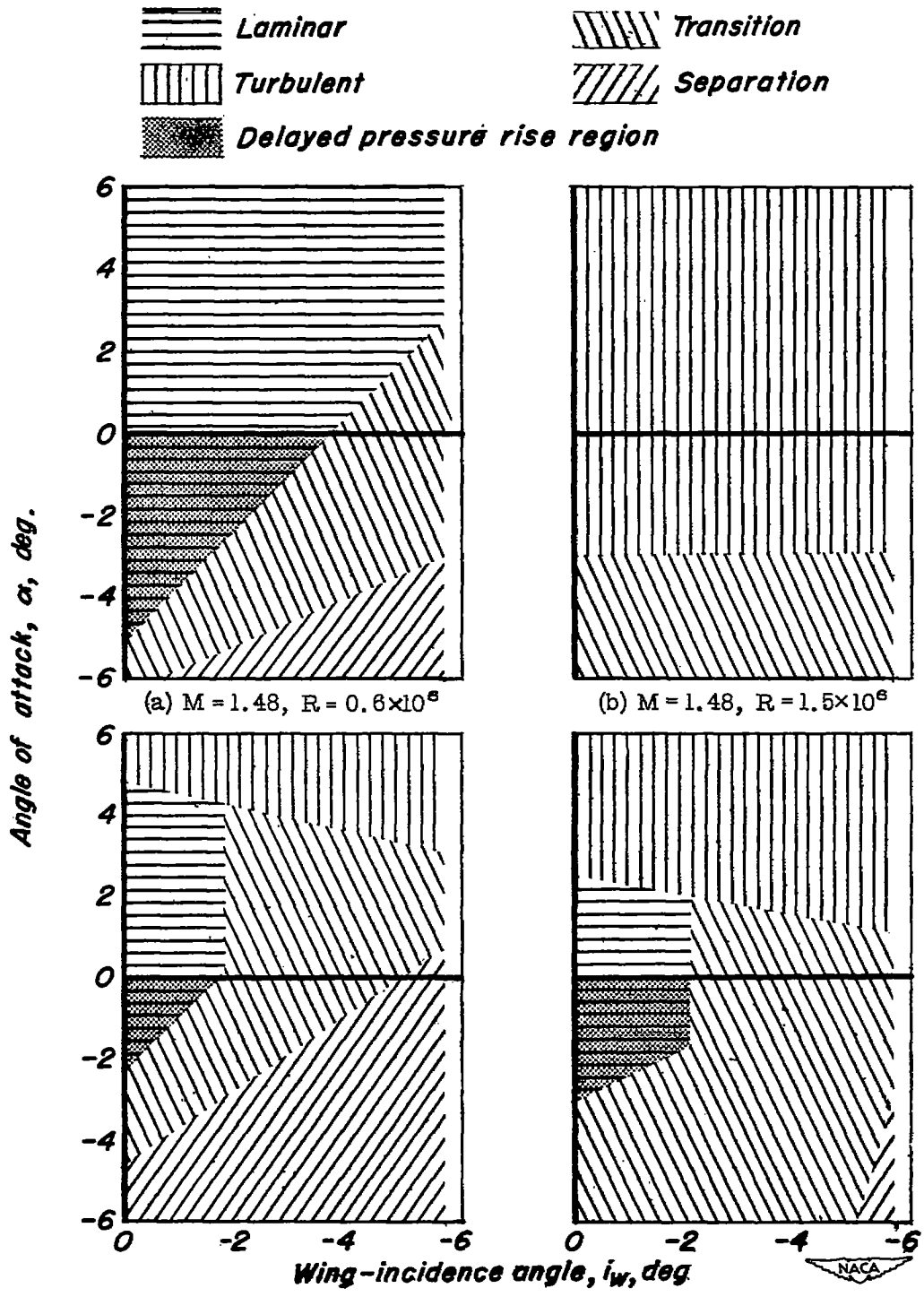

(a) M = 1.48, R = 0.6×10^6 (b) M = 1.48, R = 1.5×10^6

(c) M = 2.00, R = 0.6×10^6 (d) M = 2.00, R = 1.5×10^6

Figure 9.- Boundary-layer condition on top meridian of body at point of intersection with Mach helix from wing.

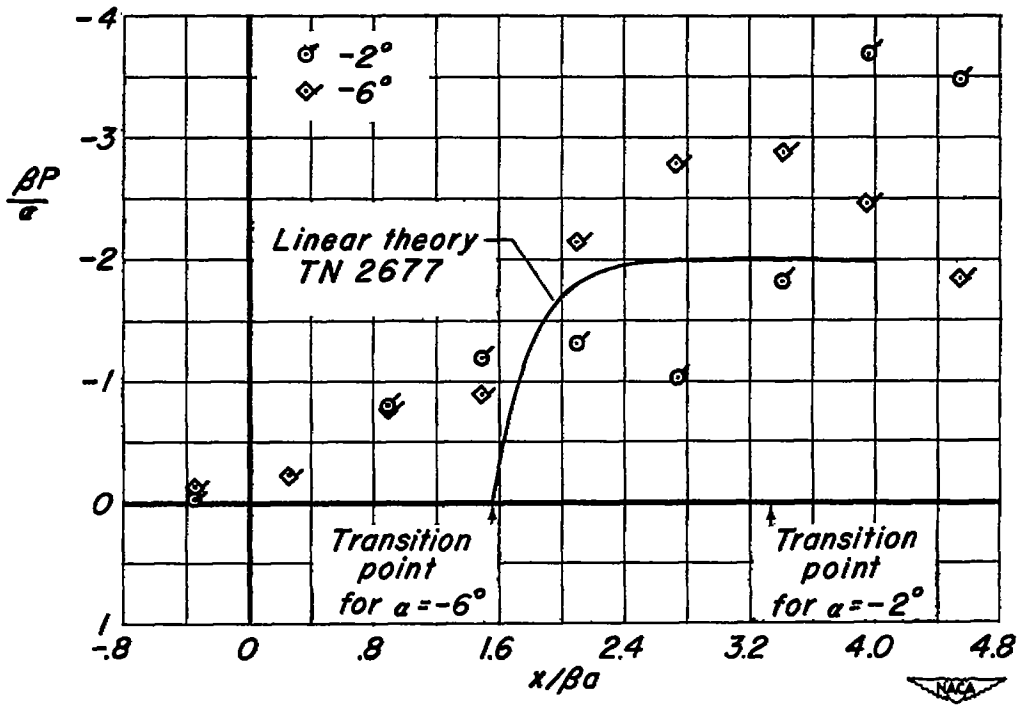

Figure 10.- Effect of transition position on pressure distribution on top meridian of body with $M = 1.48$, $R = 0.6 \times 10^6$, and $i_W = 0^\circ$.

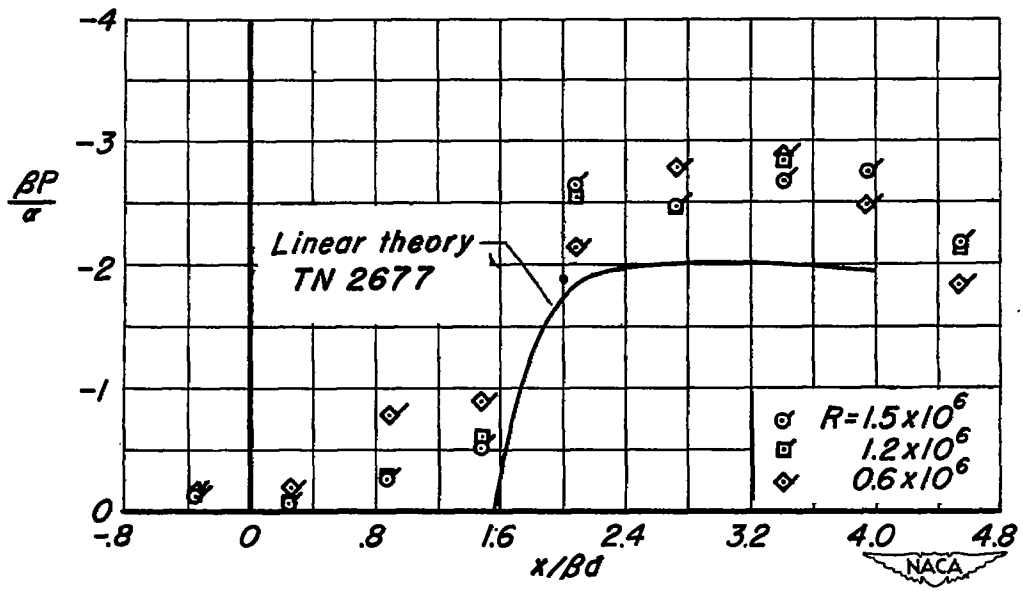

Figure 11.- Effect of Reynolds number on pressure distribution on top meridian of body with $M = 1.48$, $\alpha = -6^\circ$, and $i_W = 0^\circ$.

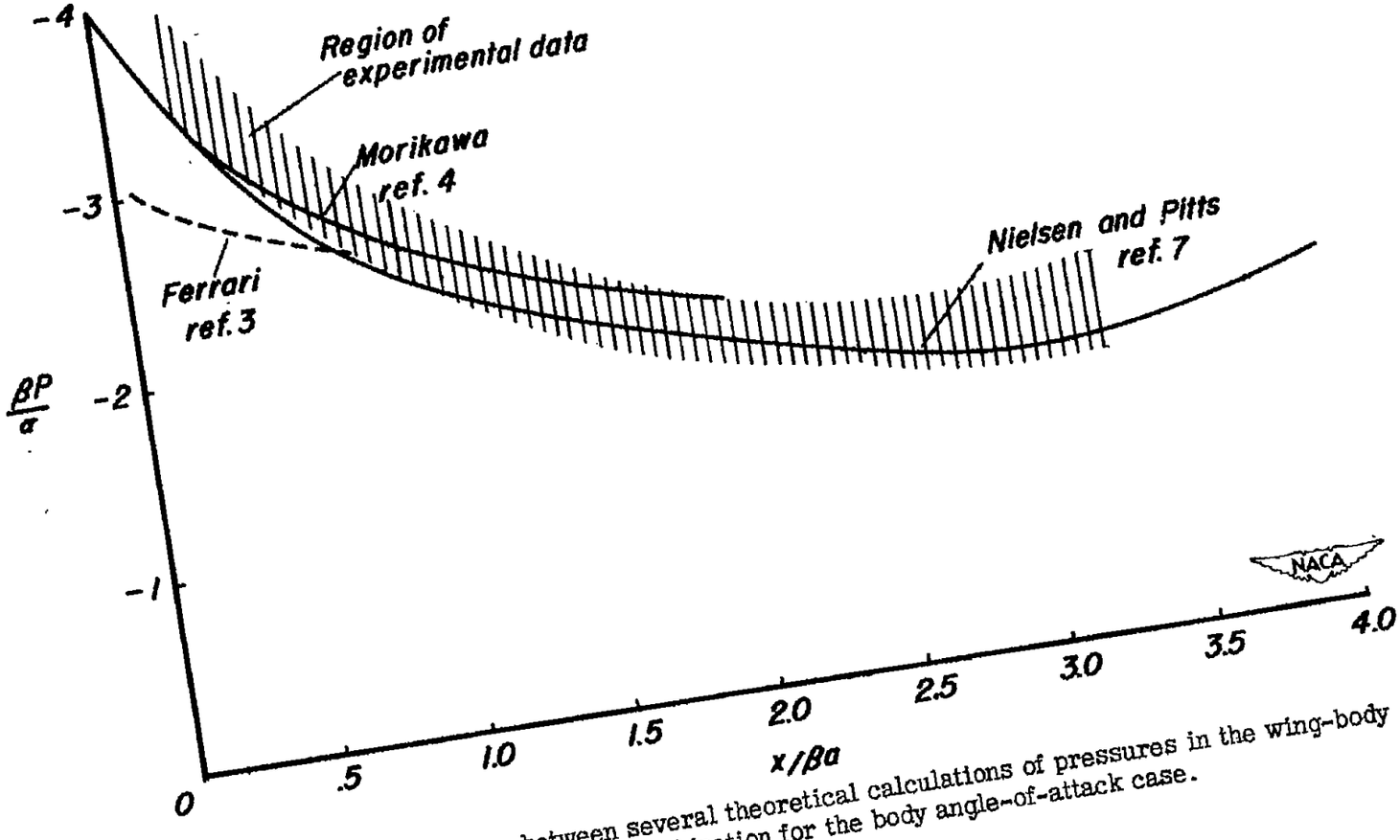

Figure 12.- Comparison between several theoretical calculations of pressures in the wing-body juncture of the combination for the body angle-of-attack case.

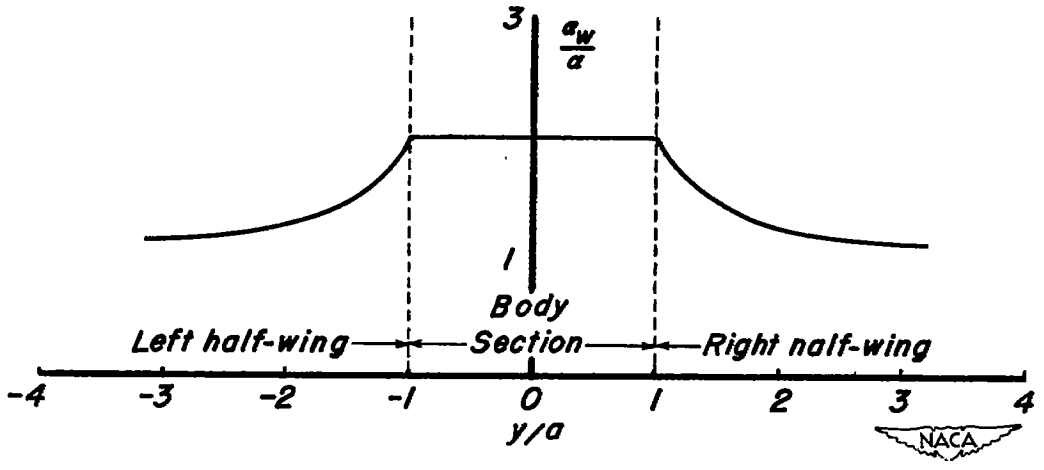

Figure 13.- Shape of wing alone with effective twist produced by body upwash field for angle-of-attack case.

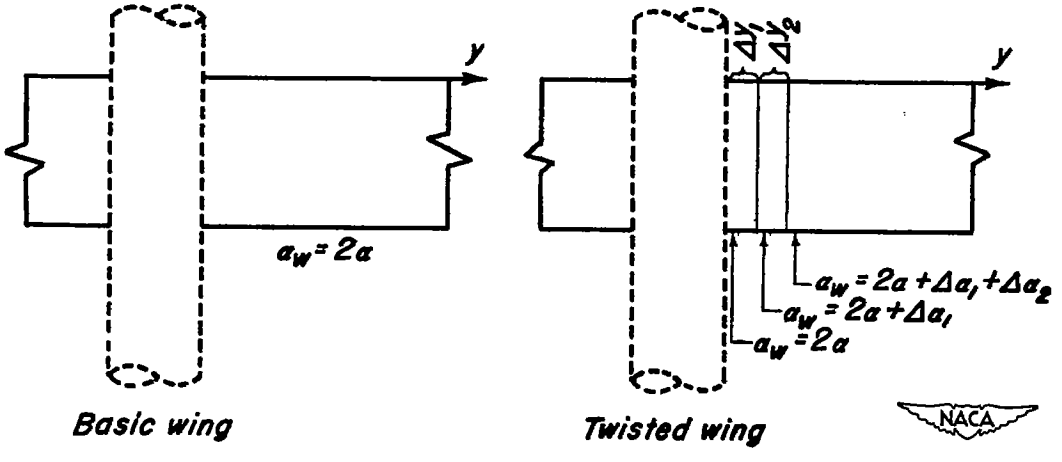

Figure 14.- Formation of twisted wing by superposition of infinite number of flat plates.

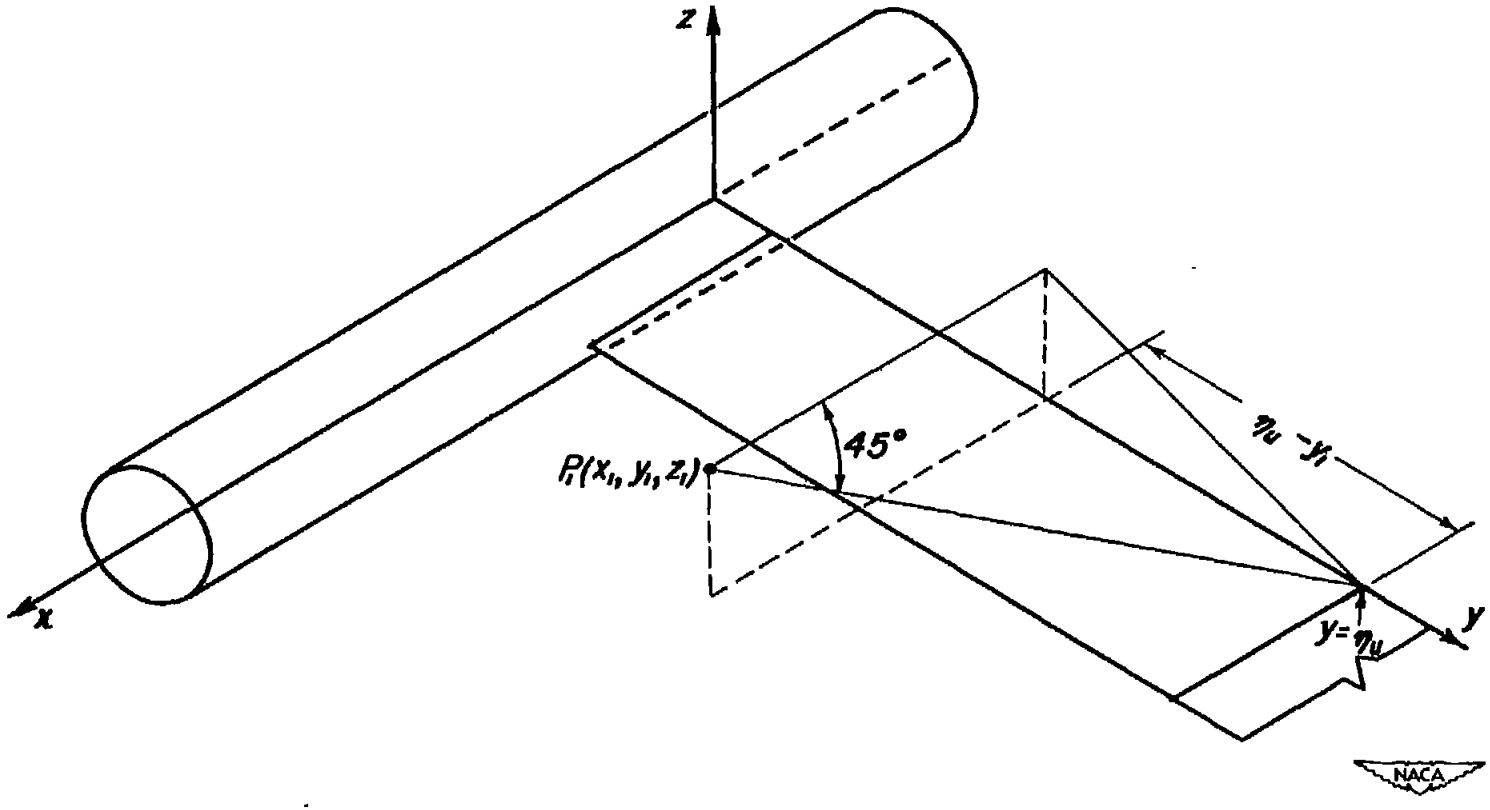

Figure 15.- Upper value of y included in the fore Mach cone emanating from P_1 for $\beta = 1$.

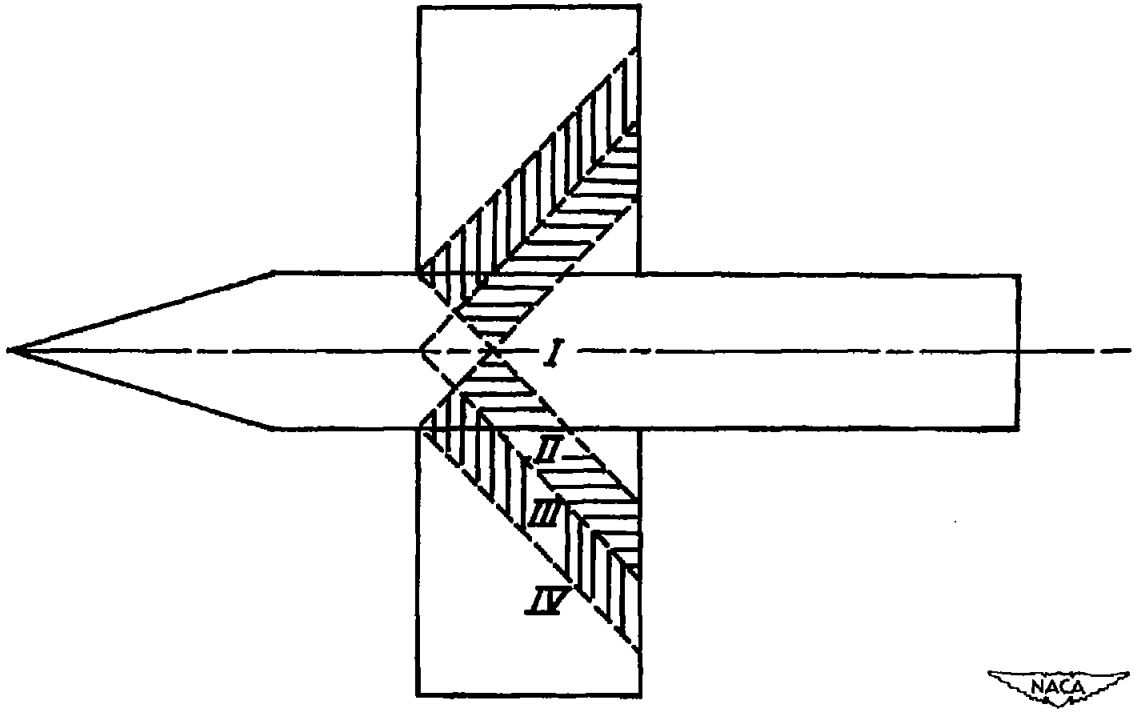

Figure 16. - Intersection of characteristic Mach cones with z = 0 plane showing corresponding regions.

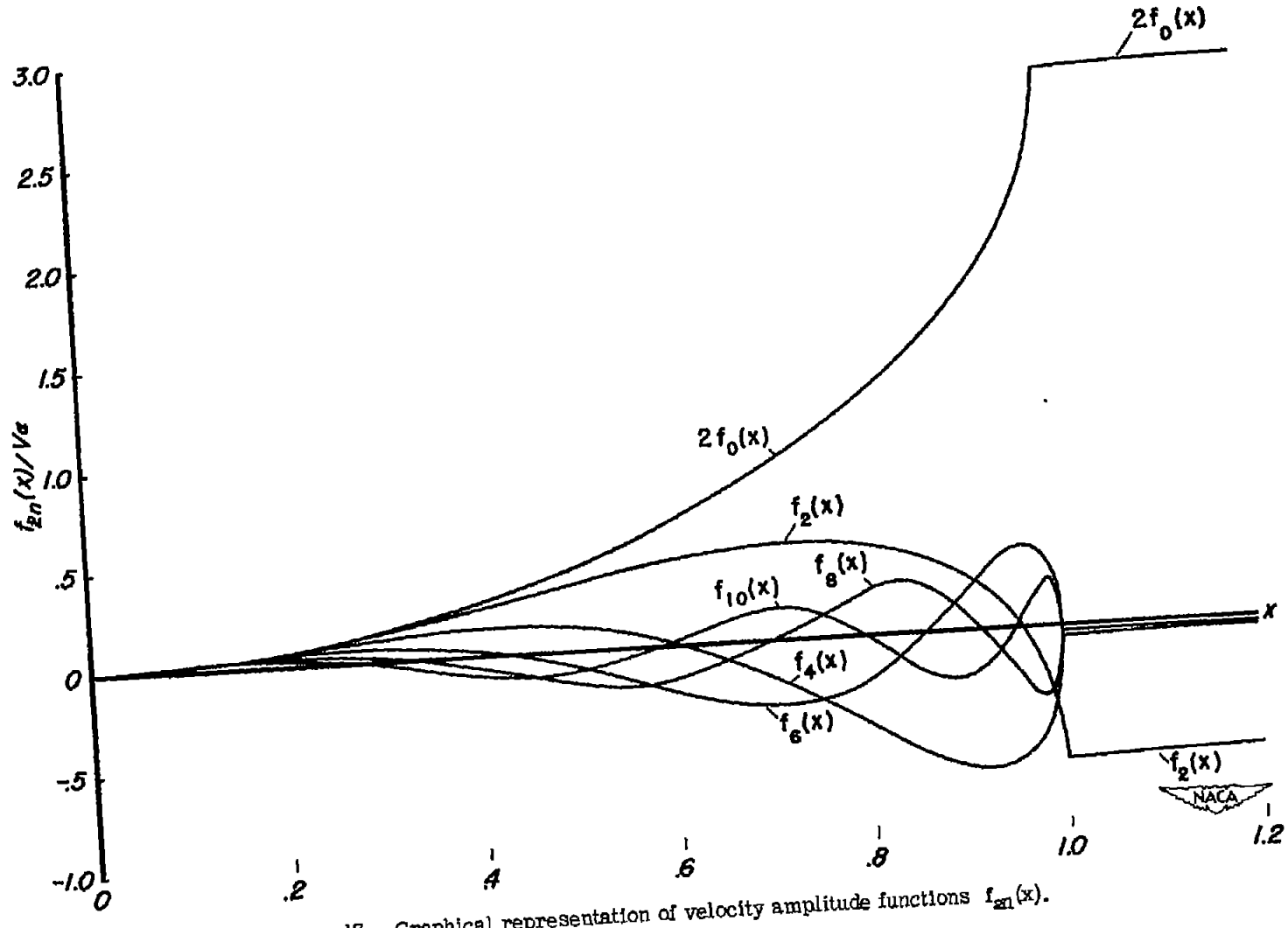

Figure 17.- Graphical representation of velocity amplitude functions $f_{2n}(x)$.

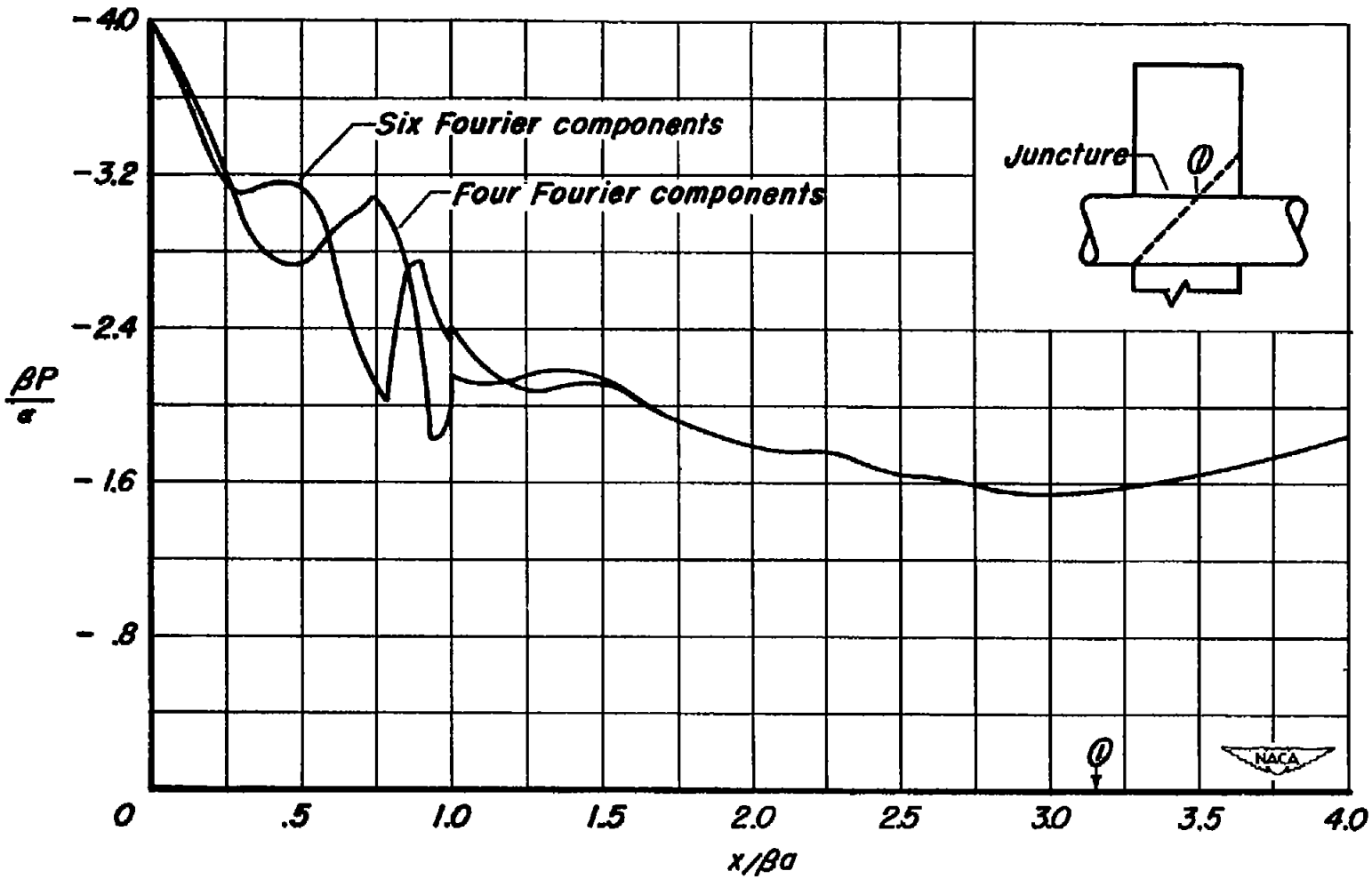

Figure 18.- Theoretical pressure distribution in wing-body juncture of combination approximated by use of four and six Fourier components.

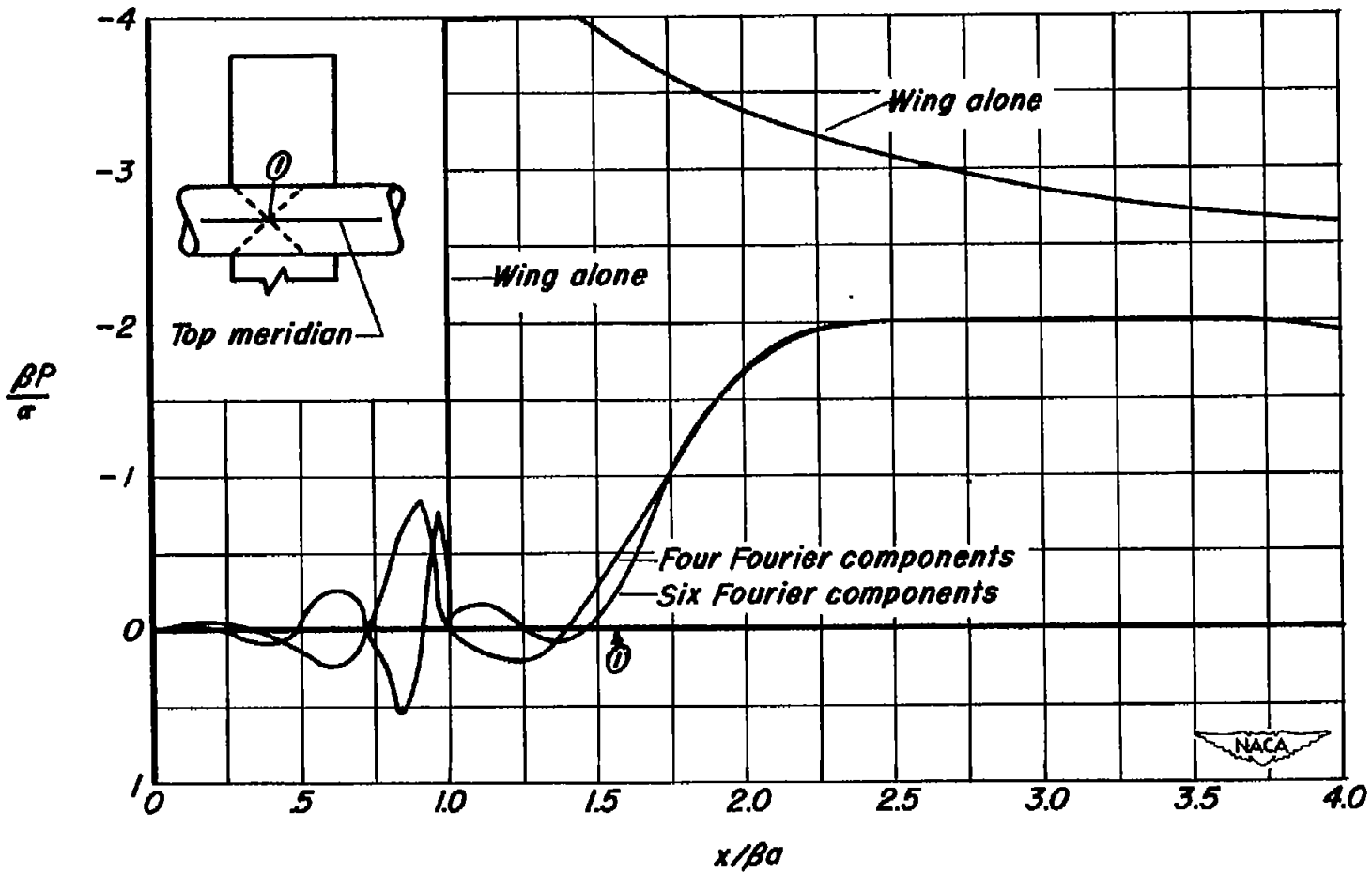

Figure 19.- Theoretical pressure distribution on top meridian of body of combination approximated by use of four and six Fourier components.

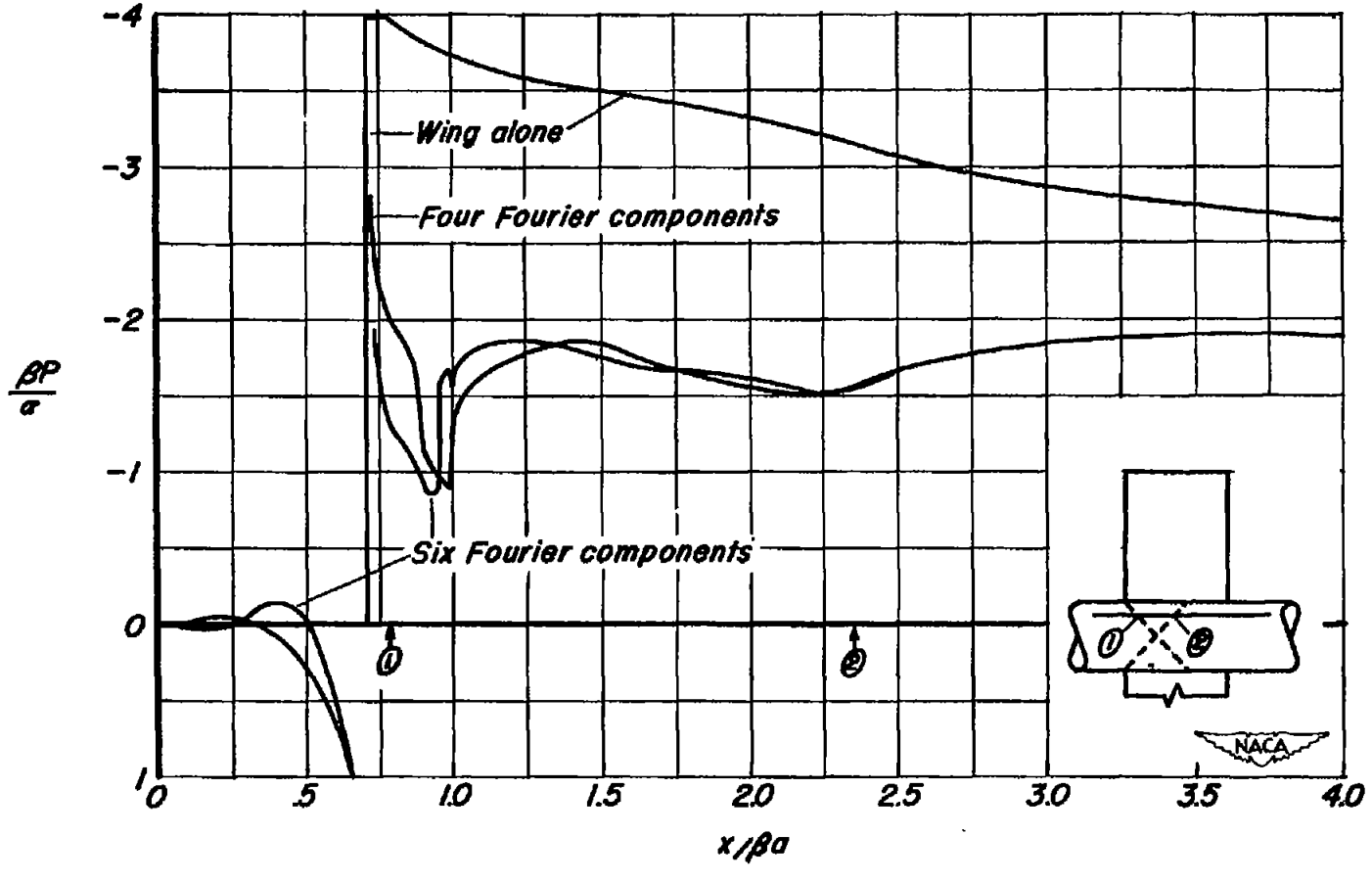

Figure 20.- Theoretical pressure distribution on $\theta = 45^{\circ}$ meridian of body of combination approximated by use of four and six Fourier components.

NACA-Langley - 4-19-54 - 1000